

High Lift Split Flaps for the Flying-V

MSc Thesis

Shadab Eftekhari



High Lift Split Flaps for the Flying-V

MSc Thesis

by

Shadab Eftekhar

To obtain the degree of Master of Science
at the Delft University of Technology
To be defended publicly on Tuesday, January 23rd, 2024 at 9:00

Student Number:	4660714	
Supervisor:	Dr. R. Vos	
Project Duration:	June, 2023 - January, 2024	
Thesis Committee:	Dr. F. Oliviero	TU Delft, Chairman
	Dr. R. Vos	TU Delft, Supervisor
	Ir. O. Stroosma	TU Delft, Examiner
	Dr. S. Asaro	TU Delft, Examiner

An Electronic version of this thesis is available at <https://repository.tudelft.nl/>

Preface

This report presents the outcomes of my MSc graduation project on the Design of High Lift Split Flaps for the Flying-V. This thesis marks the culmination of my MSc degree in Aerospace Engineering at Delft University of Technology.

I express my sincere gratitude to my supervisor, Dr. Roelof Vos, for his guidance throughout. His invaluable feedback in our bi-weekly meetings never failed to put me in the right direction during this research and his enthusiasm for the Flying-V was a great motivator.

I also thank all the amazing people associated with the Flying-V project, Eddy, Salvatore, Malkom, Burhan, Marco, Onur, Godert, Stijn and many more for their assistance in various stages of my thesis. Lastly, I am deeply grateful to my parents, from coming to The Netherlands to start my bachelor at the Aerospace Faculty of TU Delft until today when I am honored to accept my master's degree and the title of Engineer, their constant sacrifice and resilience mesmerized me. Without them I would not be where I am today.

I am filled with a range of emotions, leaving TU Delft. For over 5 years this place was my home, where I learnt so much; not only academic skills but also various life skills from the extra curricular activities during my bachelor's and master's. I met so many amazing people throughout my time here, had many great memories and made life-long friends. For these reasons I am sad to leave but at the same time happy and excited for the next chapter of my life in The Netherlands. But whatever life brings, the faculty of Aerospace Engineering at TU Delft will always be in my heart.

*Shadab Eftekhar
Delft, January 2024*

Summary

The ongoing climate crisis calls for more sustainable and fuel-efficient flying in the commercial aviation industry, which has traditionally been dominated by the Tube and Wing (TAW) configuration. Despite significant improvements in efficiency, an asymptote seems to have been reached, while air traffic continues to increase. To address these challenges, the concept of flying wings for commercial purposes has been regaining popularity, because of the ability of this configuration to reduce the non-lift generating components of the aircraft and potentially higher efficiency.

The Flying-V, a novel aircraft design, has been developing since 2016 in collaboration among the Delft University of Technology, Airbus and KLM Royal Dutch Airlines. It is a flying wing transport aircraft with a passenger capacity of 314 and a range of 15000 km, demonstrating a 20% reduction in energy consumption compared to conventional twin-aisle aircraft.

To further optimize the Flying-V's landing performance, a reduction in pitch attitude is necessary. High-lift devices, such as split flaps, can help in achieving this objective.

This report outlines the outcome of the study on High-lift Split Flaps for the Flying-V. The first part of the project adopted an experimental approach, conducting wind tunnel tests at the Open Jet Facility (OJF) of TU Delft. The experiments were conducted on a 4.6% scaled-down half-wing model of the Flying-V.

Firstly, a literature review covering research methodology, historical background on tail-less aircraft and flying wings, discussions on the low-speed aerodynamics of highly swept wings as well as low-speed wind tunnel testing was carried out. Using the knowledge gathered, the design variables for the testing of the split flaps were determined. These were the chord length, span length, chord-wise location of the hinge line, region of placement, the number of flaps and the deflection angle. Using a range of angles of attack from -5 to 30 degrees and three different speeds, 20, 25 and 30 m/s a test matrix was designed to be used during the test campaign.

The outcome of the tests lead to the selection of two flap configurations. A single-flap configuration also named Flap B, placed at 80% of the chord on region 1 which is the region closer to the root of the model. Additionally, a double-flap configuration was selected consisting of flaps C&F which were placed at 70% of both regions.

These two configurations were then analyzed in the second part of the project, using a flight performance tool developed at Delft University of Technology, PHALANX. This tool has already been used in other studies on the Flying-V. It was then concluded that the single-flap configuration was successful in reducing the pitch attitude at landing by 3° which was quite desirable. Additionally, the obscured segment and the pilot's eye altitude were reduced by 20 to 30 m and 1 m respectively which was quite significant. The possibility of reducing the approach speed was also studied which showed a reduction of 3 m/s.

The double-flap configuration was also successful in reducing the pitch attitude by about 4°, however, the inability for the aircraft to trim at forward center of gravity in Maximum Landing Mass while using this configuration was a reason to prefer the single-flap. Moreover, the added benefit of having two flaps was not significant in comparison to the single-flap configuration. The outcomes for both flap configurations are shown in Tables 5.3 to 5.8.

Table 1: The landing performance comparison between clean wing and wing with single-flaps for aft CG

Landing Characteristics	V_{app} Unchanged		V_{app} reduced
	Clean Wing	Flap B	Flap B
V_{app} (m/s)	74.5	74.5	71.5
$V_{touchdown}$ (m/s)	74.0	74.4	71.6
$\theta_{touchdown}$ (deg)	13.2	10.3	10.8
Obscured Segment (m)	102	80	88
Pilot's eye altitude (m)	28	26	27
Total landing distance (m)	1212	1182	1133

Table 2: The landing performance comparison between clean wing and wing with single-flaps for mid CG

Landing Characteristics	V_{app} Unchanged		V_{app} reduced
	Clean Wing	Flap B	Flap B
V_{app} (m/s)	74.5	74.5	71.5
$V_{touchdown}$ (m/s)	74.0	74.3	71.5
$\theta_{touchdown}$ (deg)	14.5	12.3	12.4
Obscured Segment (m)	113	87	100
Pilot's eye altitude (m)	28	27	28
Total landing distance (m)	1227	1218	1147

Table 3: The landing performance comparison between clean wing and wing with single-flaps for forward CG

Landing Characteristics	V_{app} Unchanged		V_{app} reduced
	Clean Wing	Flap B	Flap B
V_{app} (m/s)	74.5	74.5	71.5
$V_{touchdown}$ (m/s)	74.0	74.2	71.3
$\theta_{touchdown}$ (deg)	16.0	13.5	14.5
Obscured Segment (m)	126	98	114
Pilot's eye altitude (m)	29	28	29
Total landing distance (m)	1290	1256	1224

Table 4: The landing performance comparison between clean wing and wing with double-flaps for aft CG

Landing Characteristics	V_{app} Unchanged		V_{app} reduced
	Clean Wing	Flaps C&F	Flaps C&F
V_{app} (m/s)	74.5	74.5	70
$V_{touchdown}$ (m/s)	74.0	75.4	70.7
$\theta_{touchdown}$ (deg)	13.2	9.2	10.7
Obscured Segment (m)	102	73	88
Pilot's eye altitude (m)	28	26	27
Total landing distance (m)	1212	1198	1146

Table 5: The landing performance comparison between clean wing and wing with double-flaps for mid CG

Landing Characteristics	V_{app} Unchanged		V_{app} reduced
	Clean Wing	Flaps C&F	Flaps C&F
V_{app} (m/s)	74.5	74.5	70
$V_{touchdown}$ (m/s)	74.0	75.3	70.6
$\theta_{touchdown}$ (deg)	14.5	10.2	12.5
Obscured Segment (m)	113	81	104
Pilot's eye altitude (m)	28	26	28
Total landing distance (m)	1227	1219	1161

Table 6: The landing performance comparison between clean wing and wing with double-flaps for forward CG

Landing Characteristics	V_{app} Unchanged		V_{app} reduced
	Clean Wing	Flaps C&F	Flaps C&F
V_{app} (m/s)	74.5	74.5	70
$V_{touchdown}$ (m/s)	74.0	75.6	71.2
$\theta_{touchdown}$ (deg)	16.0	8.5	8.5
Obscured Segment (m)	126	77	77
Pilot's eye altitude (m)	29	26	26
Total landing distance (m)	1290	1144	1059

Note that the results for forwards CG for the double-flap configuration are in a lower landing mass. Overall, the report highlights the significance of incorporating sustainability measures in aviation, and the Flying-V project represents a promising step towards achieving more efficient and environmentally friendly air travel.

Contents

Preface	i
Summary	ii
Nomenclature	x
1 Introduction	1
1.1 Research Objective	1
1.2 Research Questions	2
1.3 Thesis Outline	2
2 Background	3
2.1 Flying-V	3
2.2 Aerodynamics of Highly Swept Cranked Wing	6
2.3 Split Flaps	10
2.4 Wind Tunnel Test	13
2.4.1 Similarity Parameter	13
2.4.2 Design of the Experiment	17
2.4.3 Uncertainties	18
2.4.4 Error Mitigation Methods	19
2.4.5 Wind Tunnel Corrections	20
2.5 Flight Performance Analysis	21
2.5.1 Aircraft Specifications	21
2.5.2 Landing Performance	22
3 Methodology	23
3.1 Wind Tunnel Experiment and Design Process	23
3.1.1 Design Variables for the Split Flaps	23
3.1.2 Test Matrix	25
3.1.3 Design and Manufacturing of Flaps	25
3.1.4 Test Set-up	27
3.2 Flight Performance Analysis	32
3.2.1 Flight Mechanics Model	32
3.2.2 Aerodynamics Model	33
3.2.3 Flight Control	34
3.2.4 Landing Maneuver	35
4 Verification & Validation	36
4.1 Reproducibility	36
4.1.1 Short-term Reproducibility	36
4.1.2 Long-term Reproducibility	39
4.2 Reynolds Number Sensitivity	39
4.3 Systematic Error Check	41
4.4 Verification of the Flight Performance Analysis	43
5 Results & Discussion	45
5.1 Aerodynamics of Split Flaps	45
5.1.1 Results of the Experiments with Single-flap Configurations	46
5.1.2 Results of the Experiments with Multi-flap Configurations	52
5.1.3 Selection of the Best Flap Configuration	57
5.1.4 Results per Design Variable	62
5.1.5 Trimming	69

5.2	Flight Performance	71
5.2.1	Landing Analysis for Wing with Single Flap configuration	71
5.2.2	Landing Analysis for Wing with Double Flap Configuration	74
5.2.3	Effect on the Landing Gear	78
6	Conclusion and Recommendations	79
6.1	Conclusions	79
6.2	Recommendations	81
	References	82
A	Test Matrix	85
B	Additional Wind Tunnel Test Results	88
B.1	Flap A	88
B.2	Flap B in R2	92
B.3	Flap C	93
B.4	Flap D	94
B.5	Flap E	98
B.6	Flaps A and D	99
B.7	Flap B on Both Regions	100
C	Wind Tunnel Test Campaign Images	102

List of Figures

2.1	CAD generated image of the Flying-V ¹	4
2.2	Modification of the Flying-V planform by Faggiano [8]	4
2.3	The original wind tunnel model constructed by Vos and Palermo [9]	5
2.4	Tuft and oil flow visualization on the half-wing wind tunnel model at 15° angle of attack [15]	6
2.5	Span wise lift distribution for an aft and a forward swept wing in comparison to an elliptical lift distribution [16]	7
2.6	Isobars on two wings with 53° sweep [16]	7
2.7	Flow pattern on the FV half-wing model at 9 degrees angle of attack [15]	8
2.8	Flow pattern on the FV half-wing model at 15 degrees angle of attack [15]	9
2.9	F-16XL in flight [17]	9
2.10	Subsonic high angle of attack case FC-25 of CAWAPI-2 [18]	10
2.11	Lift curves produced in the study by Frey et al. on the effectiveness of split flaps on lift increase of the wing [20]	11
2.12	Flap configurations for the experiment done by Wenzinger on comparison between ordinary and split flaps aerodynamics performance [21]	11
2.13	Lift, drag and center of pressure for the Clark Y airfoil with 0.2C full-span split flap [21]	12
2.14	Tail-less transport aircraft with Tail-less Combination Flap system (TCF) [23]	13
2.15	Effect of Reynolds number on $C_{L,max}$ with flaps deflected on three NACA airfoils [28]	14
2.16	Effect of scale on the lift characteristics of F-111 aircraft [28]	15
2.17	Variation of C_D with Reynolds number on NACA 23012 airfoil[28]	16
2.18	Schematics of systematic and random uncertainties [25]	19
2.19	Pilot vision during landing, modified from [43]	22
3.1	Half-wing model division for flaps placement	24
3.2	CAD model of flaps A to F placed on the half-wing wind tunnel model of the Flying-V	25
3.3	Top-view drawing of the positioning of the flaps on the half-wing model	25
3.4	Brackets used for changing the flaps' deflection angles	26
3.5	Two samples of flaps used in the wind tunnel test campaign	26
3.6	Flaps A and C mounted on the half-wing model of the Flying-V during the test campaign at OJF	27
3.7	The Open Jet Facility of TU Delft Aerospace Engineering [26]	28
3.8	The half-wing model geometry as used in a study by Empelen, Vos [47]	29
3.9	Side view of the test-set up [9]	30
3.10	Top view of the test set-up [9]	30
3.11	Rear view of the test set-up [9]	31
3.12	Block scheme overview of the PHALANX flight mechanics model [54]	32
3.13	Body (b), wind (w) and aerodynamic (a) reference frame [54]	33
3.14	General architecture of closed feedback control loop [14]	35
4.1	Comparison of repeated measurements for clean wing on 5 different days	37
4.2	Comparison of repeated measurements for flap C at 70% of the chord in Region 1 with 10° deflection	38
4.3	Comparison of repeated measurements for flap F at 70% of the chord in Region 2 with 20° deflection	38
4.4	Comparison of the results of current study and a study done by Erdinciler [13] for long-term reproducibility	39
4.5	Effect of Reynolds number variations on the aerodynamic coefficients for clean wing	40
4.6	Effect of Reynolds number variations on the aerodynamic coefficients for wing with flap E	41

4.7	Comparison of aerodynamic coefficients before and after removing bias for clean wing and wing with flaps C&F on	42
4.8	Comparison of landing performance using de Zoeten's and the clean wing data obtained from the wind tunnel test	43
5.1	CAD model of flaps A to F placed on the half-wing wind tunnel model of the Flying-V	46
5.2	Results of Flap A in Region 1 at 90% of the chord	47
5.3	Results of flap B in Region 1 at 80% of the chord	49
5.4	Results of Flap F in Region 2 at 70% of the chord	51
5.5	Results of Flaps B and E at 80% of the chord in both regions	53
5.6	Results of Flaps C and F at 70% of the chord in both regions	54
5.7	Results of Full-span flap at 80% of the chord	56
5.8	Best results of each single-flap configuration for 30° deflection angle	58
5.9	Best results of each multi-flap configuration for 30° deflection angle	60
5.10	Effect of the chord-wise hinge line location on flap performance	63
5.11	Effect of the chord length on flap performance in region 1	64
5.12	Effect of the chord length on flap performance in region 2	65
5.13	Effect of the span length on flap performance	66
5.14	Effect of the region of placement on flap performance	67
5.15	Effect of the number of flaps on flap performance	68
5.16	Determination of the aerodynamic center	69
5.17	Trimmed lift coefficient for the two selected flap configurations in comparison to clean wing	70
5.18	Pitch attitude at landing for wing with flap B with unchanged and reduced approach speed versus clean wing for aircraft trimmed at three center of gravity locations	72
5.19	Obscured segment for wing with flap B with unchanged and reduced approach speed versus clean wing for aircraft trimmed at three center of gravity locations	73
5.20	Pilot eye altitude for wing with flap B with unchanged and reduced approach speed versus clean wing for aircraft trimmed at three center of gravity locations	73
5.21	Pitch attitude at landing for wing with flaps C&F with unchanged and reduced approach speed versus clean wing for aircraft trimmed at two center of gravity locations	75
5.22	Obscured segment for wing with flaps C&F with unchanged and reduced approach speed versus clean wing for aircraft trimmed at two center of gravity locations	75
5.23	Pilot eye altitude for wing with flaps C&F with unchanged and reduced approach speed versus clean wing for aircraft trimmed at two center of gravity locations	76
5.24	Landing performance for wing with flaps C&F with unchanged and reduced approach speed and lower MLM for aircraft trimmed at forward CG location	77
B.1	Results of Flap A in Region 2 at 70% of the chord	89
B.2	Results of Flap A in Region 2 at 80% of the chord	90
B.3	Results of Flap A in Region 2 90% of the chord	91
B.4	Results of Flap B in Region 2 at 80% of the chord	93
B.5	Results of Flap C in Region 1 at 70% of the chord	94
B.6	Results of Flap D in Region 2 at 70% of the chord	95
B.7	Results of Flap D Region 2 at 80% of the chord	96
B.8	Results of Flap D Region 2 at 90% of the chord	98
B.9	Results of Flap E in Region 2 at 80% of the chord	99
B.10	Results of Flaps A and D at 90% of the chord in both regions	100
B.11	Results of Flap B at 80% of the chord in both regions	101
C.1	Different flap configurations placed on the half-wing model during the wind tunnel tests	103

List of Tables

1	The landing performance comparison between clean wing and wing with single-flaps for aft CG	iii
2	The landing performance comparison between clean wing and wing with single-flaps for mid CG	iii
3	The landing performance comparison between clean wing and wing with single-flaps for forward CG	iii
4	The landing performance comparison between clean wing and wing with double-flaps for aft CG	iii
5	The landing performance comparison between clean wing and wing with double-flaps for mid CG	iii
6	The landing performance comparison between clean wing and wing with double-flaps for forward CG	iv
2.1	Confidence intervals for a Gaussian distribution	18
2.2	The sources from which the data on FV-1000 was gathered	21
2.3	Top level specifications for the Flying-V-1000	21
2.4	Geometric specifications for the Flying-V-1000	22
3.1	Dimensions of the various flaps	26
4.1	The maximum differences and P-values of aerodynamic coefficients before and after removing the biases for clean wing and wing with flaps C&F on	43
5.1	Normalized scores in each criteria for the single-flap configuration	60
5.2	Normalized scores in each criteria for the multi-flap configuration	60
5.3	The landing performance comparison between clean wing and wing with single-flaps for aft CG	74
5.4	The landing performance comparison between clean wing and wing with single-flaps for mid CG	74
5.5	The landing performance comparison between clean wing and wing with single-flaps for forward CG	74
5.6	The landing performance comparison between clean wing and wing with double-flaps for aft CG	77
5.7	The landing performance comparison between clean wing and wing with double-flaps for mid CG	77
5.8	The landing performance comparison between clean wing and wing with double-flaps for forward CG	78
A.1	Test matrix used during the wind tunnel experiment	85
A.2	Extra measurements taken during wind tunnel test	87

Nomenclature

Abbreviations

Abbreviation	Definition
A35K	Airbus A350-1000
AoA	Angle of Attack
AoD	Angle of Deflection
CAD	Computer Aided Design
CAWPI	Cranked Arrow Wing Aerodynamics Project International
CAWP	Cranked Arrow Wing Aerodynamics Project
CG	Center of Gravity
CFD	Computational Fluid Dynamics
CS	Control Surface
DOE	Designed Experiment
DOF	Degrees of Freedom
FV	Flying-V
HLD	High Lift Device
ISA	International Standard Atmosphere
KLM	Koninklijke Luchtvaart Maatschappij (Royal Dutch Airlines)
MLG	Main Landing Gear
MLM	Maximum Landing Mass
MLW	Maximum Landing Weight
MTOM	Maximum Take-off Mass
MTOW	Maximum Take-off Weight
NASA	National Aeronautics and Space Administration
NACA	National Advisory Committee for Aeronautics
OJF	Open Jet Facility
OFAT	One Factor At a Time
PHALANX	Performance, Handling Qualities and Load Analysis Toolbox
PID	Proportional gain, Integral gain & Derivative gain
SSFT	Sub Scale Flight Testing
TAW	Tube And Wing
TCF	Tail-less Combination Flap System
TE	Trailing Edge
VLM	Vortex Lattice Method
WT	Wind Tunnel

Symbols

Symbol	Definition	Unit
A	Surface area	$[m^2]$
a	Speed of Sound	$[m/s]$
b	Wind tunnel model span	$[m]$
\bar{c}	Mean Aerodynamic chord	$[m]$

Symbol	Definition	Unit
C	Chord Length	[m]
C_D	Drag coefficient	—
C_L	Lift Coefficient	—
$C_{L,max}$	Maximum Lift Coefficient	—
C_M	Pitching moment coefficient	—
C_Y	Normal force coefficient	—
C_n	Yawing moment coefficient	—
C_l	Rolling moment coefficient	—
D	Drag force	[N]
e	Error in prescribed value	—
F	Force measured by the balance	[N]
Fr	Froude Number	—
g	Gravitational acceleration	[m/s^2]
H	Tunnel height	[m]
I	Moment of inertia	[$kg.m^2$]
K_d	Derivative control gain	—
K_i	Integral control gain	—
K_P	Proportional control gain	—
L	Characteristic Length	[m]
L	Span design variable in the wind tunnel experiment	—
L	Lift force	[N]
l	Rolling moment	[$N.m$]
L/D	Lift to Drag ratio	—
M	Pitching moment	[$N.m$]
M_{CG}	Moment around the center of gravity reference point	[$N.m$]
m	Mass	[kg]
Ma	Mach number	—
n	Yawing moment	[$N.m$]
p	Roll rate	[rad/s]
q	pitch rate	[rad/s]
R	Region design variable in the wind tunnel test experiment	—
r	Yaw rate	[rad/s]
r	Distance from the leading edge	[m]
r_{arm_x}	Distance between wing root to balance center in the x-direction on the wind tunnel model	[m]
r_{arm_z}	Distance between wing root to balance center in the z-direction on the wind tunnel model	[m]
r_{mgc_x}	Center of gravity to nose distance in the X-direction on the wind tunnel model	[m]
r_{mgc_z}	Center of gravity to wing root plane distance in the Z-direction on the wind tunnel model	[m]
Re	Reynolds number	—
S	Reference area	[m^2]
t	Time	[sec]
t/c	Thickness to chord ratio	—
u	Velocity component in x direction in body reference frame	[m/s]
v	Velocity component in y direction in body reference frame	[m/s]
V	Free stream velocity	[m/s]
V_{app}	Approach speed	[m/s]
V_S	Stall speed	[m/s]
$V_{touchdown}$	Touchdown speed	[m/s]

Symbol	Definition	Unit
w	Velocity component in z direction in body reference frame	[m/s]
Y	Normal force produces by the wind tunnel model	[N]
α	Angle of attack	[degree]
β	Sideslip angle	[degree]
γ	Flight path angle	[degree]
δ_{CS}	Control surface deflection	[degree]
δ^*	Boundary layer thickness	[m]
δ_f	Flap deflection Angle	[degree]
δ_{pitch}	Pitch control variable	—
δ_{roll}	Roll control variable	—
$\delta_{throttle}$	Throttle setting	—
δ_{yaw}	Yaw control variable	—
ϵ_β	Error in sideslip angle	[degree]
θ	Pitch attitude	[degree]
θ_{TS}	Tailstrike pitch attitude	[degree]
Λ	Sweep angle	[degree]
μ	Dynamic Viscosity	[kg/m.s]
μ	Sample mean	—
μ_b	Friction coefficient	—
σ	Sample Variance	—
ρ	Density	[kg/m ³]
ϕ	Roll angle	[degree]
ψ	Yaw angle	[degree]
ω_b	Angular rate	[rad/s]

1

Introduction

The commercial aviation industry has been dominated by the conventional Tube and Wing (TAW) configuration for the past 100 years and has made great improvements in efficiency and lowering fuel consumption [1]. In fact, it is estimated that due to the improvements in aerodynamics, structures, avionics and propulsion, the efficiency has seen an improvement of 100% [2], however, it seems that this improvement in efficiency is reaching an asymptote [3]. At the same time, air traffic is increasingly on the rise [4]. Therefore, throughout aviation history, there has been ongoing research on the concept of Flying Wings for commercial purposes. The main appeal of such configuration is instead of having separate segments for performing various tasks, such as fuselage, tail and undercarriage, these all are integrated within one system [5].

To tackle the ongoing climate crisis, the aviation industry must act towards more sustainable and fuel-efficient flying. To that end, the Flying-V, a novel aircraft design, was first conceptualized by J Benad during his internship at Airbus in Hamburg, Germany [6]. Further development of the Flying-V has been an ongoing project at the Faculty of Aerospace Engineering at Delft University of Technology since 2016 in collaboration with Airbus and KLM Royal Dutch Airlines. The Flying-V is a flying wing transport aircraft with a passenger capacity of 314 over a range of 15000 km. The wing houses the passenger cabin, the cargo compartment and the fuel tanks. Studies have shown this aircraft to have reduced energy consumption by 20% compared to a conventional twin-isle transport aircraft [7].

One of the area in which the Flying-V can be improved is landing performance. There is a need for enhancing pilot's vision by a reduction in pitch attitude and the obscured segment during landing. The goal of this thesis project is to study the possible increase in trimmed maximum lift coefficient by using split flaps which can result in a more desirable landing by improving the pilot's vision. Additionally, using flaps has other potential benefits such as reduction in approach speed, landing distance and shorter landing gears. A combination of experiment and simulation method is used for this study in which a series of wind tunnel tests were carried out at the Open Jet Facility (OJF) of the TU Delft. The data gathered from these tests were then used to advise on the best configuration of the split flap for the Flying-V. Lastly, the results were applied to the full-scale aircraft using a flight performance toolbox.

1.1. Research Objective

As mentioned, the goal of this study is to investigate the possible increase in trimmed maximum lift coefficient by using split flaps. Split flap is one of the simplest HLDs, it can be mounted using a hinge system under the inboard wing. Therefore, it is of high interest to find the best configuration of a split flap for the Flying-V. The research objective thus can be stated as :

To find an optimal split flap design for the Flying-V which increases the trimmed maximum lift coefficient resulting in a lower pitch attitude during landing as well as assessment of landing performance and pilot's vision using this optimal design.

1.2. Research Questions

The research objective is to be achieved by an experimental study of different configurations by means of wind tunnel tests conducted in the Open Jet Facility of the Faculty of Aerospace Engineering of the Delft University of Technology and analyzing the results using a flight performance toolbox. To prepare for these experiments. First, a literature study was conducted on relevant topics, namely, the Flying-V, Split flaps, Aerodynamics of highly swept cranked wings and low-speed wind tunnel testing. These studies resulted in producing the research question.

What are the aerodynamic and performance effects of split flaps on the Flying-V?

This question can then be divided into sub-questions to help break down the research. These include the following.

- What are the effects of changing the split flap's chord length, deflection angle, location of the hinge line, span, region of placement, as well as the number of flaps on the aerodynamic coefficients of the half-wing model?
- What is the effect of the different configurations of the split flaps on lift, drag, pitching moment and rolling moment coefficients?
- What is the reduction in landing pitch attitude, obscured segment and pilot's eye altitude that can be achieved by using split flaps?

1.3. Thesis Outline

This report represents the outcome of a thesis assignment on designing High-lift Split Flaps for the Flying-V. The report starts with background information on relevant topics such as the Flying-V, aerodynamics of highly swept wing, wind tunnel experiment and split flaps, as well as the flight performance analysis in chapter 2. Next, the methodology for conducting this research is discussed in chapter 3, followed by verification and validation in chapter 4. The results of the wind tunnel experiments as well as the flight performance analysis are presented in chapter 5. Finally, the report is concluded in chapter 6 along with recommendation for future work.

2

Background

This chapter serves as a summary of the literature study conducted as the initial phase of the thesis project. Section 2.1 presents the development and characteristics of the Flying-V, followed by section 2.2 discussing the aerodynamic characteristics of highly swept cranked wings. Next, information on split flaps are given in section 2.3. Wind tunnel test and corrections are discussed in section 2.4. Finally this chapter is concluded with a background on the flight performance analysis in section 2.5.

2.1. Flying-V

Due to many reasons of which the most significant ones are stability and control issues and the general public mistrust of novel commercial aircraft, the development of a flying wing for commercial purposes has been essentially on halt. While the growing demand for commercial aviation and the climate crisis calls for developing more sustainable options, one of which is the Flying-V.

The Flying-V concept emerged during an internship at Airbus by J. Benad in 2015 [7]. It is a pure flying wing with a signature V-shaped passenger cabin. The passenger cabin consists of two fuselage barrels which are positioned inside the wing and the engines are close to the center axis for a low yawing moment in case of an engine failure. It has been shown that the Flying-V promises a 20% increase in fuel burn efficiency in comparison to a conventional reference aircraft of the same mission with the same capacity and wingspan, namely the Airbus A350-900 [7].

Since 2016 the Flying-V has been developing at Delft University of Technology in collaboration with Airbus and KLM Royal Dutch Airlines. Several aspects of this novel aircraft have been studied during the following years including aerodynamics, structures and manufacturing, flight dynamics and control, environmental impact, aircraft integration, noise and airport operation. However, this section is mainly focused on the aerodynamics and performance aspects of the Flying-V. An isometric render of the Flying-V is shown in Figure 2.1.



Figure 2.1: CAD generated image of the Flying-V ¹

Aerodynamic Characteristics

During the preliminary design phase conducted as thesis research of Faggiano, a maximum lift-to-drag ratio of 23.7 at the cruise point was found. This was then compared to NASA Common Research Model with a maximum lift-to-drag ratio of 18.9, thus showing a 25% increased aerodynamic efficiency of the Flying-V. Faggiano's optimization resulted in a planform modification of the Flying-V, Figure 2.2 shows this change. Faggiano also showed that even though the Flying V is optimized at the lift coefficient of 0.26, the highest lift-to-drag ratio of the dual step optimized Flying V is attained at a lift coefficient 10% higher than the design one, at an altitude of 13,600 m [8]. This means that the Flying-V is more efficient at higher altitudes and lift coefficients.

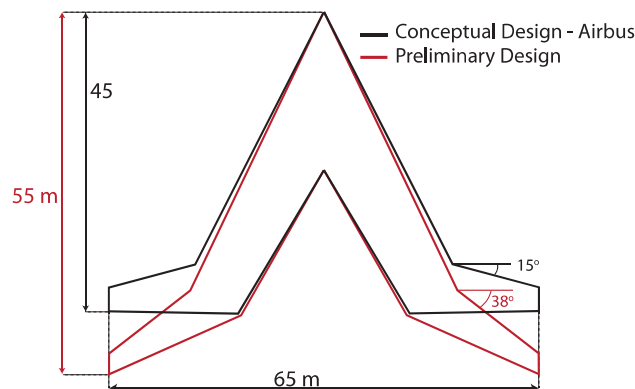


Figure 2.2: Modification of the Flying-V planform by Faggiano [8]

Based on this optimized design by Faggiano, Palermo and Vos designed a 3-meter span, 4.6% scaled-down of a half-wing of the Flying-V shown in Figure 2.3 to be tested in the open jet facility of the TU Delft [9]. In addition to the wind tunnel model a 4.6% scaled down, Sub Scale Flight Test (SSFT) model was also developed using geometric Froude scaling laws [10]. The wind tunnel model was mounted on a turntable and a 6-component force transducer enabling measurements of aerodynamic force and moments at various speeds and angles of attack. The current thesis assignment was also conducted using this half-wing model.

¹Taken from: <https://www.tudelft.nl/1r/flying-v>



Figure 2.3: The original wind tunnel model constructed by Vos and Palermo [9]

The results of the wind tunnel tests showed similar characteristics to low-aspect ratio wings such as pitch-up tendencies and vortex lift but no deep-stall characteristics were observed between angles of attack of -10 to 35 degrees. The maximum lift coefficient of 1.02 at an angle of attack of 35° with nonlinear effects starting at $\alpha = 10^\circ$ was observed. However, for the SSFT model the maximum achievable $C_{L,max}$ in horizontal steady flight was found to be 0.7 . Furthermore, a pitch break occurred after surpassing $\alpha = 19^\circ$, which made the aircraft unstable about the moment reference point. The elevon effectiveness was found to be virtually independent of the angle of attack variations. Moreover, the center of gravity was suggested to be located between 1.33 and 1.39 m behind the nose. The control surfaces could trim the aircraft in maximum lift coefficients between 0.6 and 0.7 [9].

Approach and Landing

The high angles of attack for producing the maximum lift affect the design of the landing gear for the Flying-V. The main landing gear is 5.30 m, which requires long struts to facilitate the required angle of attack for take-off. Bourget proposed in his thesis research an increase in the dihedral angle of the wings up to 16.3° to reduce the weight of the landing gear. However, this increased the rolling moment derivative due to side slip to 3.5 times larger than that of a conventional commercial aircraft, which raises the possibility of Dutch roll occurring [11]. Research by Santosh [12] considering the ground effect, showed that a reduction of 1° in the angle of attack is needed to obtain a sufficient lift coefficient, which relieved some of the rotation angle requirements on the landing gear height. Additionally, Erdinçler incorporated ground spoilers to increase lift dumping during landing, which resulted in a shorter landing distance [13].

In his research de Zoeten [14], showed that the Flying-V had a similar landing distance to A35K, while the braking distance is lower due to having a negative ground attitude of -3° . De Zoeten also incorporated the previous research done by Erdinçler, Bourget and Santosh in his simulations.

Another important aspect of landing performance is the pilot vision which is directly connected to the objective of this thesis project. It was found that the pitch attitude of the Flying-v at landing was significantly larger than A35k, which was partly due to the flare maneuver performed during landing. This also resulted in a higher obscured segment. One reason for the need to increase the pitch attitude of the Flying-V was to reduce the descent rate for a less firm landing.

Without considering the ground effect, for the SSFT model landing was predicted to occur at 15.9° angle of attack and a speed of 19.2 m/s [15]. While for the full-scale aircraft, these values were predicted to be between 14° to 17° and 72 m/s respectively [11, 14].

Flow Phenomena

Based on the studies done by Palermo [9] and Viet [15] on the half-wing model, insightful information has been gathered on the complex behavior of the flow on the wing. Due to the highly swept leading edge with a blunt nose of the Flying-V, vortices are created on the wing. These vortices tend to move around on the wing surface with changing in the angle of attack which influence the lift distribution and pitching moment. Due to this vortex lift, the lift curve slope of the aircraft is positive up to 40° angle of attack, however, because of the occurrence of pitch break around 20° , not all of this range is useful. Viet also identified the major regions of emerging vortices shown in Figure 2.4. It can be seen that a major part of the inboard wing is under the influence of vortex flow. Additionally, two vortices were formed at the mid-span of the wing and two others were observed right before and after the leading edge kink [15].

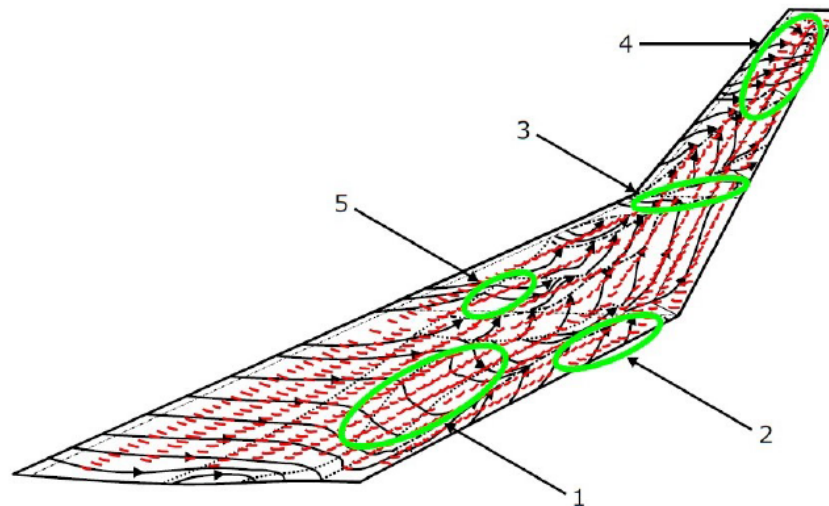


Figure 2.4: Tuft and oil flow visualization on the half-wing wind tunnel model at 15° angle of attack [15]

Research Gap

So far, the developments in the Flying-V aerodynamic design and performance have been summarized which brings us to the main objective of the current study. While the Flying-V has proved to show a 20% reduction in fuel consumption in comparison to the reference A350-900 aircraft, there are still improvements needed in flight phases such as landing. This includes a reduction in landing pitch attitude and obscured segment by increasing the maximum lift coefficient. Here the possible benefit of split flaps can be helpful. Therefore, the current thesis assignment is focused on the design and study of several split flap configurations to increase the trimmed maximum lift coefficient.

To find an optimum design for the split flaps, it is necessary to first gather enough knowledge about low-speed aerodynamics, especially concerning highly swept wings.

2.2. Aerodynamics of Highly Swept Cranked Wing

The concept of the swept wing was developed in Germany in the 1930s. The main reason behind applying sweep is to increase the drag rise Mach number, however, this also affects other aerodynamic parameters such as lift curve slope and maximum lift coefficient. The maximum lift coefficient in particular decreases, meaning that for a high-speed highly swept aircraft, more attention must be given to the low-speed regime. This translates to a need for high-lift devices. A relevant aspect to take into account for this study is span-wise lift distribution on swept wings.

Figure 2.5 shows a diagram comparing the lift distribution on an aft swept wing, a forward swept wing and an elliptical lift distribution. Note that no taper and twist is applied, as these can influence the lift distribution of the swept wing.

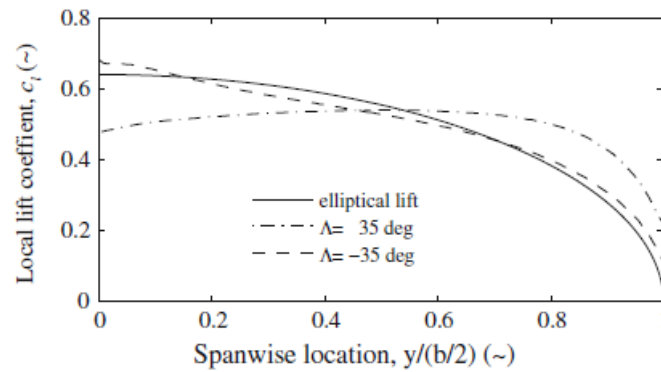


Figure 2.5: Span wise lift distribution for an aft and a forward swept wing in comparison to an elliptical lift distribution [16]

As seen, for the aft swept wing, the maximum lift coefficient is achieved further towards the tip in comparison to the other two cases. This is due to the upwash created by the inboard wing on the outboard section which increases the effective angle of attack and therefore the lift coefficient, the opposite applies to the forward swept wing.

Other relevant phenomena to take into account for swept wings are root and tip effects. These refer to the change in the isobar pattern due to the sweep. The root effect occurs due to the symmetry requirement on the junction of the two wing halves, which entails there must be no net pressure gradient perpendicular to the free stream at the wing root. For this to occur, the isobars at the root must be perpendicular to the free stream, resulting in the isobars curving backwards at the wing root. On the tip of the wing, there exists no such requirement, so the isobars curve forward, which is called the tip effect. This essentially changes the pressure distributions at the root and the tip. Figure 2.6 shows the root and tips effects on two wings with 53° sweep.

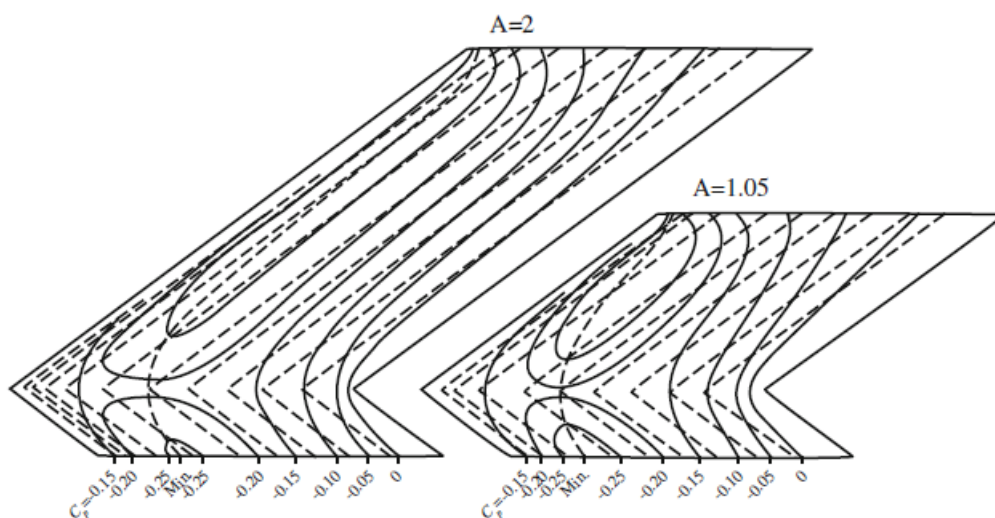


Figure 2.6: Isobars on two wings with 53° sweep [16]

The wing of the Flying-V is a cranked swept wing, which means that the leading edge has two different sweep angles. This results in some differences in the behavior in comparison to a simple swept wing.

The flow behavior on the half-wing model was studied thoroughly by Viet, using various flow visualization methods [15].

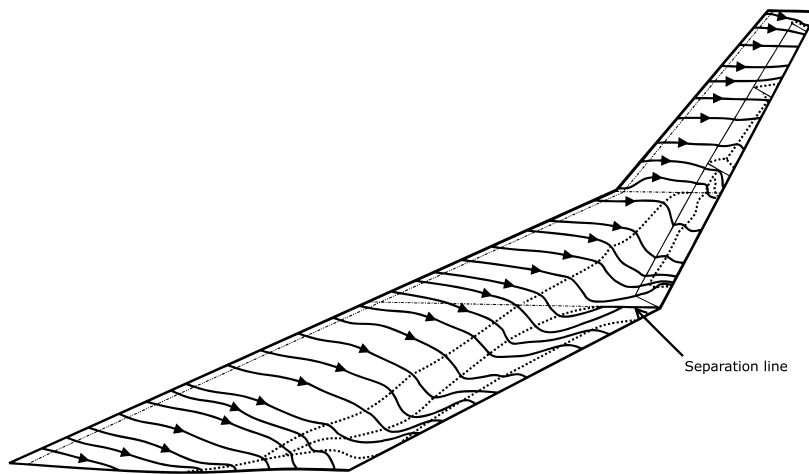


Figure 2.7: Flow pattern on the FV half-wing model at 9 degrees angle of attack [15]

As seen in Figure 2.7, the flow pattern on the FV wing has a more complex behavior than a simple swept wing. The streamlines seem to follow the direction of the flow until half way through the chord and then change direction towards the kink before becoming parallel just before the trailing edge. Additionally, there is a separation region at the kink near the trailing edge where patterns on cross-flow are visible. The flow seems to be more undisturbed at the outer wing where it follows the flow direction. At higher angles of attack there is even more complex flow patterns observed on the half-wing model. At the angle of attack of 11° vortex lift starts to generate. Figure 2.8 shows the flow pattern at 15° angle of attack. As can be seen there are regions of vortex formation for instance near the leading edge just before the outer wing, this creates a suction region on the upper surface which prevents separation occurring on the control surfaces even at higher angles of attack, adding to the lift generation. There is also much more cross flow observed, which is less significant on the region near the root.

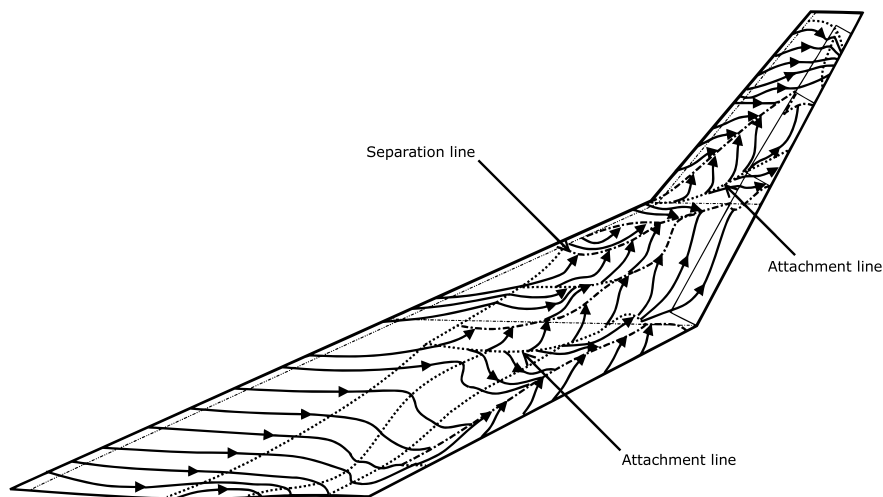


Figure 2.8: Flow pattern on the FV half-wing model at 15 degrees angle of attack [15]

A famous example of an aircraft with a cranked wing is the F-16XL. The wing of this aircraft has an aspect ratio of 1.75 and a taper ratio of 0.18. The leading edge is cranked with an inboard sweep angle of 70° and an outboard sweep of 50° . It also incorporates a varying leading edge radius, called the s-blend, this feature alongside the cranked shape produces a complex vortex lift-off which can be unsteady in high angles of attack, such as take-off and landing [17]. Figure 2.9 shows a picture taken of this aircraft in flight.



Figure 2.9: F-16XL in flight [17]

To understand the complexity of the flow on this aircraft a project was created by Lamar called the Cranked Arrow Wing Aerodynamics Project (CAWAP) which was focused on collecting a unique flight data set on the F-16-XL. Using these data it was found the Computational Fluid Dynamics (CFD) methods were not sufficient in achieving similarity with the flight data, resulting in the creation of the Cranked Arrow Wing Aerodynamics Project International (CAWAPI), where the goal was to develop CFD methods that were in agreement with the experimental data. However, the CFD methods still

fell short in predictions of two areas, namely, the low-speed high angle of attack such as take-off and landing and the transonic low angle of attack regime such as transonic cruise condition. This gave the motivation to launch a second project, CAWAPI-2 [18].

On the outer panel flowfield of the F-16XL wing, multiple complex flow phenomena occur. There are three primary vortices in this section, one from the swept inboard leading edge, one from the outboard leading edge and a counter-rotating primary vortex from the air dam. Each of these vortices also induces a secondary vortex, adding further to the complexity. A visual created using CFD from CAWAPI-2 is shown in Figure 2.10 with $Ma = 0.24$, $Re = 32 \cdot 10^6$ and $\alpha = 20^\circ$.

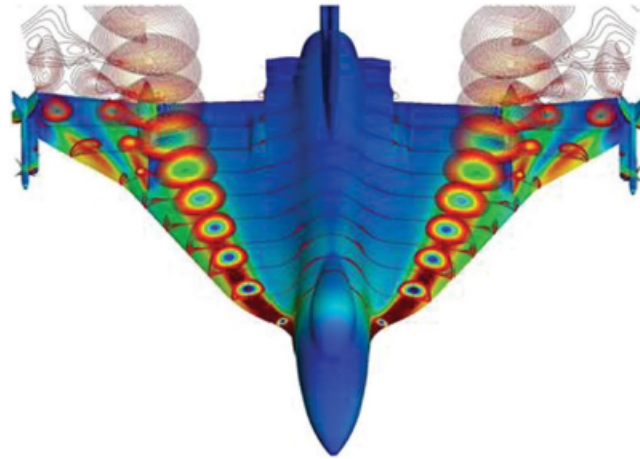


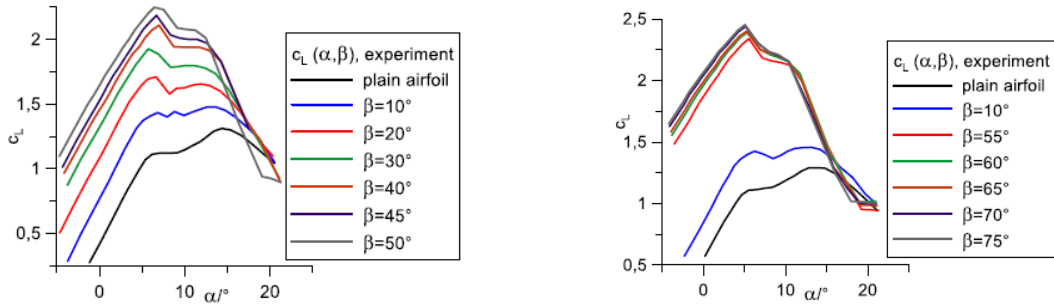
Figure 2.10: Subsonic high angle of attack case FC-25 of CAWAPI-2 [18]

Moreover, the combination of the high sweep angle and the angle of attack of the outboard wing most likely results in vortex breakdown in the near field of the wing and among interacting vortices. Vortex breakdown occurs when the flow experiences an abrupt and drastic change of structure and is an unsteady phenomenon. Another unexpected flow behavior was the development of a wake-like flow instead of a jet-like flow in the vortex core which is expected for such a highly swept wing. This was attributed to the S-blend leading edge to connect the fuselage with the wing by Hitzel [19].

2.3. Split Flaps

Split flaps are one of the simplest high lift devices, they are formed by splitting the trailing edge of the wing and using a hinge around which the lower portion of the split can rotate. The hinge line can therefore be ahead of the trailing edge. Several studies have been conducted which showed many advantages of Split flaps in comparison to the other forms, a few are discussed further.

Unlike the hinged flaps where the entire trailing edge section deflects downward, the split flaps have the advantage of not disturbing the suction side of the wing which means the boundary layer is not prone to separation at high deflection angles to achieve maximum lift. Additionally, the absence of a gap between the airfoil and the flap creates less disturbance of the boundary layer which also delays its separation [20]. The study by Frey et al. was done on a laminar wing with split flaps for a fuel cell-powered wing, which showed promising results as shown in Figure 2.11a and Figure 2.11b. The experiments were conducted at a Reynolds number of $1.1 \cdot 10^6$ for flaps deflection angles up to 75° and angle of attack sweep between -5° and 25° .



(a) Lift curves produced in the 2021 measuring campaign with flap angles up to 50 degrees

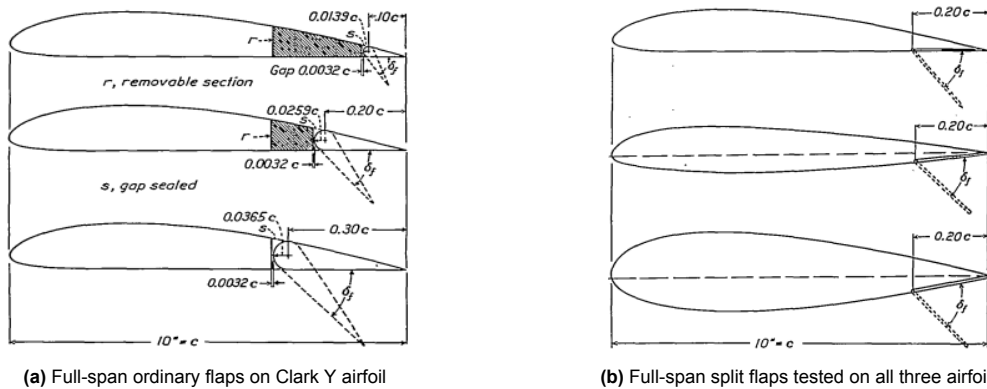
(b) Lift curves produced in the 2022 measuring campaign with flap angles of 0, 10, and 55 to 75 degrees

Figure 2.11: Lift curves produced in the study by Frey et al. on the effectiveness of split flaps on lift increase of the wing [20]

As evident by the graphs, the maximum lift coefficient had a significant increase by using split flaps with the highest increase observed for the deflection angle of 75° . Note that in these graphs β is used to show the deflection angle.

A study was conducted by Wenzinger [21] to compare the aerodynamic effects of ordinary hinged flaps and split flaps on three different airfoils, NACA 23012, Clark Y and NACA 23021. This was done by testing three different chord lengths, namely, 10%, 20% and 30% of the airfoil chord while changing the deflection angle from 0 to the angle at which the maximum lift is obtained, and the angle of attack was changed from below zero lift angle to beyond the stall angle. Furthermore, the experiments were done in a Reynolds number of 609,000 and wind speed of 80 miles per hour.

The results showed a higher increase in maximum lift coefficient provided by full-span split flaps than a full-span ordinary flap of the same width, while the lift-over-drag ratio and the drag coefficient at maximum lift stayed the same. For both the hinged and split flaps the optimum width was found to be 20% of the chord. Additionally, another advantage of the split flaps was the absence of a gap between the flap leading edge and the airfoil trailing edge as it was present in an ordinary flap. This showed promising results for split flaps. However, it should be noted that this study was done on airfoils and not full-span wings. Schematics of both flaps on airfoils for a chord length of $0.1c$ are shown in Figure 2.12



(a) Full-span ordinary flaps on Clark Y airfoil

(b) Full-span split flaps tested on all three airfoils

Figure 2.12: Flap configurations for the experiment done by Wenzinger on comparison between ordinary and split flaps aerodynamics performance [21]

As an example, the lift and drag polar for the Clark Y airfoil with split and ordinary flaps of $0.2C$ length is shown in Figure 2.13.

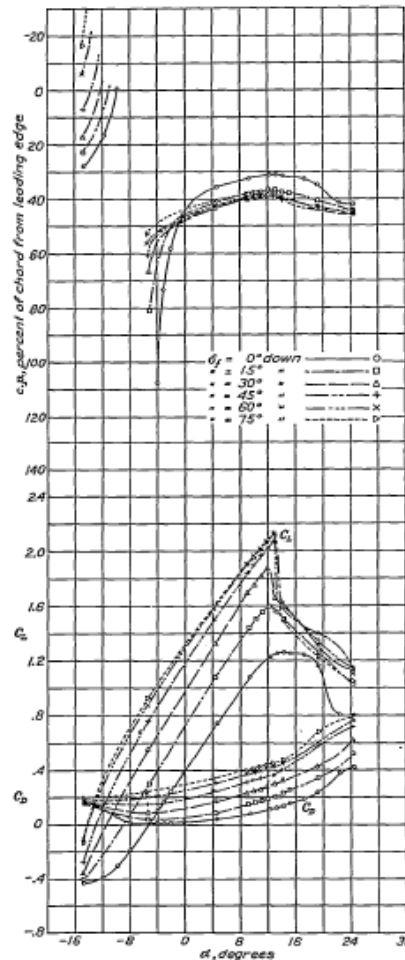


Figure 2.13: Lift, drag and center of pressure for the Clark Y airfoil with 0.2C full-span split flap [21]

Another study was done by Wenzinger [22] on the effects of full-span and partial-span split flaps on the aerodynamic characteristics of a tapered wing. The wing had a Clark Y airfoil profile equipped with various split flaps and the flaps included two sizes of constant chord and two sizes of tapered chord. The experiment was carried out with a Reynolds number of 609,000 based on the average wing chord, and a wind speed of 80 miles per hour. The flap deflection angle ranged from 0° to the angle at which the maximum $C_{L,max}$ was obtained. the angle of attack ranged from zero lift to beyond the stall angle. It was found that the tapered split flaps increased $C_{L,max}$ more for a tapered wing than the constant chord split flaps did. Additionally, for the full-span flaps the lift and drag characteristics stayed the same for both tapered and rectangular wings, but the stall angle of attack for the tapered wing lowered significantly.

For testing the partial-span flaps, two options were pursued, one was to remove the section of the flaps near the tip and the other was to remove the center section of the full-span flaps. The results showed that the lift-to-drag ratio at the maximum lift was lower when the flaps were located at the center of the wing model than when they were located at the tip. Based on this, the mounting location of the flaps were considered a design variable which were taken into account for the design of the experiment.

One notable result was that the tapered-chord flaps gave the wing a somewhat higher maximum lift in comparison to constant-chord flaps.

One more specific case of split or belly flap that has been on a tail-less transport aircraft, showed applying a belly flap in the midsection of the aircraft helped with increasing the trimmed lift coefficient up to an angle of attack of 20° , however, the maximum lift coefficient was reduced from 0.98 to 0.93. This was done in combination with wing trailing edge flaps to reduce the take-off distance [23] which was given the name Tailless Combination Flap system or TCF. A schematic of the configuration is shown in Figure 2.14.

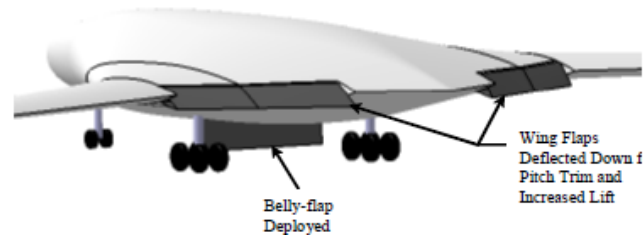


Figure 2.14: Tail-less transport aircraft with Tail-less Combination Flap system (TCF) [23]

Although this combination showed promising results in increasing the trimmed lift coefficient in the study of Hefazi et al. testing such a combination is not possible on the current half-wing model of the Flying-V due to not having the full-wing wind tunnel model. Nonetheless, it could be used as a recommendation for future studies.

Another study done by H Abbot [24], comparing the aerodynamic effects of plain and split flaps on NACA 23012 airfoil was carried out in a variable density wind tunnel of NACA. The Reynolds number for determining the maximum lift coefficient was 3,800,000, the deflection range for the plain flap was from 60° upwards to 75° downwards, and for the split flap from 0° to 90° downwards. The angle of attack ranged from below zero to above the angle at which the maximum lift coefficient was reached and for the plain flaps it extended through negative maximum lift except for flap deflections between 20° upward and the neutral position.

The study came to a similar conclusion as Wenzinger [21] regarding the higher increase in $C_{L,max}$ by using a split flap than by using a plain flap. Additionally, this study showed that the profile drag coefficient at the useful $C_{L,max}$ for take-off produced by split flaps was lower than the plain flaps, however, both performed unsatisfactorily in comparison to low-drag slotted flaps. Furthermore, in this study only flaps with a chord of 20% of the airfoil chord were tested, with deflection angle and angle of attack variations similar to Wenzinger's studies.

Overall, it can be concluded that multiple studies have confirmed that the use of split flaps is preferred to plain flaps, especially when applied to highly swept wings. Moreover, most seem to test for the three chord lengths of 10%, 20% and 30% of the plain wing chord length. The common ranges for deflection angle are from 0 to the angle at which $C_{L,max}$ occurs and for the angle of attack is below zero lift angle to above stall angle. These findings have been used in defining the design variables for conducting the experiments on the split flaps for the half-wing model of the Flying-V.

2.4. Wind Tunnel Test

Experimental simulations are common methods in Aerospace Engineering, they especially come in handy when simulating the flow with CFD is not possible, for instance, due to the high complexity of the flow. This study is partly conducted on an experimental basis, therefore a thorough understanding of wind tunnel testing is required for designing the experiment. This section starts with defining similarity parameters in subsection 2.4.1. Next, subsection 2.4.2 discusses the challenges and method of experiment design, followed by subsection 2.4.3 discussing uncertainties. Afterwards, subsection 2.4.4 presents the error mitigation methods. Lastly, wind tunnel corrections are discussed in subsection 2.4.5.

2.4.1. Similarity Parameter

Since most of the wind tunnel tests are conducted on a scaled model, similarity parameters are important for relating the results of the scaled model tests to the full-scale case. The main forces that come into play when a body moves through a fluid medium are due to inertia, gravity, viscosity and elasticity of the fluid. Dividing the inertial force by each of the other three results into three main similarity parameters, Reynolds number shown in Equation 2.1, Mach number shown in Equation 2.2 and Froude number shown in Equation 2.3. Froude number is not important for rigid bodies fully immersed in the fluid such as the wind tunnels, so it will not be considered in this study. If the scaled model has the same Reynolds and Mach numbers as the full-scale aircraft, then they are dynamically similar, meaning the forces and moments will be similar for both. Therefore, the forces on the full-scale aircraft

can be obtained by multiplying the forces on the model by $\frac{1}{2}\rho V^2 L^2$. Similarly, for the full-scale aircraft the moments can be obtained by multiplying the model moments by $\frac{1}{2}\rho V^2 L^3$. However, this rarely can become a reality [25].

$$Re = \frac{\rho V L}{\mu} \quad (2.1)$$

$$Ma = \frac{V}{a} \quad (2.2)$$

$$Fr = \frac{V}{\sqrt{gL}} \quad (2.3)$$

In these equations L is the characteristics length, V the flow speed, a the speed of sound, ρ the density, μ the dynamic viscosity and g the gravitational acceleration.

The biggest challenge in wind tunnel testing is achieving similarity between the flow in the wind tunnel and the full-scale flight. Mainly, achieving similarity in Mach number and Reynolds number at the same time is virtually impossible without having a cryogenic wind tunnel, since both of these parameters change with changing velocity.

In the low-speed regime the effects of the Reynolds number are more dominant, and as such, matching the Reynolds number is more important, however, for any experiment a careful evaluation of both Reynolds and Mach numbers must be carried out to ensure that the results can be applied to the full-scale model.

The open jet facility where the experiments were conducted can provide a maximum 35 m/s speed of the flow [26], therefore the compressibility effects can be assumed negligible and as such, matching of the Mach number is of less significance than the Reynolds number, however, due to the limitation of the facility a complete matching of Reynolds number is also not possible. This is not a problem for purposes of this study, since a higher Reynolds number increases flap effectiveness, therefore, the results of increase in lift coefficient obtained from the wind tunnel test are underestimated in comparison to the full-scale aircraft [27].

Reynolds Number and Boundary Layer Transition

Scaling effects refer to the discrepancies that occur due to using a model instead of a full-scale aircraft. Of these discrepancies, the Reynolds number plays a crucial role. To study this we must look into boundary layers.

The efforts to achieve Reynolds number similarity as much as possible between the experiment and full-scale flight is due to the significant effects the Reynolds number imposes on different characteristics. In this case, the impact on the lift coefficient is the most important as well as the effects on Flap characteristics. Figure 2.15 shows the effect of the Reynolds number on the maximum lift coefficient for NACA 23021, NACA 23012 and NACA 0012 all with split flaps deflected.

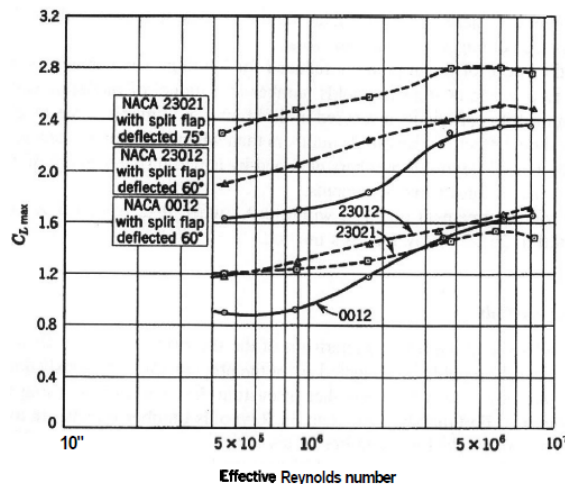


Figure 2.15: Effect of Reynolds number on $C_{L,max}$ with flaps deflected on three NACA airfoils [28]

As evident by Figure 2.15 increase in Reynolds number has a great effect on increasing the maximum lift coefficient. Another example is the effect of the Reynolds number on the lift coefficient of the F-111 aircraft, shown in Figure 2.16.

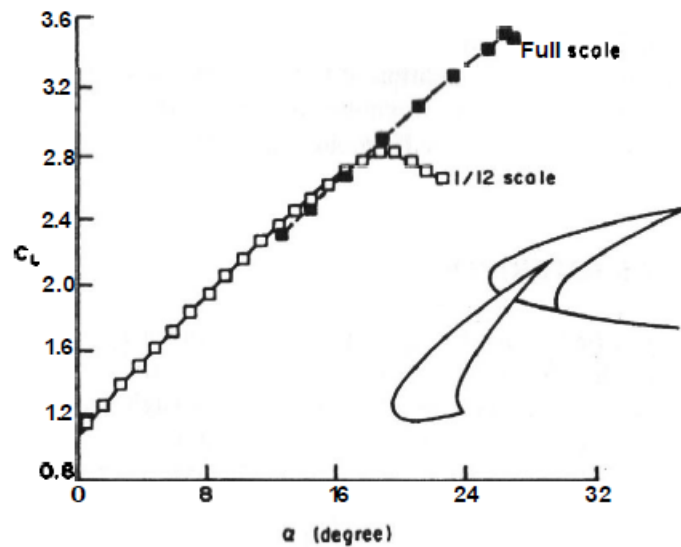


Figure 2.16: Effect of scale on the lift characteristics of F-111 aircraft [28]

It can be seen that increase in Reynolds number has increased the flap effectiveness and therefore, the performance of the flaps is underestimated in the wind tunnel test in comparison to full-scale aircraft. This assures that even though the Reynolds number cannot be matched, the flap effectiveness stays significant.

Boundary layers are formed due to the viscosity of the fluid. There is a layer in the direct vicinity of the body with a high velocity gradient, where velocity transitions from the velocity of the body to that of the free stream. There are two types of boundary layers, laminar and turbulent. A laminar boundary layer has a lower energy level which makes it more prone to separation. In the presence of an adverse pressure gradient, the laminar boundary layer transitions to a turbulent boundary layer. Turbulent boundary layers have a greater energy level and also a greater association with skin friction drag. The boundary layer properties and specifically the velocity gradients, greatly affect the overall drag of the body. The contributions to the total drag coefficient from skin friction drag for laminar and turbulent boundary layers are given by Equation 2.4.

$$C_{D, \text{laminar}} = \frac{2.656}{\sqrt{Re}} \quad (2.4)$$

$$C_{D, \text{turbulent}} = \frac{0.148}{Re^{0.2}}$$

Figure 2.17 shows the above relations for flat plates as well as NACA 23012 airfoil obtained from Jacobs et al. [28].

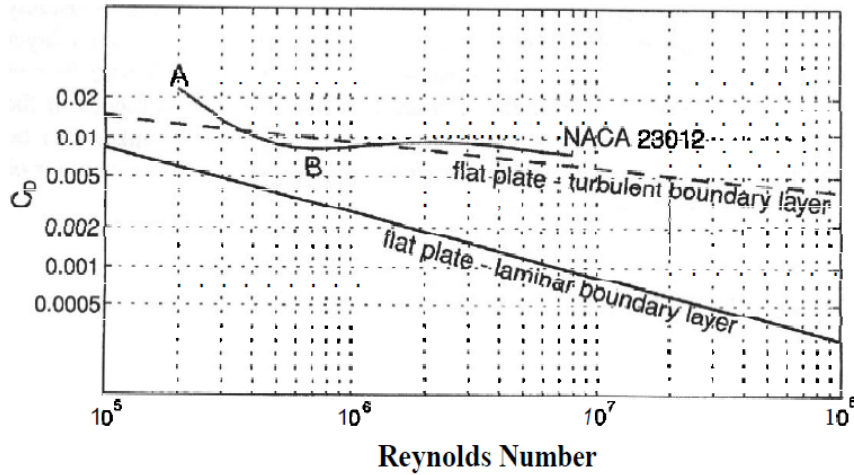


Figure 2.17: Variation of C_D with Reynolds number on NACA 23012 airfoil[28]

The boundary layer thickness is another important property. It is defined as the distance of the surface of the body to the point where the velocity in the boundary layer is 0.99 times the velocity just outside the boundary layer. The thickness of the laminar and turbulent boundary layers can be approximated using Equation 2.5 and Equation 2.6.

$$\delta_{\text{laminar}}^* = 5.2\sqrt{r^2/Re} \quad (2.5)$$

$$\delta_{\text{turbulent}}^* = 0.37r/(Re)^{1/5} \quad (2.6)$$

Where r is the distance from the leading edge. As it is evident from Equation 2.5 and Equation 2.6, both drag and boundary layer thickness are functions of the Reynolds number. Furthermore, Reynolds number also greatly affects the location of transition from laminar to turbulent boundary layer as well as the boundary layer separation.

Reynolds number in the wind tunnel test performed in OJF is roughly two orders of magnitudes lower than in the full-scale flight, while forced transition of the boundary layer does not match the Reynolds numbers, it can provide insight into the flap behavior at higher Reynolds numbers.

However, during this campaign it was decided to not pursue a forced transition since it was found in a previous research that adding trip strips for forced transition to the inboard wing, has negative effects such as reducing the usable $C_{L,max}$ of the wing [29].

In conclusion, it is crucial to consider the scale effects when performing an experimental study. These were considered during the post-processing of the data after the wind tunnel campaign was performed.

Semi-span Wind Tunnel Model

Another approach for increasing the effective Reynolds number is the use of a semi-span model [30, 31]. Using a semi-span model instead of a full-span one also improves the data quality due to better model strength, stiffness and overall fidelity. It additionally reduces production costs of the model itself and also the fact that the complicated high lift devices and propulsion system for testing need to be produced only for one wing [32].

Nevertheless, there are drawbacks to this method, one is the loss of model symmetry, therefore, requiring an important assumption; that the flow is symmetric with respect to the aircraft symmetry plane. This assumption is therefore not valid for a highly turbulent flow, however, the effect of these disturbances could be neutralized by taking time average measurements of the forces and moments which was done on the balance measurements during the experiment. Another drawback is the wall boundary layer separation, this can be tackled by installing the model on a splitter plate to reduce the effects of the wall boundary layer on the model [32], as was a part of the wind tunnel set-up.

An additional relevant factor in the assumption of symmetry is the mounting location of the model [32]. This can be changed by varying the stand-off height distance between the model symmetry plane and the tunnel wall. In a study done by Gatlin and McChee [32], where different standoff heights were

tested for a semi-span wind tunnel model, it was concluded that the matching of stall angle of attack was the most accurate for the case without a standoff. Additionally, in a study carried out by Milholen et al, [30], it was found that the standoff height had a significant effect on the aerodynamic coefficients of the model with the best agreement of the data found at a standoff height of $2\delta^*$ where δ^* is the tunnel empty sidewall boundary layer displacement thickness [30].

The main reason for this difference between the semi-span with a peniche (or standoff) and full-span data was found to be the development of a vortex on the wall in front of the standoff. This vortex had a significant effect on the flow around the model. Additionally, the presence of peniche increases the pressure difference between the top and bottom sides of the fuselage [33]. Note that all the aforementioned studies were conducted on a TAW configuration.

2.4.2. Design of the Experiment

In this subsection, a brief introduction of the chosen design variables for conducting the experiments on the split flaps is presented. Furthermore, methods for the effective design of experiments are discussed.

Design Variables

When determining the design variables covering a broad range of the design space has been considered, to gather as much valuable data possible in the limited time of the experiment. The design variables are chosen as the following. Note that a more elaborate description of the design variables is given in subsection 3.1.1.

1. Chord-wise location of the hinge line
2. Chord length (C)
3. Span (L)
4. Region (R)
5. Deflection angle (δ_f)
6. Number of flaps
7. Angle of attack (α)
8. Free stream velocity (V)

Each of these criteria could have multiple variations, which could ultimately lead to a significant number of data points being measured, leading to an inefficient test campaign. Therefore firstly, a method for the experiment design had to be chosen. There are different possible approaches in experiment design, two of which are the simplest approach, the One Factor At a Time (OFAT) and Designed Experiments (DOE).

OFAT

In this approach each parameter is changed on its own. Meaning that each data measurement is accounting for a change in one factor at a time while the rest of the variables are fixed. This approach can be useful if there are not many data points to be measured, however, for testing the split flaps it is not recommended to use OFAT. This meant that a Designed Experiment (DOE) approach had to be taken.

DOE

This approach requires fewer resources, while it estimates the effects of each factor more precisely. Additionally, it allows for systematic estimation of the interactions between different variables. One of the methods for Designed Experiment is Factorial Design. They are especially used for experiments with a large number of variables. Using this method enables examining both the Main effects, which are defined as the response change due to a change in the level of an individual variable and the Interaction effects which are the change in a main effect due to a change in some other variable. Using this method a test matrix was developed for the experiment. While creating this test matrix it could be noticed that some data combinations were duplicated, this is due to aliases. Overall, n-way interactions are aliased with m-way interactions where $n + m = N_{variables}$.

2.4.3. Uncertainties

In addition to the general method for the design of the experiments we need to take into account the statistical uncertainties and how to mitigate them. There are two main categories of uncertainties, random and systematic [34]. In this subsection, these are further discussed.

Random uncertainties

The random uncertainty, also known as precision shows the spread of the mean of the data set. This uncertainty occurs when measurements taken for identical conditions, differ from one another. For random uncertainties to be detected a sufficient number of data points may be gathered. These data result in creating a pattern called the probability distribution. The most commonly used probability patterns are Gaussian or normal and the associated distributions that are created from sampling Gaussian populations. To mitigate the random uncertainties, a high confidence level must be shown in the gathered data. A Gaussian distribution is shown in Equation 2.7

$$f_n(y) = \frac{1}{\sigma\sqrt{2\pi}} \exp\left(\frac{-(y-\mu)^2}{2\sigma^2}\right) \quad -\infty < y < \infty \quad (2.7)$$

Where the mean can be computed using Equation 2.8

$$\mu = \frac{1}{N} \sum_{i=1}^N y_i \quad (2.8)$$

And the variance is computed using Equation 2.9

$$\sigma^2 = \frac{1}{N-1} \sum_{i=1}^N (y_i - \mu)^2 \quad (2.9)$$

The variance can then be used to determine the confidence interval of the data. The confidence level in the data increases by increasing the offset from the mean value. This is shown in Table 2.1.

Table 2.1: Confidence intervals for a Gaussian distribution

Offset from the mean	Confidence level
1σ	68.2%
2σ	95.4%
3σ	99.7%
4σ	99.9%

The random errors in a wind tunnel can be caused by small perturbations or turbulence in the flow.

Systematic Uncertainties

Systematic uncertainties are also known as biases. They stem from causes such as instrument drift, thermal gradients, creep or incorrect model settings. Therefore, the impact of such errors is present in all measurements and more difficult to detect. This results in a perceived mean which is shifted from the true mean and must be mitigated. One way to achieve this is by taking zero measurements at the beginning and end of each run during the wind tunnel test. It was assumed that the biases would behave linearly and therefore, the biases taken at the beginning and the end were used to linearly interpolate the biases for in between. Each of these interpolated values were then deducted from the corresponding raw data to assure systematic errors are mitigated as much as possible.

To give a better understanding of the uncertainties discussed, Figure 2.18 is taken from Barlow et al. [25].

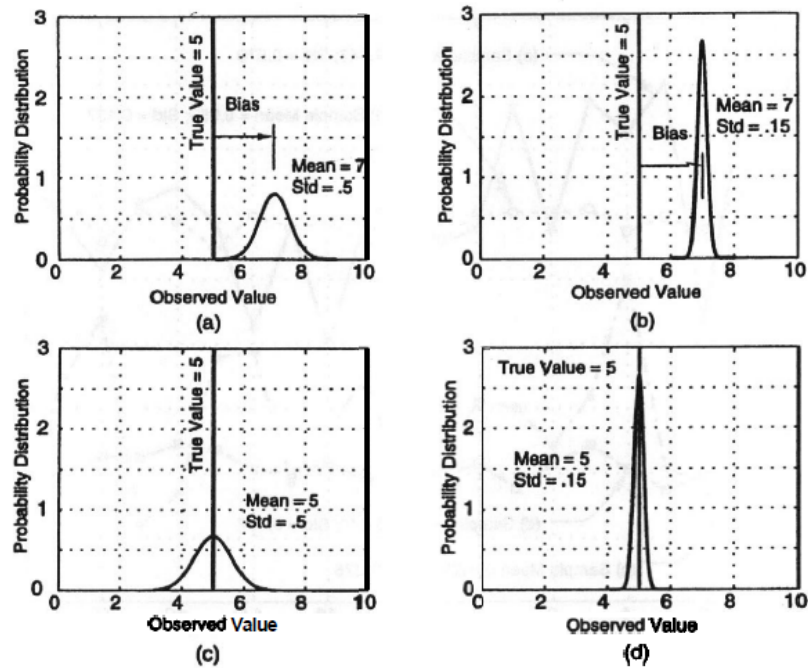


Figure 2.18: Schematics of systematic and random uncertainties [25]

Graphs a and b both show systematic uncertainties since their means are shifted from the true mean of the distributions. On the other hand, the precision of graphs b and d are more than a and c since the deviation from the mean value is less for b and d. This means that fewer measurements are required to achieve a certain precision level for b and d than it is for a and c.

2.4.4. Error Mitigation Methods

Now that different types of uncertainties are introduced, practical methods for improving the data quality are explored. These are for the most part taken from Montgomery [35].

Randomization

Randomization is a significant pillar of statistical methods in experiments. It applies to both the usage of material or set-up as well as the order of testing of the data. By using randomization it is aimed to average out the effect of perturbations present in the measurements. These perturbations can include instrument drift, structural creep, temperature changes and alike, which can create systematic errors. It is also possible to use computer programs to impose this randomization on the data.

For the experiments that are conducted in the current study, due to the time constraint, randomization for the most part was not applied. However, after each configuration change, zero-speed measurements were taken to assure systematic errors are mitigated as much as possible. Additionally, the environmental condition of the wind tunnel facility were checked frequently to ensure consistency.

Replication

Replication refers to an independent repeat run of each factor combination. It allows for an estimation of the experimental error which can help in determining if the observed differences in the data are truly statistically different. Another advantage of replication is obtaining a better estimation of the true mean. As shown in Equation 2.10.

$$\sigma_y^2 = \frac{\sigma^2}{n} \quad (2.10)$$

So by increasing n , we can get a better estimation of the variance, meaning that without replication we cannot know the reason for differences between two data points. Note that replication and repeated measurements are different. For example, if between two configurations the pressure stays the same, there should be a reset to an intermediate pressure in between the two measurements before going back to the original pressure. In the current study, between each configuration change the tunnel must

be shut down even if the same velocity is taken for two consecutive measurements, this way replication is ensured. Moreover, a number of data points were chosen to be repeated during the test campaign to ensure reproducibility. This is discussed further in section 4.1.

Blocking

Blocking is the method for increasing the precision of the measured data. It is achieved by reducing the differences in the set-up for each measurement. For example, instead of removing or changing the whole set-up each time, sub-parts are added or removed. This was used in the current study, where the half-wing model was installed at the beginning of the campaign and remained there for the entirety of the experiment. Flaps and brackets then were added to or removed from the model. In order to assure the flaps and brackets were placed at the exact same location for each run, a template was designed using 3D Experience and cut using the facilities at the aircraft hall of the aerospace faculty. The template was then used to mark the exact locations of mounting the flaps and brackets on the wing model. Note that, even though significant care was taken to mitigate errors, the mounting of flaps and brackets were still done manually and prone to some errors.

2.4.5. Wind Tunnel Corrections

Despite the availability of many correction methods, most of these methods were designed for conventional aircraft models. As such, the assumptions for these corrections to be valid are not applicable to the Flying-V model. Therefore, previous experimental studies conducted on the half-wing model have not included any corrections.

Palermo [9] did not apply any open jet wind tunnel corrections to his experiments mainly due to the fact that the streamline corrections identified in literature have been applied under the assumption of two-dimensional flow which was not representative of the flow over the Flying-V. Thus, it was preferred to not apply corrections than applying partially correct ones.

Garcia [36], investigated different open jet wind tunnel corrections but concluded that applying them to the studies on the Flying-V was not possible. Since the assumptions used for developing these methods could not be held for the Flying-V model. Furthermore, not all data is deemed correctable due to the non-linearity or unsymmetrical flow conditions for aileron deflections.

Similarly, Viet [15] also decided to not impose corrections. He argued that the corrections for the dynamic pressure and the angle of attack could not outweigh the potential error that stemmed from the corrections. Same applies to the works of Johnson [37], Erdinciler [13] and Nolet [38].

It has thus been decided to not correct the data to also be consistent with previous studies done on the Flying-V model.

2.5. Flight Performance Analysis

After obtaining data on the half-wing wind tunnel model of the Flying-V, they needed to be analyzed for the full-scale aircraft. For an aircraft to be certifiable by the European Union Aviation Safety Agency (EASA) and the Federal Aviation Administration (FAA), as well as being attractive for the customers, the results of the performance plays a pivotal role. In this research the focus was on landing analysis. Firstly, the specifications of the aircraft model used are given in subsection 2.5.1. Next, a description of the landing maneuver is presented in subsection 2.5.2.

2.5.1. Aircraft Specifications

Firstly, it should be noted that this thesis project was conducted in two phases, one was the experimental study using the half-wing wind tunnel model and the other was flight performance analysis using the full-scale simulation developed by de Zoeten during his thesis [14]. However, the work of de Zoeten was also based on many other studies done on the Flying-V throughout years. Therefore, it is important to document where each information is resourced from. A brief summary is given in this subsection. The Flying-V model studied was the model developed by Oosterom, FV-1000, which is the largest of the Flying-V family and has similar mission profile to Airbus A350-1000 [39]. Table 2.2 shows other relevant sources for developing the model.

Table 2.2: The sources from which the data on FV-1000 was gathered

Item	Source [9, 11, 13, 39–43]
Aerodynamic data	Odilila and the WT experiment
Inertia tensor	Claeys
Centre of Gravity range	Cappuyns
Planform geometry	Oosterom
Airfoil geometry	Palermo
Nacelles geometry	Airbus
Pylons geometry	Erdirncler
Landing gear position	Bourget
Landing gear struts	Bourget
Landing gear wheels	Airbus
Engine position	Pascual

Odilila is a Vortex Lattice Method (VLM), used to analyze and optimize aerodynamic performance. This software has been created and validated by Airbus [41]. Furthermore, the top-level specifications of the FV-1000 are shown in Table 2.3.

Table 2.3: Top level specifications for the Flying-V-1000

Item	Value [9, 11, 13, 39–41, 43]	Unit
Number of passengers	361	-
Payload mass	67	10^3 kg
MTOM	259	10^3 kg
MLM	193	10^3 kg
Dry thrust	707	kN
Thrust-to-weight ratio	0.278	-
Approach speed	74.6	m/s

Note that the approach speed changes for the cases with flaps on, later on, which is described in section 5.2. Finally, the geometrical parameters used in the simulations are shown in Table 2.4.

Table 2.4: Geometric specifications for the Flying-V-1000

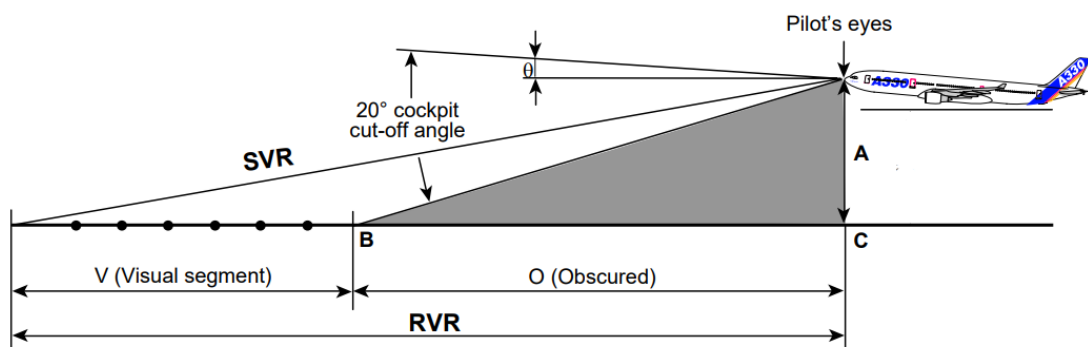
Item	Value	Unit
Reference span	65	m
Aircraft length	57	m
Reference area	883	m ²
Aspect Ratio	4.8	-
Mean aerodynamic chord	18.7	m
x-coordinate forward CG limit	29.4	m
x-coordinate mid CG limit	30.6	m
x-coordinate rearward CG limit	31.7	m
CG Range	2.34	m
x-coordinate nose landing gear	6.5	m
x-coordinate main landing gear	31.8	m
θ_{ground}	-3	deg
θ_{TS}	19.2	deg
$\Lambda_{c/4}$	55.8	deg
$(t/c)_w$	0.130	m
x-coordinate engine	37.4	m
y-coordinate engine	4.7	m
z-coordinate engine	0.8	m

2.5.2. Landing Performance

Landing starts when the aircraft descends below the screen height of 50 ft as defined by CS25 regulations [44]. Additionally, the approach speed in which the aircraft arrives at the screen height is defined as Equation 2.11 where V_S is the stall speed.

$$V_{app} \geq 1.23V_S \quad (2.11)$$

The landing maneuver consists of an airborne phase followed by de-rotation and ground-run. Additionally, the landing field length is defined as the horizontal distance paved by the aircraft from the screen height to standstill divided by a safety factor of 0.6 [45, 46]. One objective of this research was to determine whether using split flaps would reduce the pitch attitude at landing and the obscured segment to improve pilot vision. A schematic of the pilot vision definitions during landing, from Airbus [43] is shown in Figure 2.19.

**Figure 2.19:** Pilot vision during landing, modified from [43]

For these analyses the pilot's eye is assumed to be located 1.87 m behind the nose and 1 m above the aircraft center line. Additionally, the pilot's nose angle is assumed to be 25.7 degrees.

3

Methodology

During this thesis project a wind tunnel test campaign was performed to obtain experimental data about the designed flaps. Using these data an estimate of the best flap design and location was selected. Subsequently, the effect of these flaps on landing performance of the full-scale aircraft was evaluated. This chapter discusses the methodology followed for the flap design and wind tunnel experiment in section 3.1 followed by the methodology for the flight performance analysis in section 3.2.

3.1. Wind Tunnel Experiment and Design Process

In this section the methodology followed for the wind tunnel test and flap design is explained. Firstly, subsection 3.1.1 presents the design variables used for the experiment. The Test matrix is introduced in subsection 3.1.2. Next, the design and manufacturing of the flaps are described in subsection 3.1.3, followed by the test set-up description in subsection 3.1.4.

3.1.1. Design Variables for the Split Flaps

For the wind tunnel campaign a broad design space was used, this was done to assure different design options could be explored in the limited time of the campaign. The design variables were chosen as:

1. Chord-wise location of the hinge line
2. Chord length (C)
3. Span (L)
4. Region (R)
5. Deflection angle (δ_f)
6. Number of flaps
7. Angle of attack (α)
8. Free stream velocity(V)

Below each of these design criterion is explained.

Chord-wise location of hinge line

This variables refers to the placement of the flaps in the chord-wise direction. There were three options, 90%, 80% and 70% of the local chord. This was closely related to the flap chord length and was chosen as a variable to test the difference in performance in cases where the trailing edges of the flaps and wing either meet or do not meet. This is referred to as 0.9C, 0.8C and 0.7C.

Span (L)

The span has been taken as the span-wise length of each region while keeping some margins with the engine location. Figure 3.1 show the regions and spans.

Region (R)

This variable refers to the location on the inner wing where the flaps are placed. R1 is the region closer to the root and R2 the region closer to the kink. The division has been done based on the location of the engine and landing gear which are shown on Figure 3.8. Additionally, the division of the model in 3D Experience is presented in Figure 3.1.

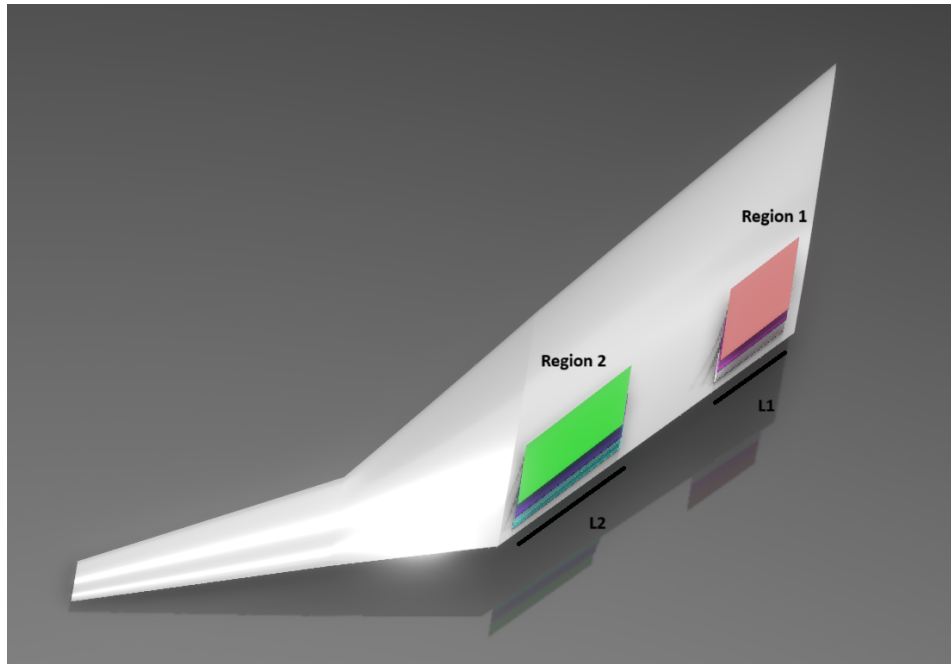


Figure 3.1: Half-wing model division for flaps placement

Chord Length (C)

Following the literature study it was noticed that many experiments conducted on flaps have included three variations of chord length namely, 10%, 20% and 30% of the local chord length. Therefore, the same approach has been followed in this thesis project. Since the Flying-V half-wing model has a complicated geometry with multiple curvatures a certain airfoil section had to be chosen as the datum for the local chord. The datum has been taken as the root chord for region 1 and the kink chord for region 2.

Deflection Angle (δ_f)

This criteria was also determined based on the literature study. It was found that typical values for the deflection angle for experimental studies on flaps started below the zero lift angle and above the stall angle. Ranges of 5° to 75° were often used in other studies. Therefore, for this study a deflection angles of 10° , 20° , 30° , 45° , 60° were chosen in order to cover a wide range while staying within the reasonable numbers of measurement points given the limited time of the experiment. The deflection angles are measured relative to the flow direction on the wing.

Number of Flaps

This criterion indicated whether only one of the regions had flaps placed on them or multiple regions were occupied.

Angle of Attack (α)

The angles of attack chosen were [-5, 0, 5, 10, 12, 14, 16, 18, 20, 22, 24, 26, 28, 30]

Free Stream Velocity

This criterion is mainly used to check for the effect of Reynolds number on the aerodynamic coefficients. Therefore, most of the configurations were tested only at 0 and 20 m/s. To check for the effects of velocity change seven configurations were measured for two additional velocity of 25 and 30 m/s.

3.1.2. Test Matrix

Using these design variables firstly all the possible combinations were laid out in a large table. However, to adhere to the Design of Experiment method and to have an efficient experiment only a part of these data points were chosen. This resulted in a test matrix, throughout the research before the experiment, a few changes were made to the test matrix, therefore only the latest update is shown in Appendix A. During the wind tunnel campaign due to having additional time an extra test matrix was developed to be used for testing extra configurations. One noteworthy configuration was a full-span flap setting on the inboard wing which was not initially considered.

3.1.3. Design and Manufacturing of Flaps

The determination of the design criteria and the test matrix resulted in six different flaps, these were in the form of a parallelogram and were installed on the wing in the direction parallel to the trailing edge. The six designs were created based on the chord length and the span length of the flaps and were named A to F. Figure 5.1 shows these flaps as designed in 3D Experience.

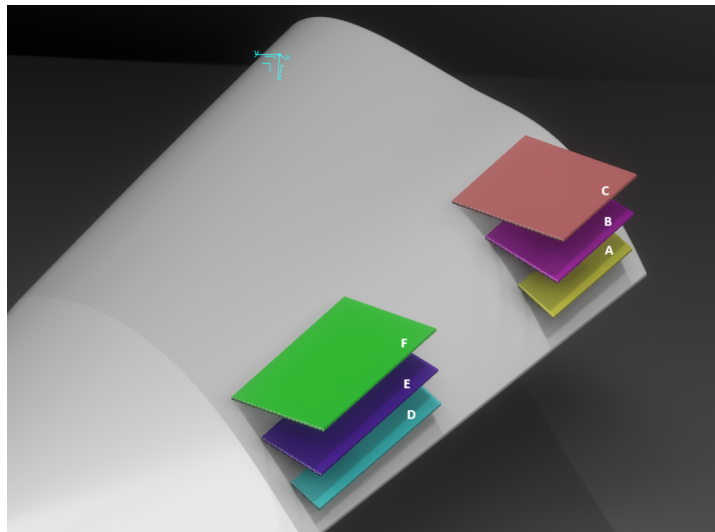


Figure 3.2: CAD model of flaps A to F placed on the half-wing wind tunnel model of the Flying-V

Additionally, Figure 3.3 shows a top view drawing of the flaps on the half wing model with dimensions in mm. Since the largest flaps are covering the smaller ones in this drawing the chord wise location variation has been included to help with visualization.

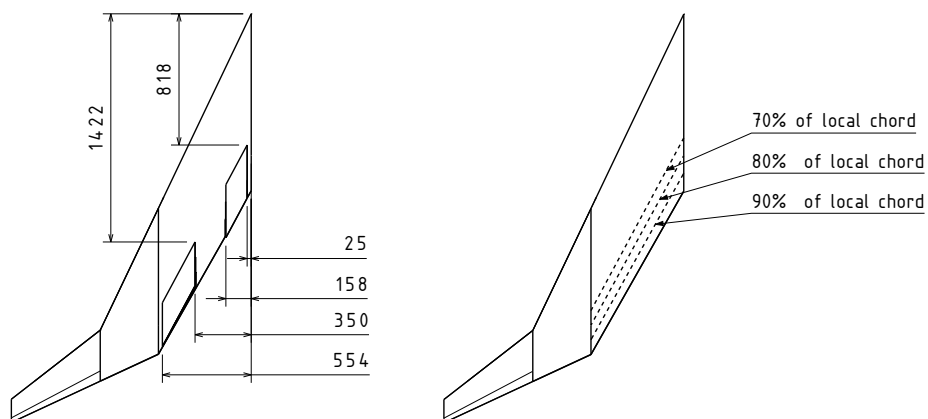


Figure 3.3: Top-view drawing of the positioning of the flaps on the half-wing model

As seen, the flaps have a shape of a parallelogram with dimensions summarized in Table 3.1.

Table 3.1: Dimensions of the various flaps

Flap name	Base (mm)	Height (mm)
A	280	52
B	280	105
C	280	157
D	430	43
E	430	86
F	430	133

In addition to the flaps, several brackets were designed to be used for changing the deflection angles. The drawings and designs were done using 3D Experience. The brackets were 3D printed and the flaps were made using watercut on aluminium sheets. A sample of a few brackets is shown in Figure 3.4.

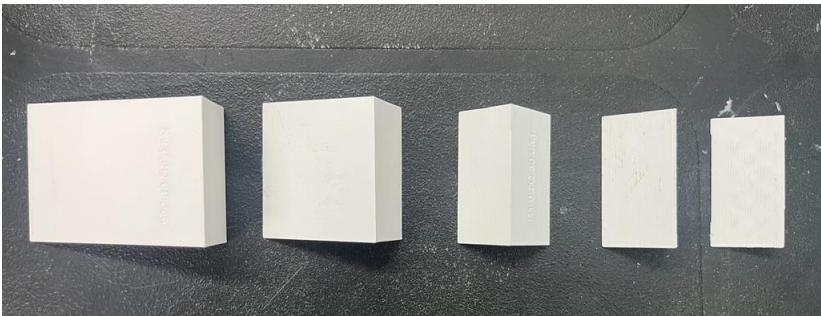


Figure 3.4: Brackets used for changing the flaps' deflection angles

Additionally, the watercut versions of flaps A and C are shown in Figure 3.5



(a) Flap A

(b) Flap C

Figure 3.5: Two samples of flaps used in the wind tunnel test campaign

Furthermore, the flaps were set up on the wind tunnel model as shown in Figure 3.6.



(a) Flap A mounted on region 2

(b) Flap C mounted on region 1

Figure 3.6: Flaps A and C mounted on the half-wing model of the Flying-V during the test campaign at OJF

During the test campaign, the flaps and brackets were changed manually after each measurements. Extensive photographing and documentation was used to assure outmost similarities in the experiment set-up.

3.1.4. Test Set-up

Similar studies to the current research have been performed previously on the Flying-V using the same methods. The experiments were carried out during a wind tunnel test campaign in the Open Jet facility of the Aerospace engineering faculty. The split flaps were mounted on a 4.6% scaled half-wing model of the Flying-V. A full wing cannot be used due to the size restrictions of the OJF.

The Open Jet Facility

The Open Jet Facility is a low-speed, closed-circuit wind tunnel. It consists of an octagonal nozzle cross-section with dimensions of $2.850 \text{ m} \times 2.850 \text{ m}$ and a test room of $13 \text{ m} \times 8 \text{ m}$. The maximum test section velocity is 35 m/s [26]. A large fan powered by a 500 kW electric motor drives the airflow. After this fan, the flow passes a long diffuser and is guided by two rows of corner vanes resulting in a 180° rotation. To reduce turbulence the flow goes through several dense wire meshes in the settling chamber, before blowing into the test section through a contracting nozzle. Additionally, to keep the temperature of the flow constant the heat is removed after the test section by a 350 kW radiator system. Finally, before entering the fan, the flow is again redirected 180° by two rows of corner vanes. A schematic of the OJF is shown in Figure 3.7

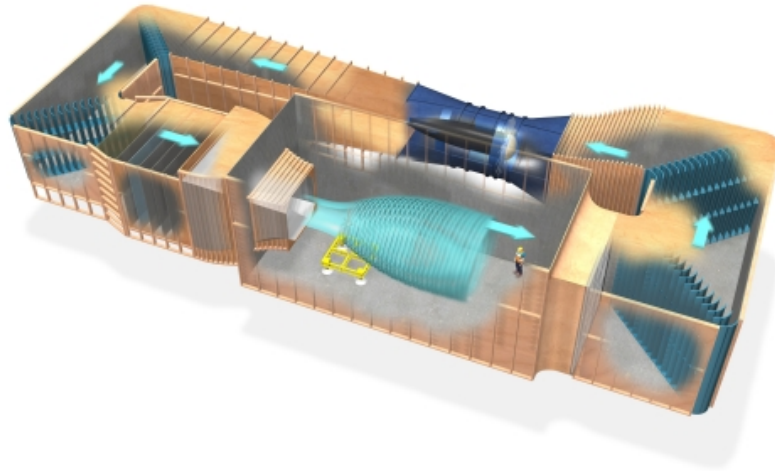


Figure 3.7: The Open Jet Facility of TU Delft Aerospace Engineering [26]

The half-wing Model

The half-wing model is generated using the geometric Froude scaling laws as described by Palermo [9] and Viet [15]. It has a semi-span of 1495 mm and a chord-wise length of 2547 mm, with 64.5° inboard and 37.9° outboard leading edge sweep and thickness to chord ratio of 0.16 at the root section. The model represents exactly a half wing of the Flying-V Sub-scale Flight Testing (SSFT) model which is scaled as 4.6% of the aircraft. It is divided into three main sections, the inboard, mid and outboard sections, the midsection contributes to the transition from the higher to lower sweep angle.

This model houses 4 adjustable control surfaces. Three of which, namely, CS1, CS2 and CS3 are part of the original design. CS1 is the most inboard surface located on the midsection, working as the main elevator and CS3 as the aileron, CS2 is the central control surface used for both lateral and longitudinal control, making it an elevon [9]. A 4th control surface, CS4 has been more recently added as a rudder for directional control [37]. It must be noted that all the control surfaces were kept on zero-deflection during the wind tunnel tests. There were a few reasons for this decision, one was that CS1 and CS2 were damaged long before the experiment and could not be adjusted, another reason was the limited time of the wind tunnel which made having an even larger test matrix by involving CS deflections undesirable, lastly, it was decided to first study the flap performance isolated from the interactions with control surfaces. Involving the control surfaces was meant to occur during a second wind tunnel test campaign which could not happen due to scheduling conflicts.

Moreover, the half-wing model has been manufactured out of a sandwich of three layers of fiberglass, a foam core and another three layers of fibreglass to ensure a stiff model which is less prone to aeroelasticity effects.

As mentioned before, in this study the split flaps were only located on the inboard section, while taking into account the space reserved for the engines and the landing gears on the full-scale aircraft. Figure 3.8 shows top and rear views of the half-wing model geometry where all the dimensions are in mm.

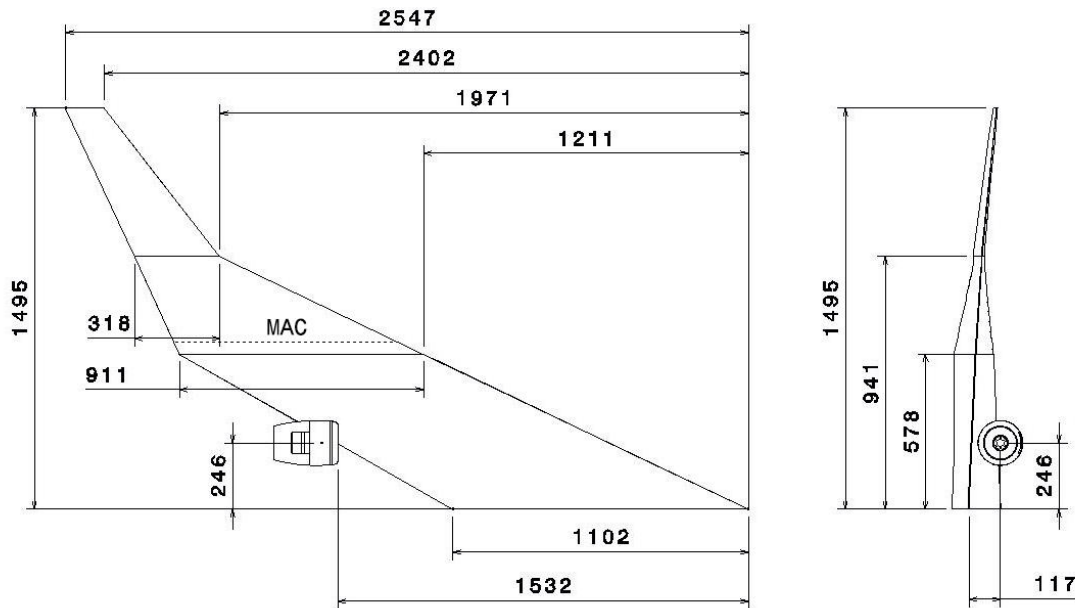


Figure 3.8: The half-wing model geometry as used in a study by Empelen, Vos [47]

Balance Set-up

In order to stay consistent with the previous and ongoing experimental studies conducted on the half-wing model, a test set-up similar to the ones used by Palermo [9], Garcia [36], Viet [15] and Erdinçler [13] was used. The forces and moments in X, Y, and Z directions on the model were measured using an external balance, each data point was measured for a duration of 10 seconds and averaged out to reduce errors, these data were then saved by the computer.

The balance was placed onto a turntable which was placed on top of a flat plate. This flat plate could be used to adjust the height of the set-up and also provide a solid base which did not move during the experiment. On top of the turntable, a splitter plate was placed to separate the boundary of the jet from the measurements, the leading edge of this splitter plate was built in an elliptical shape to avoid the separation of the incoming flow. A reflection plate was put in between the splitter plane and the balance to ensure the balance was not in direct contact with the jet flow to minimize noise and perturbations in the data. Finally, the model was set on top of the reflection plate and connected to the balance through a model support which connected both balance and the model through an aluminium plate located at the root of the model. Below schematics of the set-up are shown.

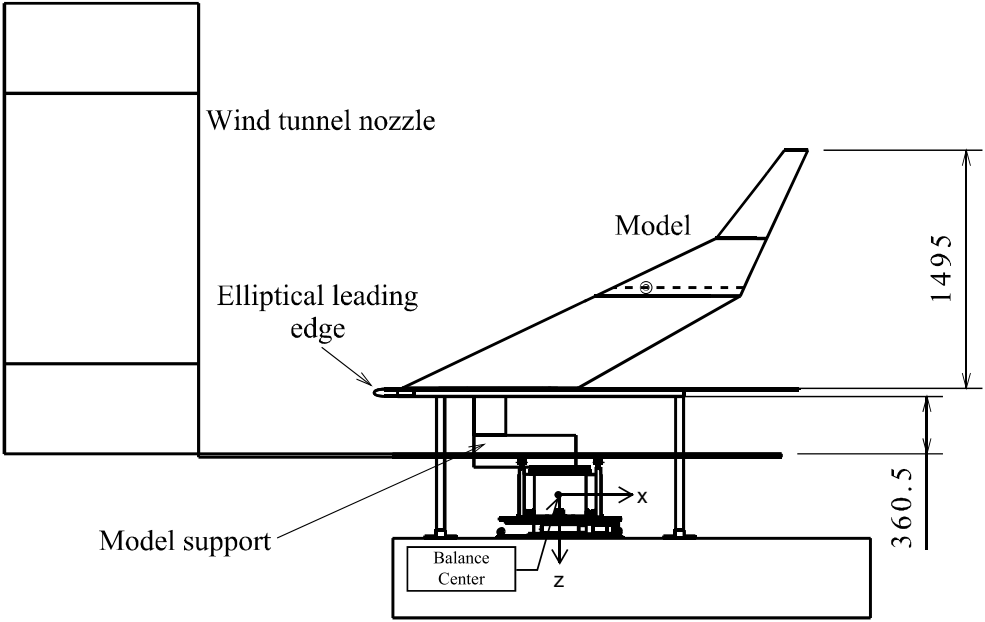


Figure 3.9: Side view of the test-set up [9]

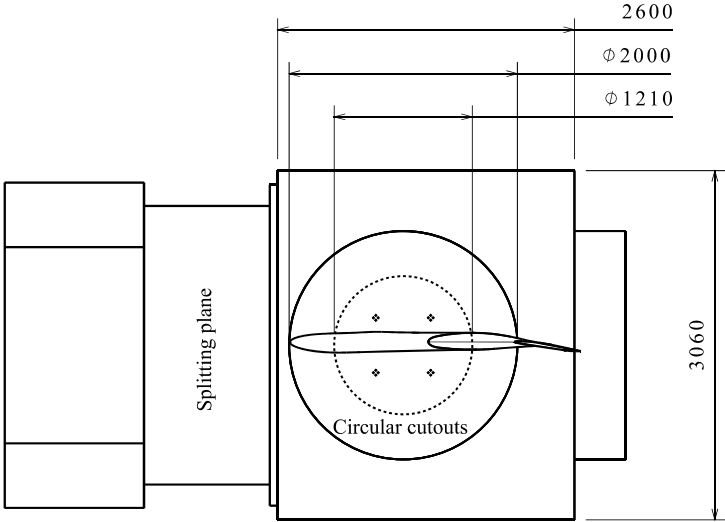


Figure 3.10: Top view of the test set-up [9]

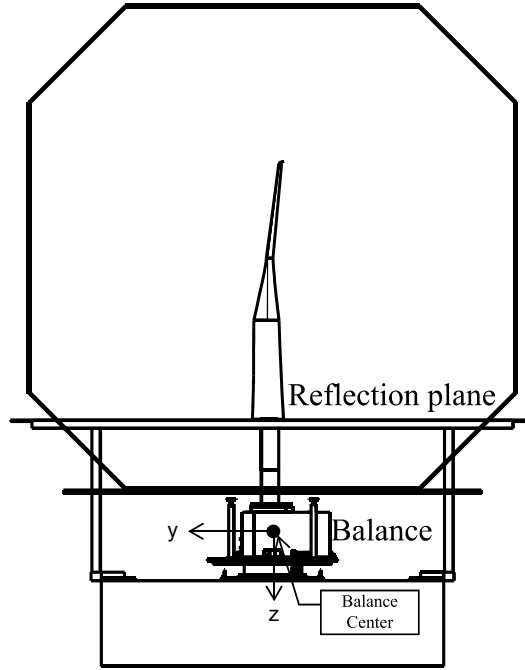


Figure 3.11: Rear view of the test set-up [9]

The forces and moments namely, F_x , F_y , F_z , M_x , M_y and M_z , are measured using an external balance. These measurements are taken around the balance center, in the coordinate system of the balance itself and therefore, must be transferred into the wind axis system. The aerodynamic forces and moments are determined in the wind axis system, using Equation 3.1 to Equation 3.6. Note that these equations are set up with the assumption that the angles of sideslip and roll are zero.

$$L = -F_y \cos \alpha - F_x \sin \alpha \quad (3.1)$$

$$D = F_x \cos \alpha - F_y \sin \alpha \quad (3.2)$$

$$Y = F_z \quad (3.3)$$

$$M_{CG} = M_z + F_y \cdot (r_{\text{arm}_x} - r_{\text{mgc}_x}) - F_x \cdot r_{\text{arm}_z} \quad (3.4)$$

$$l = -M_x + F_y \cdot r_{\text{arm}_z} \quad (3.5)$$

$$n = M_y - F_x \cdot (r_{\text{arm}_z} + r_{\text{mgc}_z}) \quad (3.6)$$

Where r_{arm_x} and r_{arm_z} are the wing leading edge to the balance center distance in x and z directions respectively. Similarly, r_{mgc_x} and r_{mgc_z} are the leading edge distance to CG of the wing in x and z direction respectively. These can also be expressed in the non-dimensional format. Equation 3.7 shows the force coefficients, namely lift, drag and normal forces.

$$C_L = \frac{L}{qS} \quad C_D = \frac{D}{qS} \quad C_Y = \frac{Y}{qS} \quad (3.7)$$

Equation 3.8 shows the moment coefficients which are pitching moment coefficient, rolling moment coefficients and yawing moment coefficient.

$$C_{M_{CG}} = \frac{M_{CG}}{qS\bar{c}} \quad C_l = \frac{l}{qSb} \quad C_n = \frac{n}{qSb} \quad (3.8)$$

3.2. Flight Performance Analysis

The second part of this research was a flight performance analysis to apply the outcome of the wind tunnel experiment on the full-scale Flying-V. The analysis was focused on landing performance. This section provides a description of the flight mechanics model in subsection 3.2.1, the aerodynamics model subsection 3.2.2 and the pilot and flight control system in subsection 3.2.3. Lastly, the landing maneuver is described in subsection 3.2.4.

3.2.1. Flight Mechanics Model

The landing analysis was conducted using the Performance, Handling Qualities and Load Analysis Toolbox (PHALANX) developed at the Delft University of Technology. This toolbox integrates disciplinary sub-models into a flight mechanics model. PHALANX was implemented in several other research projects on unconventional aircraft [48–52]. But more importantly it has been used for the Flying-V analysis. In his thesis, de Zoeten [14] used and tailored PHALANX for analysis of different flight phases of the Flying-V including landing. The process with which PHALANX works has been thoroughly discussed in de Zoeten's work [14], however a summary is provided in this subsection.

In this toolbox, it is assumed that Earth is flat, non-rotating, exerts a constant gravitational acceleration and has a still atmosphere which adheres to International Standard Atmosphere (ISA) [53]. The purpose of the model is to provide the time evolution of relevant parameters, through solving a set of equations of motion (EOM) at each time instant. PHALANX creates a framework for simulation of flight with 6 Degrees of Freedom (DOF), which can be reduced to 3 DOF in case of longitudinal motion. A block scheme of a flight mechanics model created using PHALANX [54] is shown in Figure 3.12.

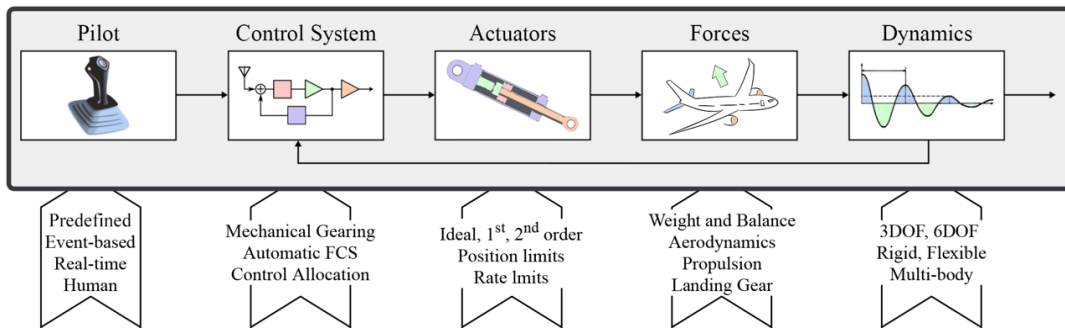


Figure 3.12: Block scheme overview of the PHALANX flight mechanics model [54]

The pilot provides input for the control system which translates these inputs into control surface deflection and a throttle setting. It is assumed that the control surface actuators are operating ideally, meaning that they deflect the control surfaces instantly.

Classic rigid body dynamic equations are used, where external forces and moment contributions of different aircraft components are summed in body frame and used to propagate the aircraft state. Equation 3.9 and Equation 3.10 show these equations. Note that the external forces and moments are functions of angle of attack, sideslip, flight Mach number, angular rates of roll, pitch and yaw and control settings.

$$\begin{Bmatrix} \dot{u} \\ \dot{v} \\ \dot{w} \end{Bmatrix} + \begin{Bmatrix} p \\ q \\ r \end{Bmatrix} \times \begin{Bmatrix} u \\ v \\ w \end{Bmatrix} = \frac{q_\infty S}{m} \begin{Bmatrix} C_X(\alpha, \beta, Ma, p, q, r, \delta) \\ C_Y(\alpha, \beta, Ma, p, q, r, \delta) \\ C_Z(\alpha, \beta, Ma, p, q, r, \delta) \end{Bmatrix} + g \begin{Bmatrix} -\sin \theta \\ \cos \theta \sin \varphi \\ \cos \theta \cos \varphi \end{Bmatrix} \quad (3.9)$$

Where u, v, w are the airspeed components with respect to the body frame of reference, X, Y, Z are the external forces excluding gravity. p, q, r are the angular rates of roll, pitch and yaw.

$$I \begin{Bmatrix} \dot{p} \\ \dot{q} \\ \dot{r} \end{Bmatrix} + \begin{Bmatrix} p \\ q \\ r \end{Bmatrix} \times I \begin{Bmatrix} p \\ q \\ r \end{Bmatrix} = q_\infty S_c \begin{Bmatrix} C_l(\alpha, \beta, Ma, p, q, r, \delta) \\ C_m(\alpha, \beta, Ma, p, q, r, \delta) \\ C_n(\alpha, \beta, Ma, p, q, r, \delta) \end{Bmatrix} \quad (3.10)$$

Where l, M and n are the external moments about the center of gravity.

Finally, the moment of inertia tensor is given in Equation 3.11

$$I = \begin{bmatrix} I_{xx} & -I_{xy} & -I_{xz} \\ -I_{xy} & I_{yy} & -I_{yz} \\ -I_{xz} & -I_{yz} & I_{zz} \end{bmatrix} \quad (3.11)$$

The dynamics of the aircraft are governed by the external forces and moment. The external forces considered are, aerodynamics, propulsive, gravitational, and ground contact forces. A brief description of the aerodynamic forces is given in subsection 3.2.2 and for the rest the reader is referred to de Zoeten's thesis [14]. Note that these external forces and moments are translated into the aircraft body frame of reference through transformation matrices. The body, wind and aerodynamic reference frames are shown in Figure 3.13.

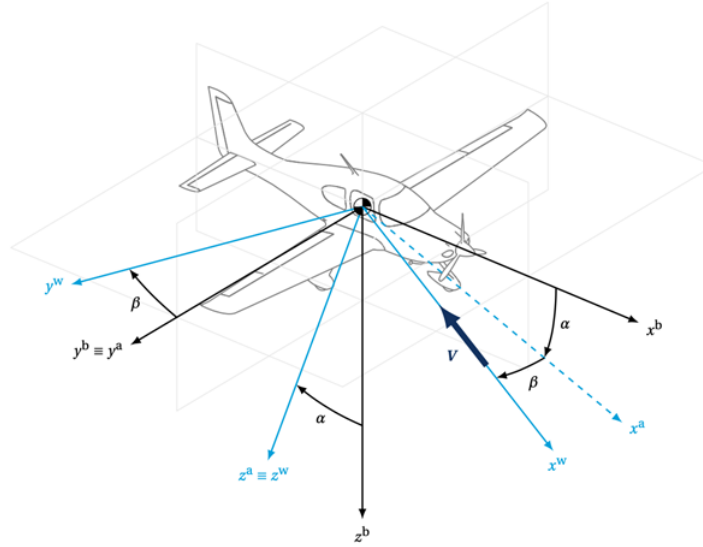


Figure 3.13: Body (b), wind (w) and aerodynamic (a) reference frame [54]

PHALANX also has a built-in trimming function based on a predetermined, altitude, air speed, sideslip angle and Euler angular rates p , q , r . The trimming algorithm works by minimizing the linear and angular accelerations in the body reference frame as well as the error in the sideslip angle ϵ_β . Therefore the objective function to be minimized is shown in Equation 3.12.

$$\min f(\phi, \theta, \psi, \delta) = \|\dot{u}, \dot{v}, \dot{w}, \dot{p}, \dot{q}, \dot{r}, \epsilon_\beta\| \quad (3.12)$$

The Euler angles and control settings $\delta = (\delta_{roll}, \delta_{pitch}, \delta_{yaw}, \delta_{throttle})$ that minimize the objective function are found by a gradient-descent optimization algorithm. Where δ_{roll} shows pilot moving the stick in lateral direction (positive right), δ_{pitch} shows a longitudinal stick deflection (positive forward), δ_{yaw} is a pedal input to control the rudder (positive right) and $\delta_{throttle}$ shows the throttle setting.

The trim function depends on the degrees of freedom and the equations of motion. Assuming a 2D EOM represents a symmetric flight and therefore eliminates δ_{roll} , δ_{yaw} and the Euler angles ϕ and ψ . To get the trimmed conditions either a flight path angle γ or a thrust setting $\delta_{throttle}$ must be prescribed.

3.2.2. Aerodynamics Model

This subsection presents a description of the aerodynamic sub-model used in the flight performance analysis of the Flying-V.

The aerodynamic forces and moment used in the analysis were produced initially using a Vortex Lattice Method developed and verified by Airbus, called Odilila [41]. VLMs are based on the assumption that the flow is incompressible, inviscid and irrotational which imposes some limitations. Despite this, they are widely used in the conceptual and preliminary design phases due to low computational cost and ability to calculate lift curve slope, induced drag and stability derivatives.

One important note is that for the landing analysis during current research the aerodynamics data

obtained from the wind tunnel test were used to replace or modify the forces and moments of the Odilila model. Therefore, the aerodynamic model used is a combination of experimental and VLM data. The experimental data were scaled to match the full-scale aircraft to be usable alongside the rest of the Odilila data which were not replaceable due to the lack of experimental data.

The aerodynamic forces and moments were transferred to the body reference frame and ranged from the angle of attack of -5 to 20 degrees. The reason for not going beyond 20 degrees was the pitch up tendency observed in the previous wind tunnel tests conducted on the Flying-V half-wing model. Moreover, Mach numbers ranged from 0.2 to 0.85 and the contributions due to non-zero angles of sideslip, Euler angular rates and control surface deflections were calculated under the superposition assumption. Which meant that these contributions were completely decoupled and linear.

A general formulation of the forces and moments outputted by Odilila is shown in Equation 3.13. Here F_0 represents the contribution of the airframe alone at zero angle of sideslip and angular rate ω_b .

$$F(\alpha, Ma, \beta, \omega_b, \delta_{cs}) = F_0(\alpha, Ma) + \frac{\partial F(\alpha, Ma)}{\partial \beta} \beta + \frac{\partial F(\alpha, Ma)}{\partial \omega_b} \omega_b + \frac{\partial F(\alpha, Ma)}{\partial \delta_{cs}} \delta_{cs} \quad (3.13)$$

As mentioned in subsection 2.5.1, the Flying-V model used in these analysis was FV-1000 designed by Oosterom [39]. The control surfaces have also been modelled such that the outboard CS of the main wing of the Flying-V is categorized as an elevon due to its function in both pitch and roll control, while the inboard control surface is categorized as an elevator since it is only used for pitch control. The deflection limit of the CS's is assumed to be 30 degrees. Additionally, the contributions of ground spoilers as designed by Erdinciler have been added as a reduction of 0.16 in C_L during the ground run after touchdown.

Since Odilila can only predict the lift induced drag, the Zero-lift drag and Transonic wave drag were added manually, using imperial relations [55–58] and as such prone to inaccuracy since these imperial relations are based on conventional aircraft. In addition to this there are other limitations to Odilila due to not accounting for viscous effects. These are for instance, inability to predict stall characteristics or non-linear behavior. The lift curve slope predicted by Odilila is also linear due to inability to account for vortex lift which has been shown to occur on the Flying-V [15]. However, this last short coming is partially negated by using experimental data from the wind tunnel test which do account for vortex lift. Furthermore, since modelling accuracy of high lift devices by Odilila are limited, the contribution of the split flaps have been modelled by changes to the aerodynamic forces and moments.

3.2.3. Flight Control

For flight control a pilot has been modelled that provided control variable values that were converted to control surface deflections and a thrust setting by the Flight Control System (FCS). These control variables included δ_{pitch} , δ_{roll} , δ_{yaw} and $\delta_{throttle}$ and can assume a value between -1 and 1 [14].

The pilot input in each maneuver, such as landing is modelled by incorporating different controllers that aim to minimize the error in prescribed values of the variables. This means that each value is assigned a target and a closed feedback loop is used which compares the current value to the target value and then feeds the error (e_t) into a PID controller.

A PID controller consists of a Proportional gain K_p , and Integral gain K_i and a Derivative gain K_d . These gains are multiplied by the current error, time-integrated error and current time derivative of the error respectively. Then they are summed up to obtain the output of the PID controller (u_t) as shown in Equation 3.14. To achieve the desired behavior of the system these gains must be tuned.

$$u(t) = K_p e(t) + K_i \int_0^t e(\tau) d\tau + K_d \frac{de(t)}{dt} \quad (3.14)$$

An architecture of the closed feedback loop system is shown in Figure 3.14.

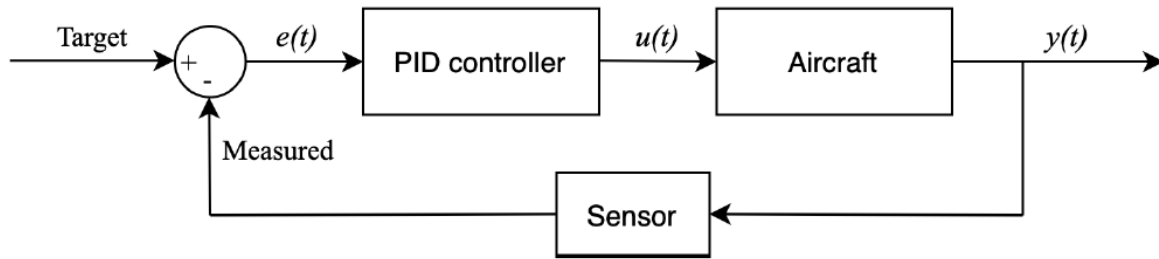


Figure 3.14: General architecture of closed feedback control loop [14]

3.2.4. Landing Maneuver

Finally, the main goal of the flight performance analysis, the landing maneuver is discussed in this subsection. Landing maneuver is started when the aircraft arrives at the screen height which is taken as 50 ft above the runway following a glide slope of -3° . The maximum lift coefficient was assumed to occur at an angle of attack of 18° . Since it was observed that a pitch break occurred at an angle of attack of 20° and therefore using 18° assured the pitch break does not occur. Based on these the stall and approach speeds were calculated. These are discussed in section 5.2.

The landing maneuver is performed with a flare movement, this is to reduce the touchdown rate from approximately 12 ft/s to 6 ft/s. According to CS25 [44], the maximum descent rate at Maximum Landing Mass (MLM) is 10 ft/s and 6 ft/s is considered generally a firm touchdown but still acceptable. This has been implemented such that the pilot increases the flight path angle by pulling the nose up. The degree to which this pull-up is performed depends on the approach speed. These numbers depend on the flap configuration and are discussed in section 5.2.

The pull-up maneuver occurs when the aircraft is 1 m above the runway, where the pilot attempts to increase the flight path angle to the reference touchdown angle. The nose is raised to increase lift, to prevent over rotation the pull-up is stopped when the aircraft descends below 1 m. During the flare maneuver the thrust is reduced to idle while taking the spool-down time into account. After the aircraft touches down on the runway, de-rotation starts which should be done as quickly as possible, since braking can start only when the nose landing gear touches the ground. The target pitch rate during the de-rotation is -3 deg/s. Afterwards, braking is initiated by deflecting the ground spoilers, setting the main gear friction coefficient to μ_b and activating the controllers. The controllers maximize the downforce while keeping at least 8% of the weight on the nose landing gear. The landing simulation is done using 2D equations of motion, since only symmetric motion is considered.

4

Verification & Validation

This chapter presents the Verification and Validation of the results obtained from wind tunnel experiments and flight performance simulations. Validation and verification are essential parts of a reliable research and help ensure the obtained results are sound and compatible to previous research. Verification is done to check whether the right model and procedure is followed, while validation checks whether the outcome is right.

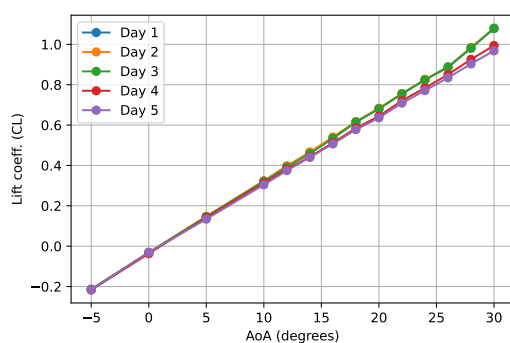
The chapter starts with discussing reproducibility of the wind tunnel results in section 4.1. Next, Reynolds number sensitivity is discussed in section 4.2, followed by systematic error check in section 4.3. Lastly, section 4.4, presents the verification of the flight performance analysis.

4.1. Reproducibility

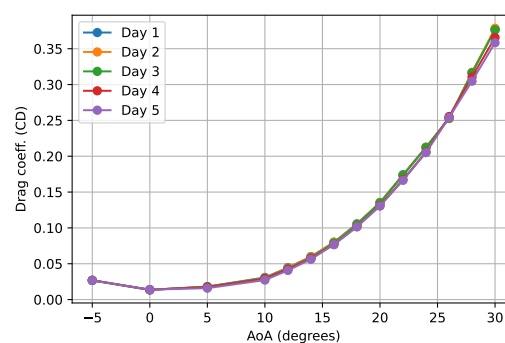
To make sure the results of the wind tunnel experiment are not subject to systematic errors, one method is to check for their short and long term reproducibility. For checking the short term reproducibility, some measurements were selected to be repeated during the wind tunnel campaign, the outcomes are presented in subsection 4.1.1. On the other hand the long term reproducibility is checked using the previous experiments conducted on the half-wing model, explained in subsection 4.1.2.

4.1.1. Short-term Reproducibility

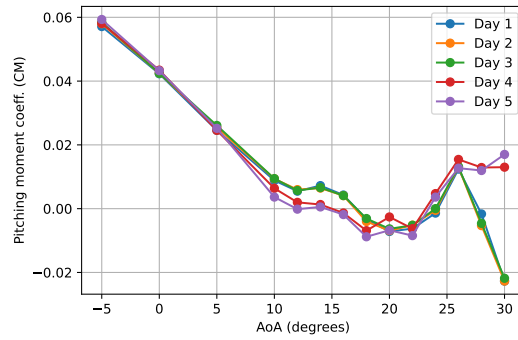
To check for short term reproducibility, some of the measurement data were chosen in a random manner to be measured multiple times during the wind tunnel campaign. There were quite a few repeated measurements for the clean wing and for each flap configuration but for conciseness only clean wing shown in Figure 4.1 and flap C and flap F are shown in Figure 4.2 and Figure 4.3 respectively.



(a) Lift coefficient



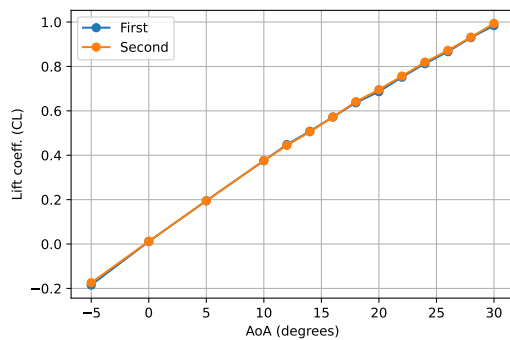
(b) Drag coefficient



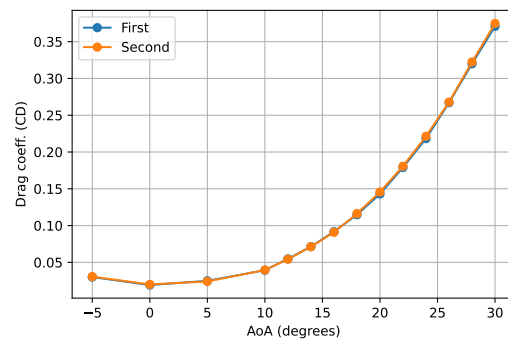
(c) Pitching moment coefficient Vs. Angle of attack

Figure 4.1: Comparison of repeated measurements for clean wing on 5 different days

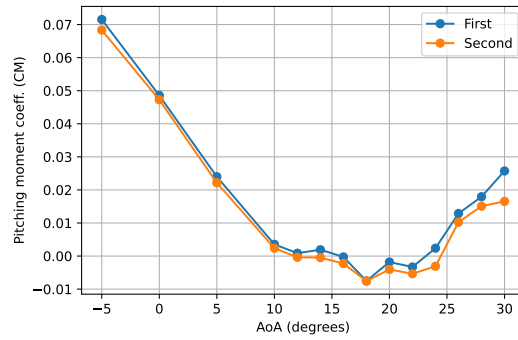
There is quite a close similarity for lift and drag coefficients for different measurements. Day 3 seems to have a slightly higher lift coefficient, this can be attributed to temperature differences. As for the pitching moment diagram the overall behavior of the wing follows the same pattern over different days however, there is a large difference after the angle of attack of 25 degrees. We can see the pitch break occurring at about 22 degrees angle of attack resulting in an unpredictable behavior, additionally, after the angle of attack of 20 degrees strong vortices are generated on the suction side and flow separation on the wing causes non-linear and unpredictable flow behavior causing a change in the aerodynamic center and large changes in the pitching moment coefficient. Overall, the maximum difference between various measurements was 0.1 for lift coefficient, 0.02 for drag coefficient and 0.04 for pitching moment coefficient. It should be noted that the performance of flaps has been compared to the clean measurements taken at the same day, mitigating the differences that the clean wing has shown in various days.



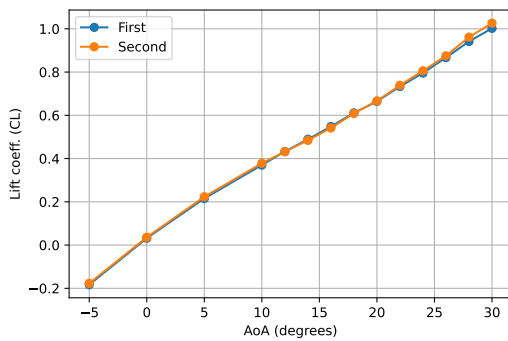
(a) Lift coefficient



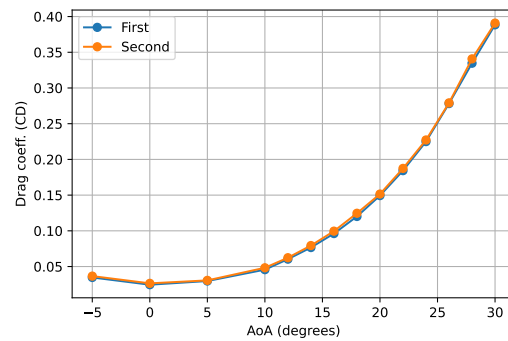
(b) Drag coefficient



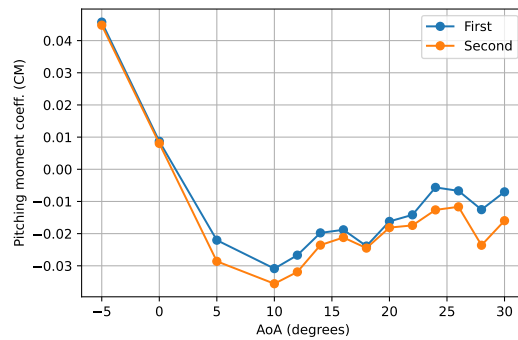
(c) Pitching moment coefficient Vs. Angle of attack

Figure 4.2: Comparison of repeated measurements for flap C at 70% of the chord in Region 1 with 10° deflection

(a) Lift coefficient



(b) Drag coefficient



(c) Pitching moment coefficient Vs. Angle of attack

Figure 4.3: Comparison of repeated measurements for flap F at 70% of the chord in Region 2 with 20° deflection

As can be seen the lift and drag coefficients for the repeated measurements are very similar to the first measurements for both flaps with a difference between the means of the two measurements being a maximum of 0.02 and 0.01 respectively. There are some differences in the pitching moment coefficient amounting to 0.01 at maximum, for the two measurements despite them having the same overall behavior. These can be attributed to slight differences in the installation of the flaps or small variations in the dynamic pressure due to different temperatures. Even though there was a great care taken in having identical conditions during the wind tunnel experiment, slight variations were unavoidable.

4.1.2. Long-term Reproducibility

For long-term reproducibility, the results of the wind tunnel were compared to the results of previous wind tunnel tests done on the half-wing model by Erdinçler [13]. As evident by Figure 4.4, there is a great compatibility in lift and drag coefficients with 0.06 and 0.03 difference, respectively. There is a slight change of lift gradient observed at Erdinçler's data starting from the AoA of 15 degrees where a higher lift is produced than current study. This may be due to higher vortex lift produced in Erdinçler's experiment which affects the slope of the lift curve. Other reasons maybe due to slight differences in environmental conditions and the set-up or the calibration of the balance. Note that some elements during the wind tunnel tests are prone to errors because of mostly being done manually. For example the test set-up is built from scratch each time, the wing is calibrated at zero using human eye and the balance calibrations can differ. Therefore, slight changes are expected in between campaigns. However, these differences are so insignificant that it can be concluded that a systemic error or mistake has not occurred.

Regarding the pitching moment coefficient graph, the two data set are quite similar until 22° AoA, where the pitch break happens. After that Erdinçler's data show a more negative pitching moment most probably, due to a larger shift in aerodynamic center. However, again a significant similarity is achieved in pitching moment behavior with a maximum difference of 0.02, which previously was deemed the most difficult one.

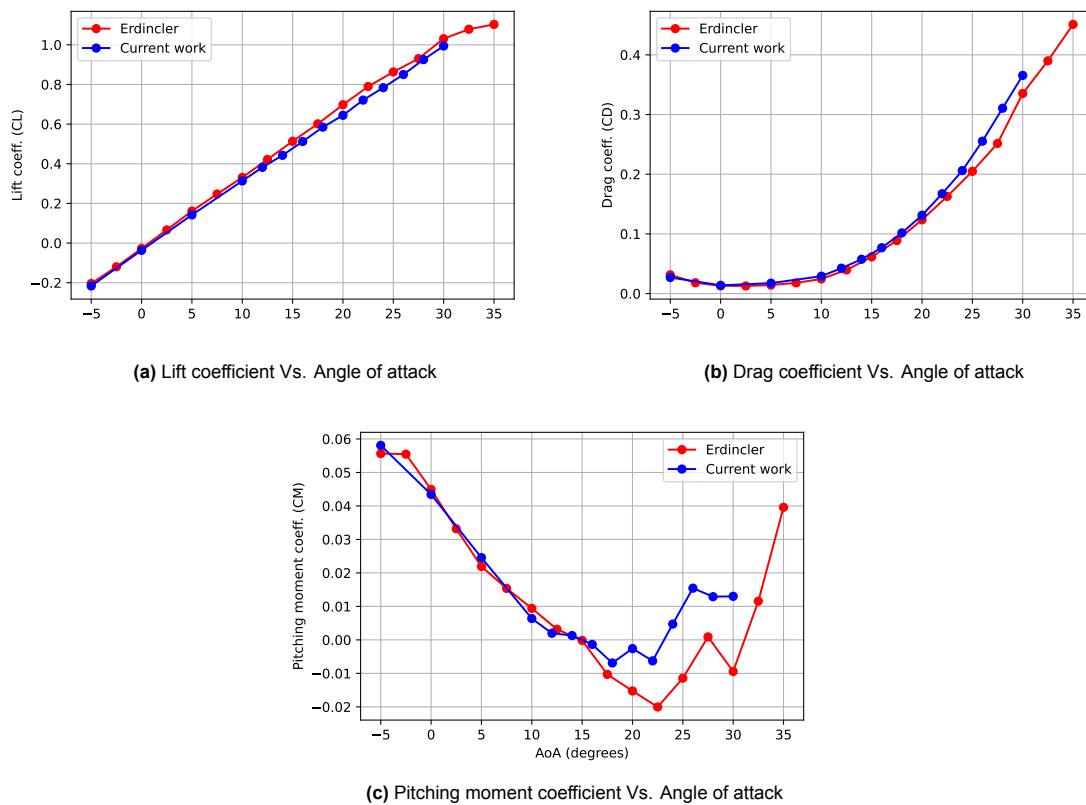


Figure 4.4: Comparison of the results of current study and a study done by Erdinçler [13] for long-term reproducibility

4.2. Reynolds Number Sensitivity

One method for verification of the results of the wind tunnel experiment is checking for Reynolds number sensitivity. It should be noted that the means for controlling the Reynolds number at the OJF is limited to small changes in the flow velocity. To achieve this a few measurements were chosen at random before the experiment to be tested for three velocities namely, 20, 25 and 30 m/s, whereas the other measurements were done at 20 m/s only. The results for clean wing cases are shown in Figure 4.5. Note that due to limitations of the OJF and the imposed vibrations on the model the higher the velocities were the lower maximum measurable angle of attack was.

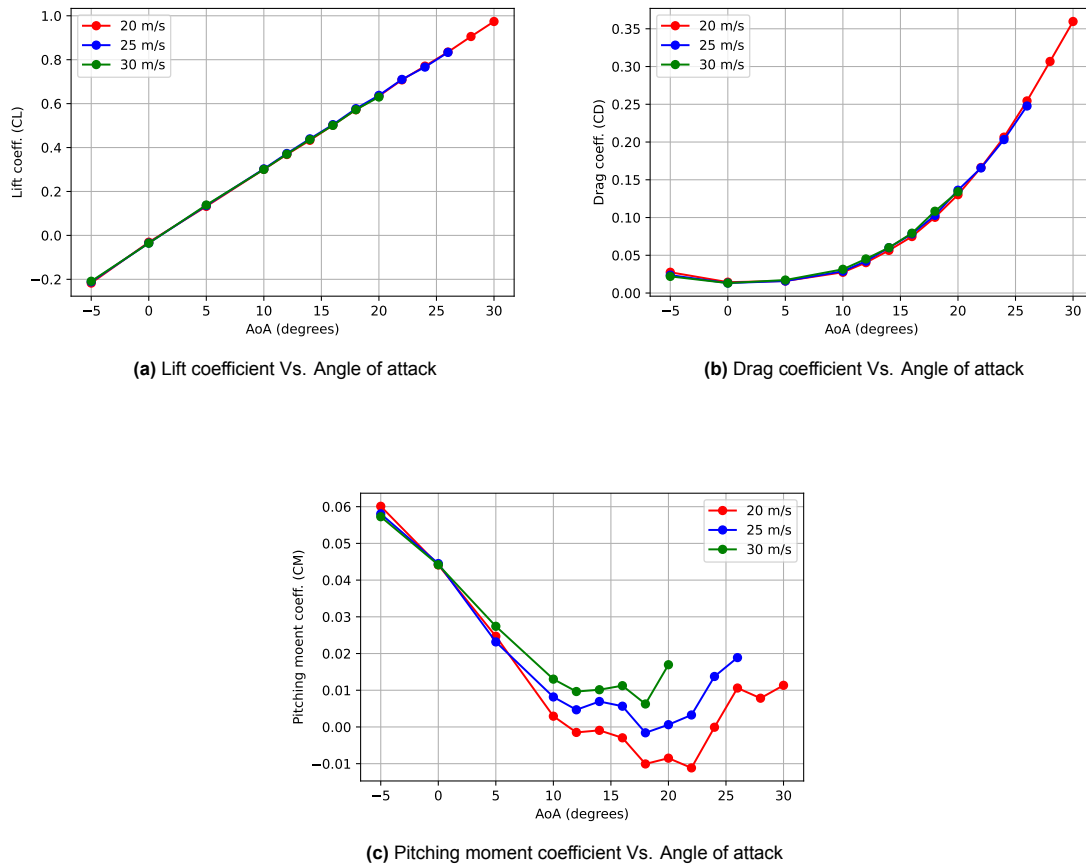


Figure 4.5: Effect of Reynolds number variations on the aerodynamic coefficients for clean wing

There is a significant compatibility between the lift and drag curves for the three cases. There seems to be a slight drag rise after the angle of attack of 10 degrees for the 30 m/s case. This can be attributed to the onset of vortices from the leading edge of the model, this can increase flow separation and due to the higher velocity it appears to occur the earliest on the highest Reynolds number case. This is not unexpected. Unlike the lift and drag coefficients, larger differences are observed for the pitching moment coefficient. While the overall behavior of the pitching moment coefficient curve is identical in all three cases, the values differ. The graphs diverge after the angle of attack of 5 degrees and the cases with larger Reynolds numbers show a more positive value of pitching moment coefficient. The reason for this behavior can be the fact that separation on the outer wing occurs earlier for the cases with higher Reynolds number meaning there is a loss of force behind the center of gravity while the inner wing is generating strong lift resulting in a more positive pitching moment. This phenomena does not occur as intense for the lowest Reynolds number and therefore the pitching moment coefficient takes on more negative values. Another interesting observation is that there is a much smaller difference between 25 and 30 m/s than there is between 20 and 25 m/s. This can hint to the conclusion that the model behavior is independent of Reynolds number effects after a certain limit. However, this experiment is not a sufficient evidence to arrive at this conclusion for certain but can be stated as an assumption for future reference.

The changes in Reynolds number were also experimented for a few configurations with flaps on. The results for the case of flap E on the wing is shown in Figure 4.6

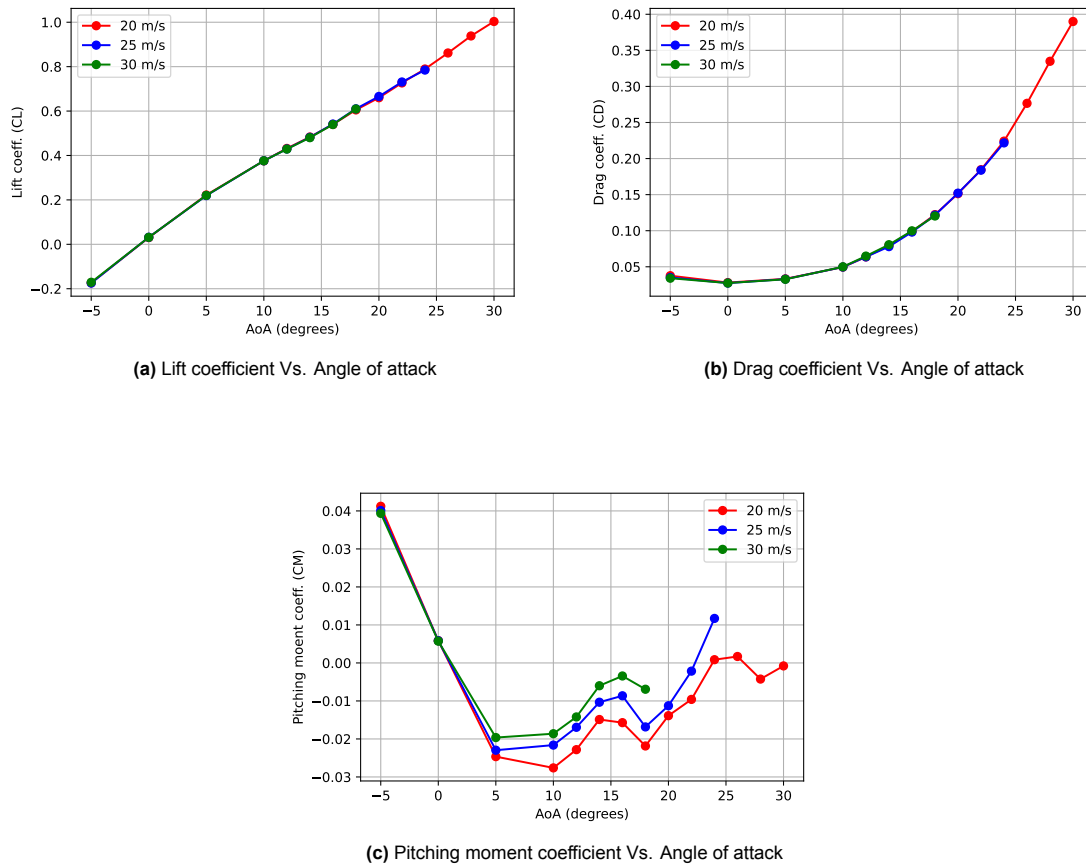
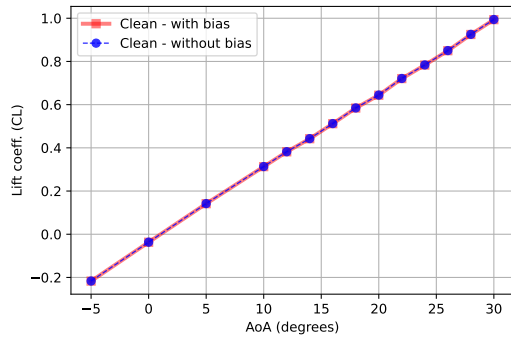


Figure 4.6: Effect of Reynolds number variations on the aerodynamic coefficients for wing with flap E

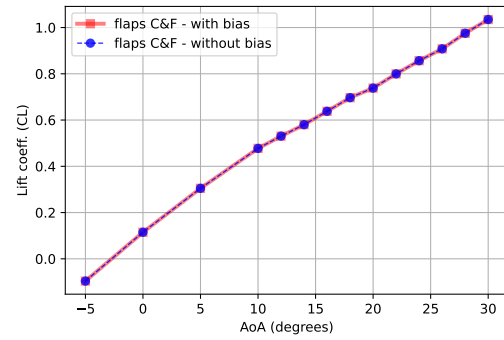
The same conclusions can be made for this case with flaps on. There are no significant differences in lift and drag coefficients as was for the clean wing. The pitching moment coefficient shows more distinction between the three different speeds, however, these differences are less than the case with clean wing, meaning that the presence of the flap in region 2 delays the loss of lift and the effect of velocity on changing of the aerodynamic center.

4.3. Systematic Error Check

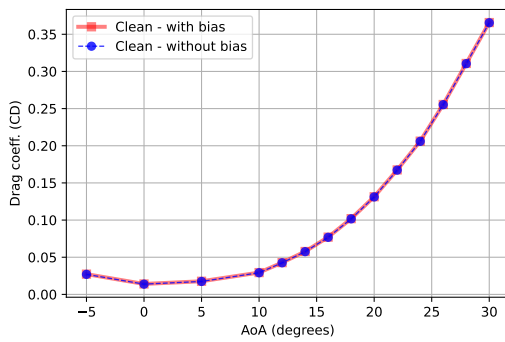
A way to assure the quality of data obtained from the wind tunnel model is to check for the presence of systematic errors. If present, there would be a consistent drift in the data. To check for this, at the beginning and end of each measurement, bias measurements were taken, with the wind speed of 0 m/s and AoA of 0° . These measurements then were interpolated for the whole range of the angle of attack to find the bias for each measurement point. The biases were then subtracted from each corresponding value to remove the noise in the measurements. If there is a large differences between the values before and after the bias is removed, it is an indicator of a systematic error. This can occur due to instrument drift, thermal gradients, creep or incorrect model settings. Figure 4.7 shows C_L , C_D and C_m coefficients before and after the biases are removed for clean wing and wing with flaps C&F on.



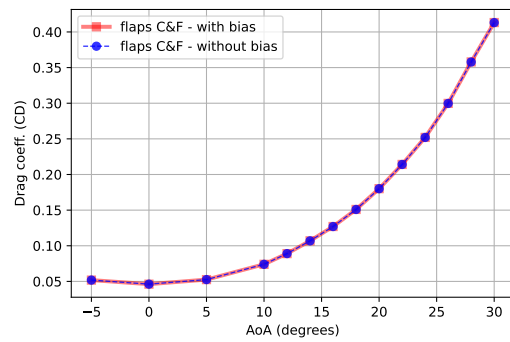
(a) Lift coefficient Vs. angle of attack before and after removing the bias for clean wing



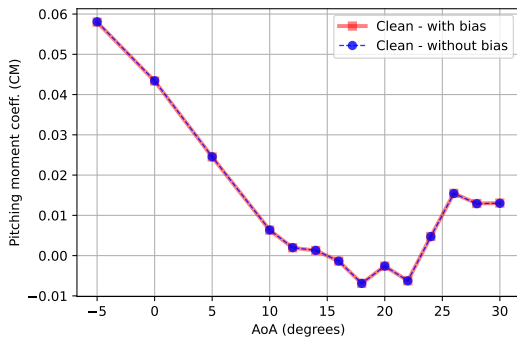
(b) Lift coefficient Vs. angle of attack before and after removing the bias for wing with flap C&F on



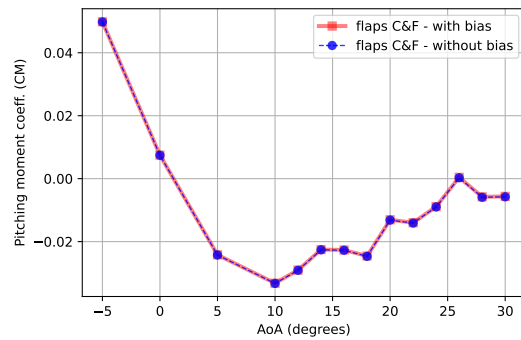
(c) Drag coefficient Vs. angle of attack before and after removing the bias for clean wing



(d) Drag coefficient Vs. angle of attack before and after removing the bias for wing with flaps C&F on



(e) Pitching moment coefficient Vs. angle of attack before and after removing the bias for clean wing



(f) Pitching moment coefficient Vs. angle of attack before and after removing the bias for wing with flaps C&F on

Figure 4.7: Comparison of aerodynamic coefficients before and after removing bias for clean wing and wing with flaps C&F on

As observed in Figure 4.7, there are insignificant differences between the data straight from the measurements and the case were the noise is removed. This proves the absence of systematic errors. To put this in more quantitative perspective, the maximum differences between the two data series and their respective P-values were calculated and are shown in Table 4.1.

Table 4.1: The maximum differences and P-values of aerodynamic coefficients before and after removing the biases for clean wing and wing with flaps C&F on

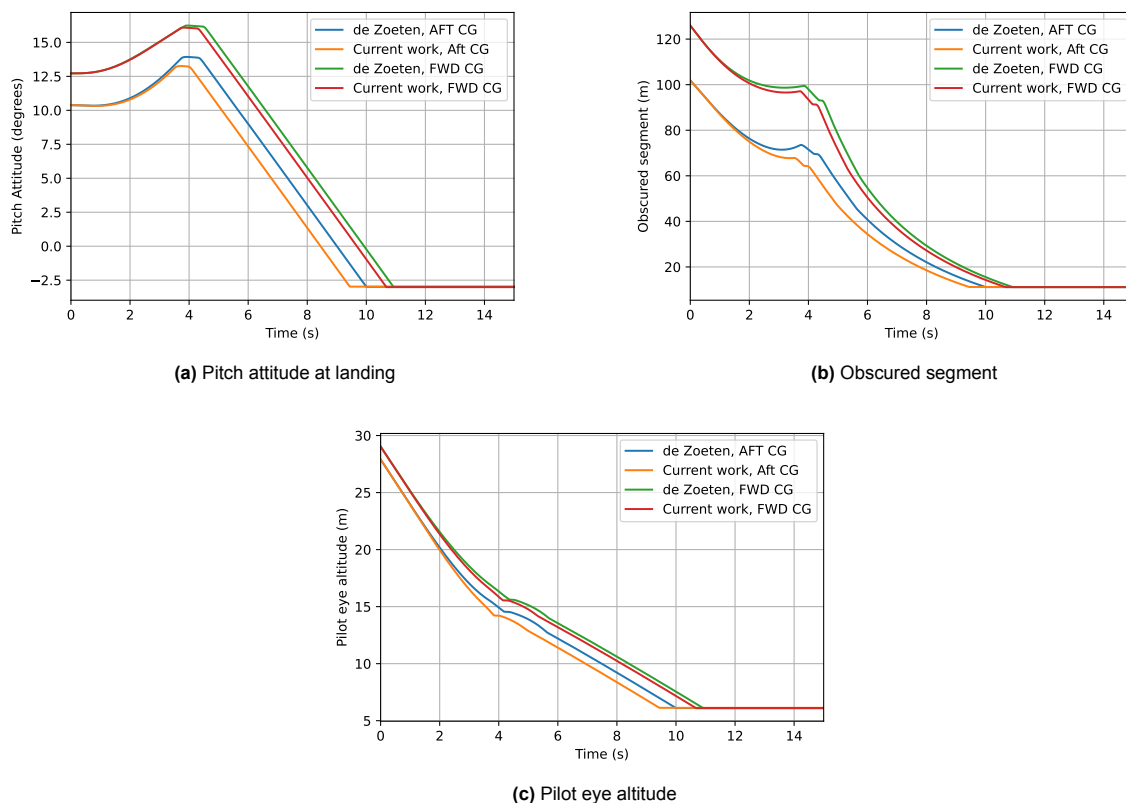
Aerodynamic property	Maximum difference for clean	P-value for clean	Maximum difference for flaps C&F	P-value for flaps C&F
C_L	-0.00414	0.99672	-0.00084	0.99944
C_D	0.006194	0.99510	0.00069	0.99944
C_m	-0.00200	0.99841	0.01167	0.99077

As shown in Table 4.1, there is an extremely small difference in the data measurement caused by noise which results in a very high P-value. This indicates that there were no systematic error occurring during the wind tunnel test experiment and a high quality of data was assured. This was achieved, by close monitoring of the environmental conditions such as temperature and pressure throughout the campaign and accurate calibration of the balance as well as maintaining out-most consistency in the set-up of the experiment.

4.4. Verification of the Flight Performance Analysis

After being assured of the validation and verification of the experimental data. The flight performance analysis must also be verified. In this section, the analysis performed in this study is compared to the results obtained by de Zoeten in his thesis [14], for further read on the verification of the flight performance model it is advised to refer to his findings.

To assure the verification of flight performance model for landing analysis, the experimental data from the clean wing measurements were fed into PHALANX and the results were compared to the data obtained by de Zoeten. To avoid overcrowding the diagrams, mid CG has not been shown.

**Figure 4.8:** Comparison of landing performance using de Zoeten's and the clean wing data obtained from the wind tunnel test

Firstly, note that the goal of the analysis was not matching the results of two data set precisely,

since de Zoeten's data were obtained using Odilila and the current data were obtained from the wind tunnel test. Additionally, the wind tunnel data were scaled to match the full-scale aircraft, which was prone to some unavoidable error. At the time of the writing of this thesis, a completely valid method of scaling the wind tunnel data for the Flying-V is being studied and not yet realized. However, there is a great similarity between the two analysis which is sufficient for verifying the applied method for landing analysis. For further analysis, the clean wing results of the wind tunnel have been used as the baseline.

5

Results & Discussion

This chapter presents the results of the wind tunnel experiment and the flight performance analysis of this thesis project and therefore, is divided into two main sections. Firstly, section 5.1 presents the results and discussion of the Wind Tunnel Experiment. Next, section 5.2 presents the results and discussion of the landing performance analysis.

5.1. Aerodynamics of Split Flaps

As discussed in chapter 3, before conducting the experiments, six variations of flaps were designed in addition to different brackets for applying the deflection angles. In this section, results for a selection of single flap and multi flap configurations are shown. The plots that are shown and discussed are the following where the coefficients are defined in Equation 3.7 and Equation 3.8:

- **Lift coefficient (C_L):** this is the most important criterion to judge the flap performance on, since the first goal of deploying flaps is increasing the lift coefficient
- **Drag Coefficient (C_D):** flap deployment shall not cause a significant increase in drag, otherwise it deteriorates the overall performance of the wing
- **Pitching moment coefficient versus the angle of attack (C_M Vs. α) and versus the deflection angle (C_M Vs. δ_f):** it is important that deploying the flaps and changing their deflection angle have minimal effect on the change in pitching moment of the wing, otherwise there will be a need for trimming the wing using control surfaces which can negate the increase in lift by the flap
- **Rolling moment coefficient (C_l):** this criterion was considered to check whether the flaps could potentially be used for roll control as well

Note that there were in total six single-flap, four double-flap and one full-span flap tested, therefore, not all the results are shown in this section to avoid repetition. The flaps not shown here can be found in Appendix B. As a reminder an illustration of the CAD model of the wing with different flaps is shown in Figure 5.1.

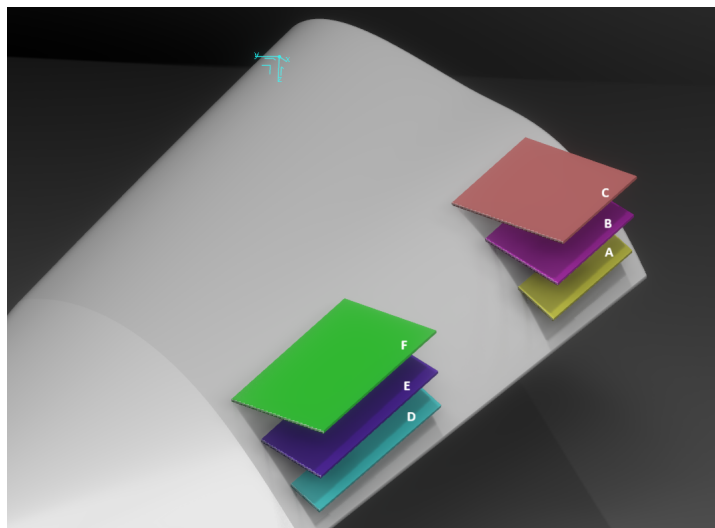


Figure 5.1: CAD model of flaps A to F placed on the half-wing wind tunnel model of the Flying-V

5.1.1. Results of the Experiments with Single-flap Configurations

Firstly, the results of the tests conducted with only one flap on the wing model are shown. The flaps shown are A on region 1 placed at the 90% of chord, B in region 1 placed at 80% of the chord and F in region 2 placed at 70% of chord.

Flap A

A refers to the case where the flap has a chord wise length equal to 10% of the root chord of the half-wing model and a span equal to L1 that is the span of the region 1 which is the region closer to the root of the wing as explained in chapter 3. Please note that the number of tests conducted using each flap were not the same. Flap A was tested on both regions R1 and R2 and on R2 its chord-wise position was also changed.

The results of testing flap A on region 1 are shown in Figure 5.2. While an increase in lift coefficient of 0.12 is obtained, the deflection angle at which it occurs is the highest one (60°). By having a 10° deflection angle there is a maximum increase of 0.04 in lift coefficient. On the other hand, the drag rise is also quite small for this flap, which is not surprising given the small size of flap A. Looking at the pitching moment graphs, we can see a pitch break around 24° angle of attack, however, adding the flap seems to have minimal effect on the pitching moment when comparing to clean wing. Another desired outcome of the flap is minimal change in pitching moment by changing the flap's deflection angle, which holds true for flap A.

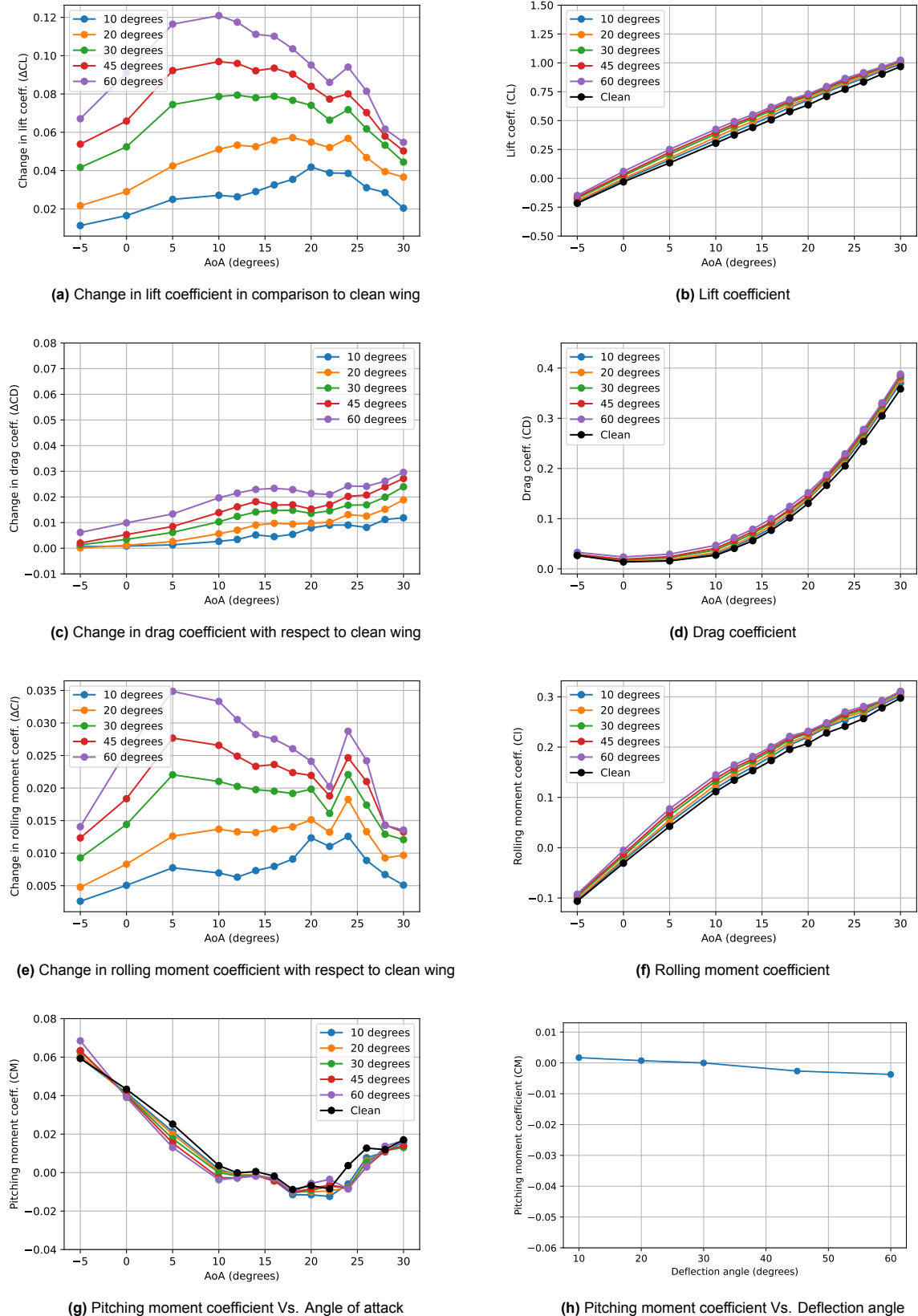


Figure 5.2: Results of Flap A in Region 1 at 90% of the chord

If we look at the flap behavior, we can see a clear distinction between different ranges of angle of

attack. Starting from the low AoA of 5° to 10° it is observed that the increase in lift coefficient is on the rise, with AoD of 60° and 45° arriving at their highest increase in lift coefficient at 10° AoA. This could indicate that, at 5° the flow at region 1 is still quite undisturbed and follows the direction of free stream flow. If the AoA is increased to 9° we can see the effect of cross flow at region 1 getting stronger, however, no separation has occurred yet. The presence of the cross flow nonetheless starts to affect the aerodynamic performance of the flap such that increase in lift reaches a maximum at 10° AoA. This can also be observed in drag increase, where from 0 to 10 degrees the increase in drag for all deflection angles follows an upwards trend.

From 12° to 20° there seems to be a more stable region where the change in lift coefficient and drag coefficient stay at the same value for all deflection angles. At these angles the vortex roll-up is getting stronger which creates a vortex lift. This seems to be compensating for the cross flow occurrence near the trailing edge on region 1 which leads to a positive outcome for lift increase but is less dependent on the increase of angle of attack.

After the AoA of 20° , the increase in lift goes down for all AoD except for a small rise on 24 degrees AoA. We also observe the pitch break at 24° AoA, after which the increase in lift reduces rapidly. These angles are considered high which can create a large amount of cross flow and separation, combining with the pitch break it is expected that the performance of flaps deteriorates. However, the fact that the flaps have a quite stable performance up until the pitch break and even continue to produce additional lift after that is a desirable outcome.

It should be noted that no flow visualization methods were used during current research and therefore the statements on the flow behavior on the wing and the current data must be taken with caution. Nonetheless, there seems to be an explanation for the behavior of flaps regarding the flow patterns. It is definitely an interesting research to look at the flow patterns on the wing while having the flaps mounted, in the future.

Considering the outcome of all the experiments with flap A on, shown either in this section or Appendix B, the case where flap A was placed on region 1, indicates a clear superiority, especially in lift increase. Therefore, the best case for flap A was chosen to be the case where it is placed on region 1, at 90% of the chord. For conciseness this is referred to as A in 0.9C R1 from now on.

Flap B

This flap was the most tested one. It was placed on both regions 1 and 2 on the 0.8C chord-wise position as well as testing for both regions at the same time. Additionally, due to extra time it was tested for full-span case next to flap E. The results for the multi flap cases are shown later on. Note that since flap B refers to L1 span and 0.2C chord length, two versions were made with one having 80% of the chord length of the root chord for R1 and the other 80% of the chord length of the kink chord for R2. Figure 5.3 shows the case where the flap is positioned in region 1. For the results of the other tests with flap B refer to Appendix B.

It is seen in Figure 5.3 there is a significant increase in lift, even with lower deflection angles. There also is not a big difference between 45 and 60 degree deflection angles. It is quite impressive how flap B has a large increase in lift throughout different AoA even for lower deflection angles, however, we do see a big jump between 20° and 30° AoD.

The drag rise is slightly more than flap A but that is to be expected due to larger size of flap B. The maximum increase in rolling moment coefficient is about 0.04. Additionally, the pitching moment behavior is quite similar to clean wing with pitch break occurring around 22° angle of attack. Furthermore, the change in pitching moment coefficient with deflection angle is quite small.

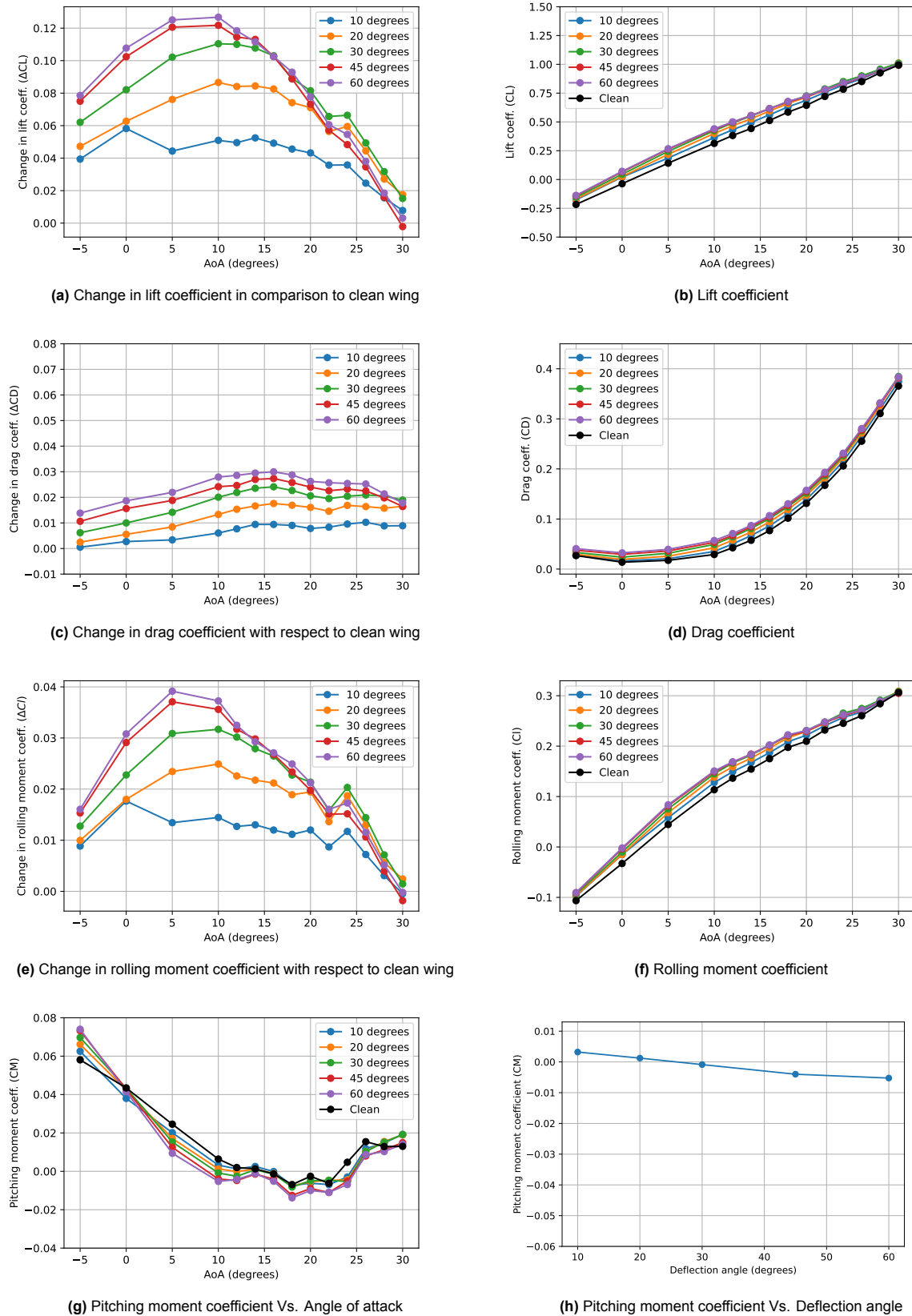


Figure 5.3: Results of flap B in Region 1 at 80% of the chord

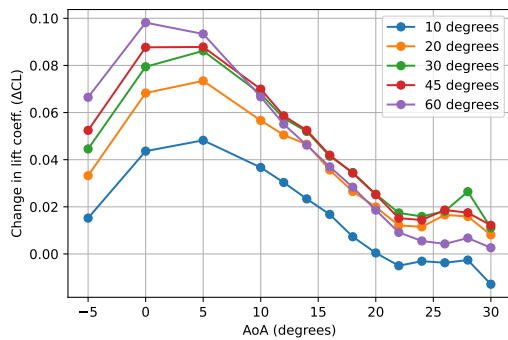
Similar to flap A, the maximum increase in lift is achieved at 10° AoA for all cases except for 10

degree AoD. However, the lift increase is declined between the AoA of 10 and 20 degrees. Nonetheless a minimum 0.08 increase in lift coefficient is maintained for the three larger AoD. The change in the $C_L - \alpha$ curve gradient after 10° AoA is also visible which indicates the generation of vortex lift. Moreover, the effect of pitch break is quite clear in the lift coefficient graphs where after AoA of 22° the flap performance declines. The separation on the wing seems to be amplified by flap B and cause a large drop in lift increase, even though the drag stays more or less constant. Another noticeable thing is that after the pitch break the flap B at 30° deflection angle continues to produce lift and surpasses all the other AoD.

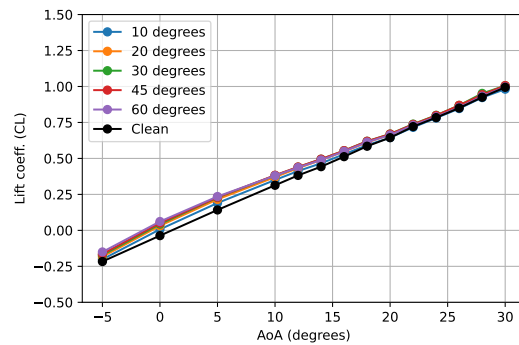
Flap F

This flap has a span of L2 and chord-wise length of 30% of the chord at region 2, making it the largest flap in terms of surface area. F was tested on 0.7C at region 2 only. Figure 5.4 shows the results for this flap. The increase in lift is lower than flap B while also having a larger drag increase. Additionally, there is a large increase in rolling moment coefficient with respect to clean wing.

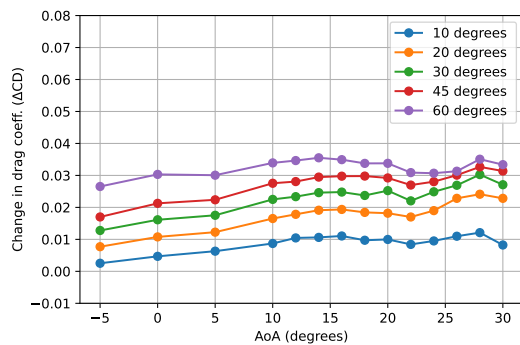
The change in pitching moment coefficient in comparison to clean wing is quite noticeable. Which can be attributed to the location of the flap. Since region 2 has a larger moment arm to the CG than region 1, the effect of flap placement on pitching moment is more prevalent. It also produces a nose down pitching moment when increasing the deflection angle which is expected since flap F is placed in region 2, behind the aerodynamic center.



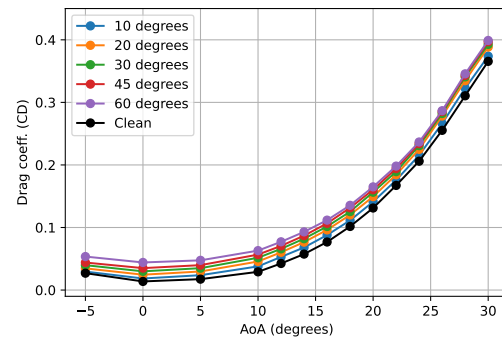
(a) Change in lift coefficient in comparison to clean wing



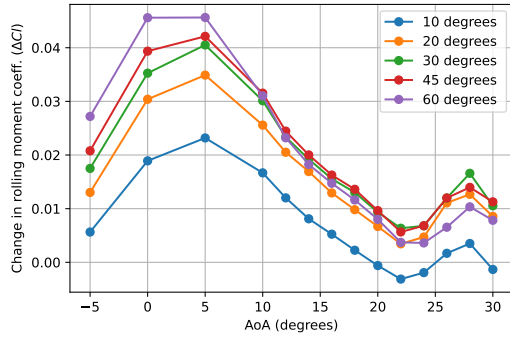
(b) Lift coefficient



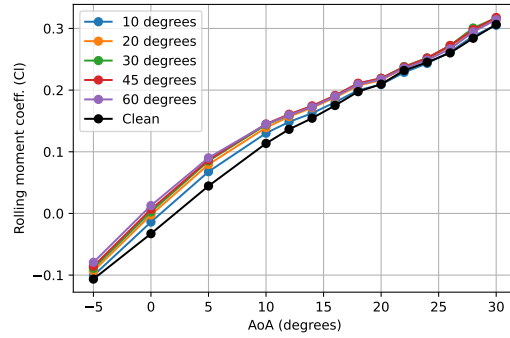
(c) Change in drag coefficient with respect to clean wing



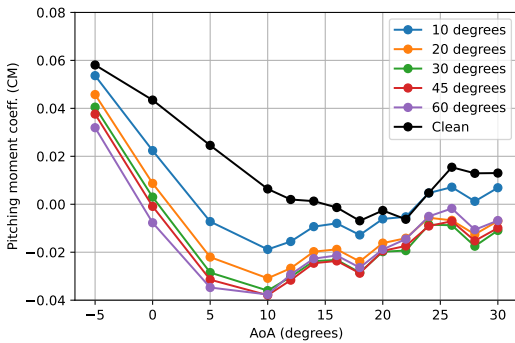
(d) Drag coefficient



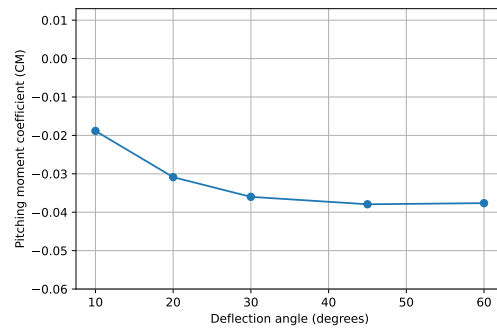
(e) Change in rolling moment coefficient with respect to clean wing



(f) Rolling moment coefficient



(g) Pitching moment coefficient Vs. Angle of attack



(h) Pitching moment coefficient Vs. Deflection angle

Figure 5.4: Results of Flap F in Region 2 at 70% of the chord

It is valuable to compare the flap behavior to previous cases. Unlike A and B the highest lift coefficient increase is achieved early on, at the AoA of 0° or 5° depending on the deflection angle. At the 5° AoA, the flow over region 2 is still experiencing low disturbance and follows the pattern of the incoming flow on the wing. By increasing the AoA, it is expected that the cross flow gets much stronger on region 2, even resulting in separation near the kink. This is one reason for the performance of flap F deteriorating already after 5 degree AoA. When increasing the angle of attack further the cross flow gets stronger and a separation starts to occur. With this the flap performance goes down rapidly. For 10 degree AoD the flap stops increasing lift after 20° and even causes a slight lift reduction, essentially acting as a spoiler.

We can also observe a change in behavior of pitching moment vs AoA where the slope changes sign at 10° AoA, but maintaining a somewhat constant slope until 30°. It can be concluded that even though there is not a drastic pitch break, placing the flap on region 2 requires a larger moment for trimming the wing from the control surfaces. The effect of region of placement is discussed further in subsection 5.1.4.

5.1.2. Results of the Experiments with Multi-flap Configurations

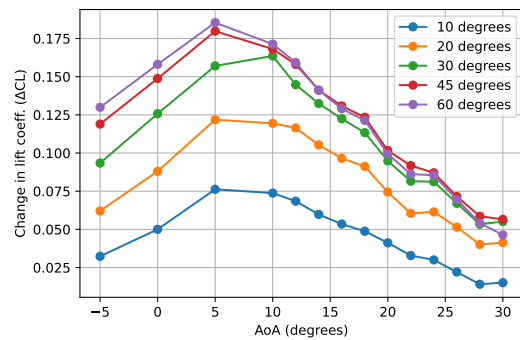
For testing the multi-flap configurations, it was initially only planned to place the two versions of flap B on both regions, however, due to additional time more configurations were tested. The results of the multi-flap experiments are shown in this subsection.

Flaps B and E

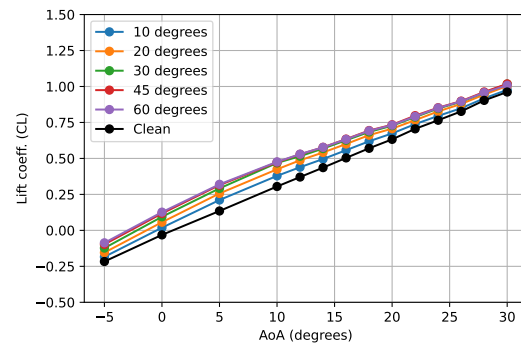
For this, flap B was placed on R1 and flap E on R2 both at 80% of the chord. Figure 5.5 shows the results. The increase in lift coefficient is significantly higher than single-flap cases but behaves similarly to flap F in terms of achieving the highest increase in lift coefficient at 5° AoA. It could be concluded that the flow in region 2 is more dominant than region 1. The decline in lift coefficient is however, less rapid than F. Even at the low AoD of 10 degrees the flaps continue to perform well.

As it is expected the increase in drag is also higher in comparison to single flaps. The increase in drag has an upward trend until 10° AoA and becomes more or less constant afterwards. One reason for this could be the fact that the change in the slope of pitching moment Vs AoA curve occurs at 10° but stays very close to zero up until 25° AoA, meaning there is no pitch break and therefore no significant drag rise.

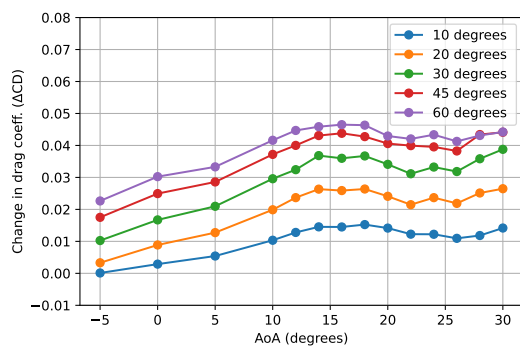
There is a significant increase in rolling moment which is desirable. Additionally, the change in pitching moment with changing deflection angle is low. The flaps seem to produce a nose down moment which means the lift produced by E placed behind the aerodynamic center is dominant.



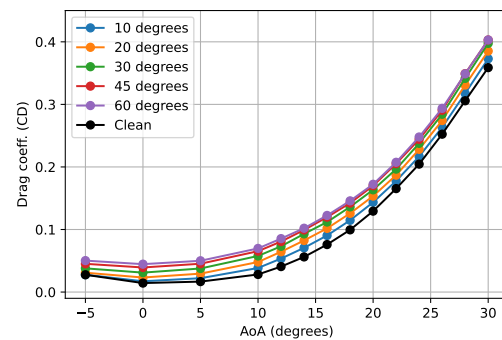
(a) Change in lift coefficient in comparison to clean wing



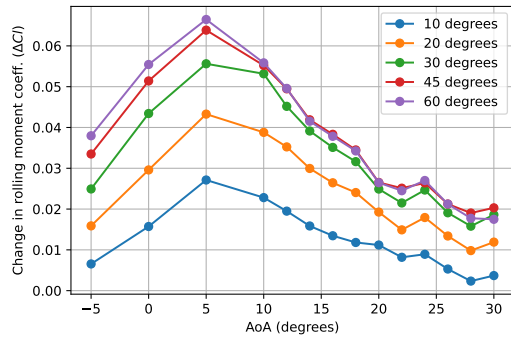
(b) Lift coefficient



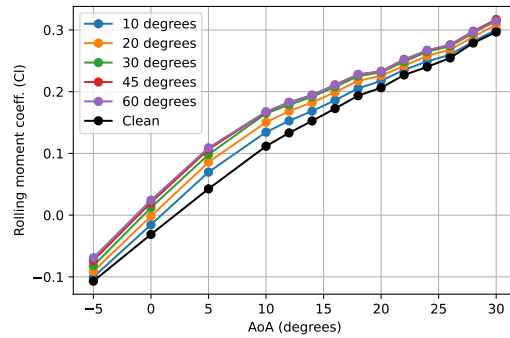
(c) Change in drag coefficient with respect to clean wing



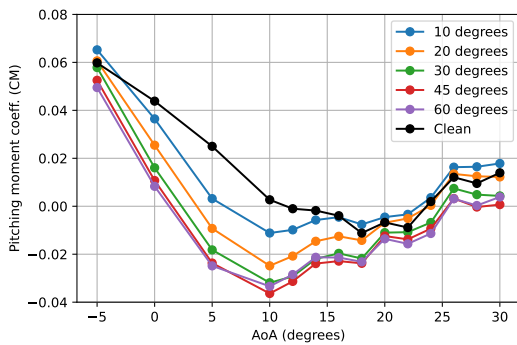
(d) Drag coefficient



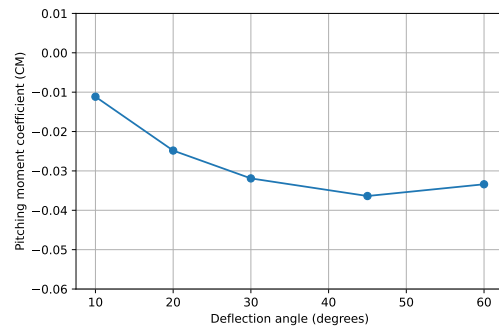
(e) Change in rolling moment coefficient with respect to clean wing



(f) Rolling moment coefficient



(g) Pitching moment coefficient Vs. Angle of attack



(h) Pitching moment coefficient Vs. Deflection angle

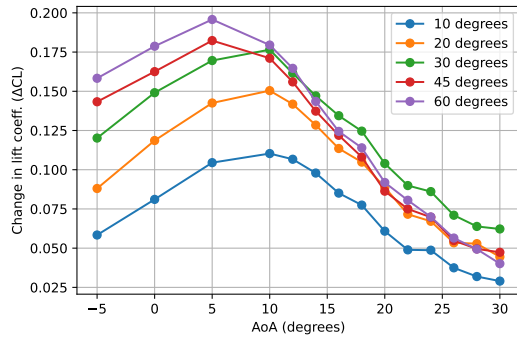
Figure 5.5: Results of Flaps B and E at 80% of the chord in both regions

Flaps C and F

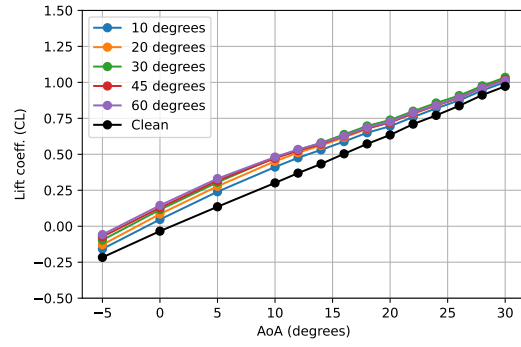
For this, flap C was placed at 0.7C on region 1 and flap F was placed at 0.7C on region 2. There seems to be an improvement in comparison to the B&E case shown in Figure 5.5 in terms of increasing lift coefficient. Another interesting behavior is that the flaps at 30° AoD start to surpass larger AoDs after 14 degrees AoA. This could be due to the large size of the flaps which hastens separation if placed at large deflection angles. Nonetheless, the flaps perform quite well in all deflection angles. The trends at which the lift increases is similar to B&E.

The increase in drag is also higher than B&E due to larger size of the flaps, however, seems to be more stable throughout with no significant change after 10° AoA.

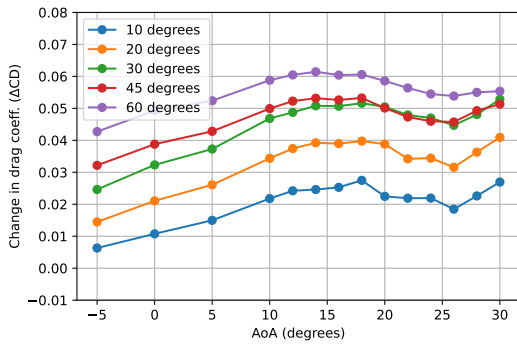
There is also a large rolling moment coefficient produced. Change in slope of the pitching moment vs AoA curve occurs at 10° but it remains very close to zero showing an acceptable longitudinal stability when using the flaps. The flaps also produce a nose down pitching moment with insignificant changes with changing the deflection angle.



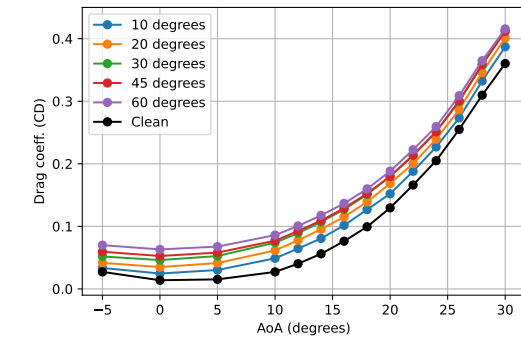
(a) Change in lift coefficient in comparison to clean wing



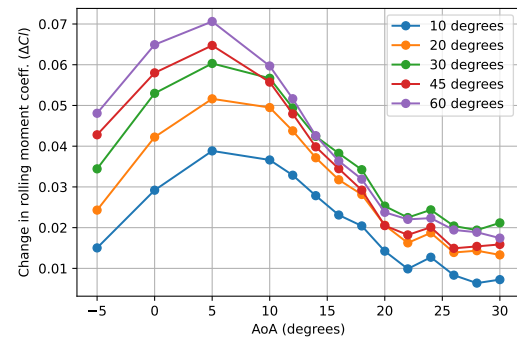
(b) Lift coefficient



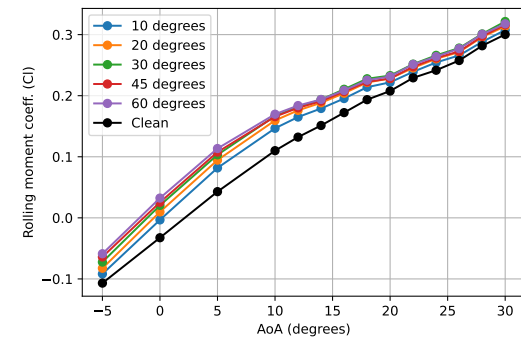
(c) Change in drag coefficient with respect to clean wing



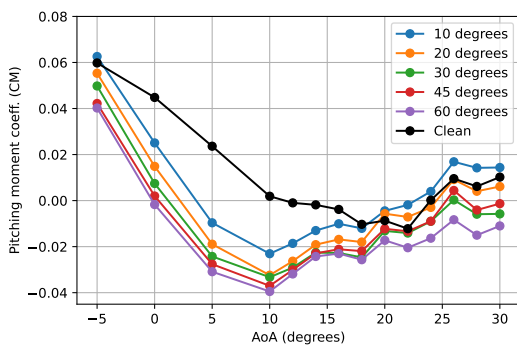
(d) Drag coefficient



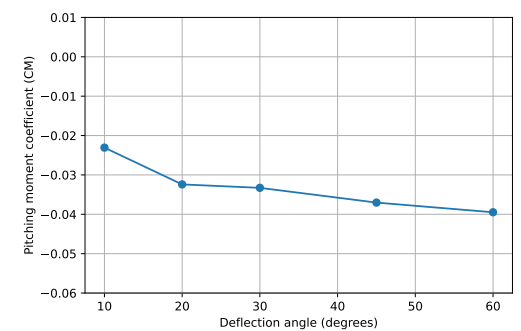
(e) Change in rolling moment coefficient with respect to clean wing



(f) Rolling moment coefficient



(g) Pitching moment coefficient Vs. Angle of attack



(h) Pitching moment coefficient Vs. Deflection angle

Figure 5.6: Results of Flaps C and F at 70% of the chord in both regions

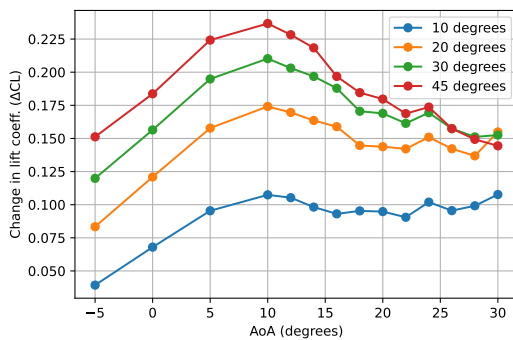
Full-Span

Lastly, the case of having flaps on the full span of the inboard wing was tested. Note that, these measurements were not originally planned and therefore there was a lower level of accuracy involved. This was achieved by placing the two versions of B on R1 and R2 and then placing E in the middle region all on 0.8C. There was still a small region which was not covered. Additionally, the 60° deflection angle was not tested due to the limitation of the balance measurements and the OJF.

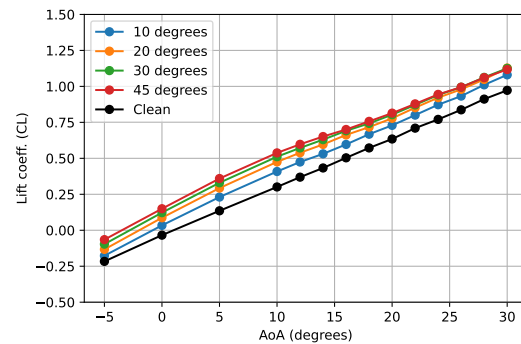
As expected, the increase in lift is higher than the two-flap cases. The case with 10° performs significantly poorer than higher AoD's. But the overall trend in the behavior of lift increase is similar to double-flap configurations. As expected there is also higher drag than double-flap. The behavior has also changed where the drag increase follows an upward trend until about 14° AoA and stays constant afterwards except for 10° AoD where drag continues to increase.

Additionally, the increase in rolling moment coefficient is also higher than previous cases. Looking at the pitching moment coefficient graphs, there is a change of sign of the slope around 10° , however, the wing seems to be stable throughout. Although the difference between clean wing and full-span is significant, meaning the trimmed state of the wing is more disturbed than the double-flap cases.

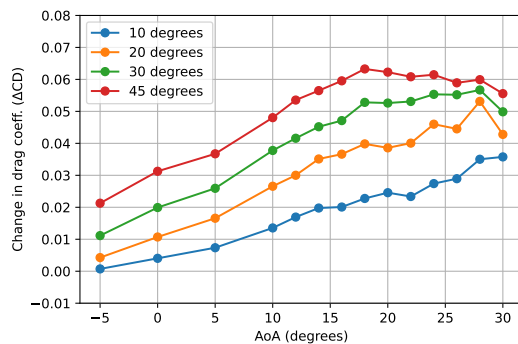
There is also a small change in pitching moment with deflection angle, with the moment being nose down throughout meaning the resultant lift was being produced behind the CG.



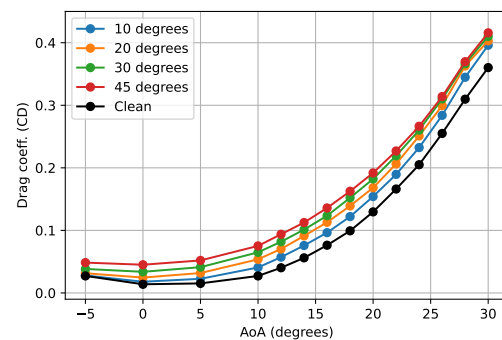
(a) Change in lift coefficient in comparison to clean wing



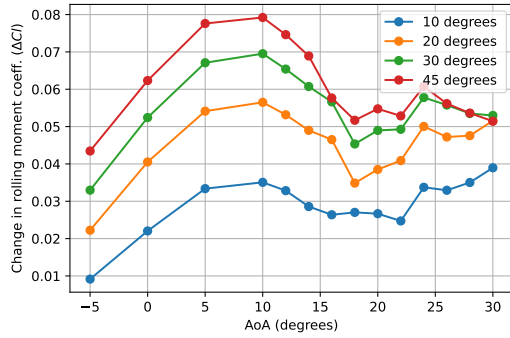
(b) Lift coefficient



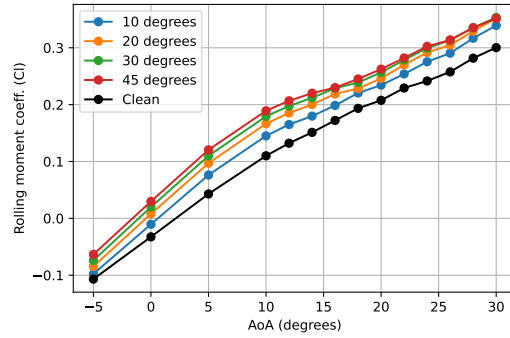
(c) Change in drag coefficient with respect to clean wing



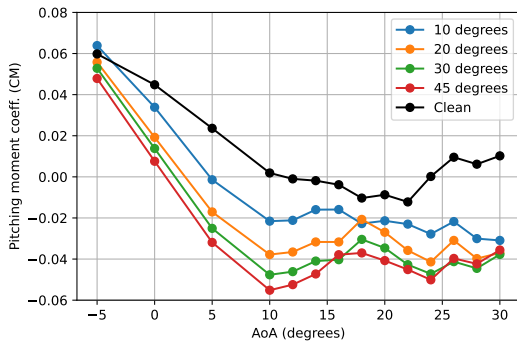
(d) Drag coefficient



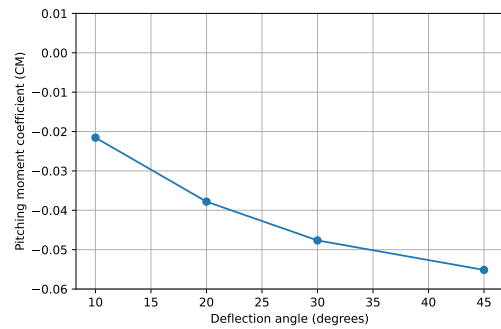
(e) Change in rolling moment coefficient with respect to clean wing



(f) Rolling moment coefficient



(g) Pitching moment coefficient Vs. Angle of attack



(h) Pitching moment coefficient Vs. Deflection angle

Figure 5.7: Results of Full-span flap at 80% of the chord

Now that different configurations have been discussed, it is time to compare them together to select the best configuration for each flap in subsection 5.1.3.

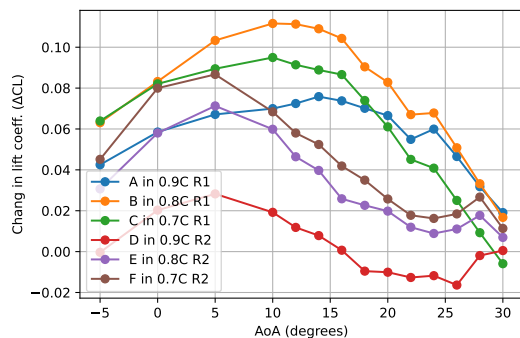
5.1.3. Selection of the Best Flap Configuration

In this section, the process for selecting the best flap configuration is laid out. Firstly, the single-flaps and multi-flap configurations have been compared separately. The methodology was comparing the performance of each flap for deflection angle of 30° in each of the criteria. This deflection angle was chosen as a middle ground considering the range of the angles that were tested. After analyzing the graphs a trade-off was set up to select the final flaps.

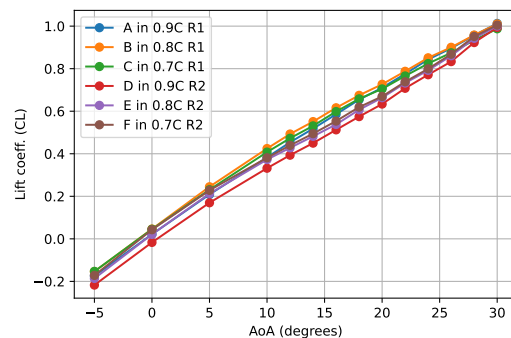
Single-flap Configurations

As mentioned, the results for the deflection angle of 30° for each configuration were compared in each of the measured criteria. The results are shown in Figure 5.8. Starting with lift coefficient, flap B in 0.8C R1 is producing significantly more lift in comparison to the others, which is a big plus for this flap. Flap D is performing significantly worse than the rest, making it an undesirable option. Moreover, flaps E and F seem to generate a higher lift up until 5° deflection angle and then their lift generating ability is reduced, whereas B, C and A are more consistent in increasing lift throughout. Moving on to drag, C and F produce more drag than the rest which is expected since those are the two largest flaps. D has lowest drag production again due to its small size. Looking at the L/D graph we can see that the smallest flaps, A and D have the highest lift over drag, followed by B and E and the worst performing are C and F. The graph makes perfect sense since it is attributing the performance to the size of the flaps. Furthermore, F is producing the highest rolling moment, followed by B and E, with B having a more consistent increase throughout.

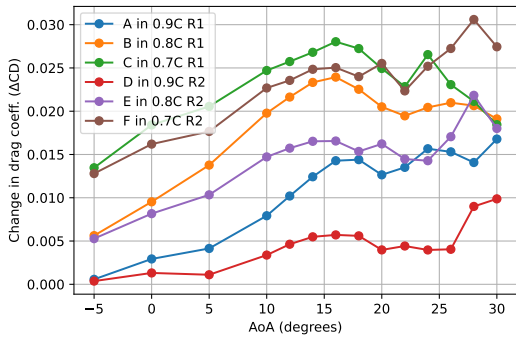
Based on the pitching moment versus the angle of attack graph we can see a better stability with A, B and C flaps, since there is a smaller change in pitching moment with angle of attack. Additionally, the pitching moment coefficient starts to follow an upward trend around 10° for D, E and F flaps, even though the wing is still stable up until 22° . Whereas, the pitching moment coefficient is following a slope closer to zero for A, B and C with a pitch break occurring around 24° . All of these show a better longitudinal stability when using flaps A, B and C. The pitching moment coefficient versus deflection angle graph also confirms this by showing the difference in the slope of the curve for A, B and C in comparison to D, E and F. The small magnitude of which the pitching moment coefficient is changing with deflection angle should also be taken into account. As such the change in pitching moment caused by the flaps on region 1 is essentially zero.



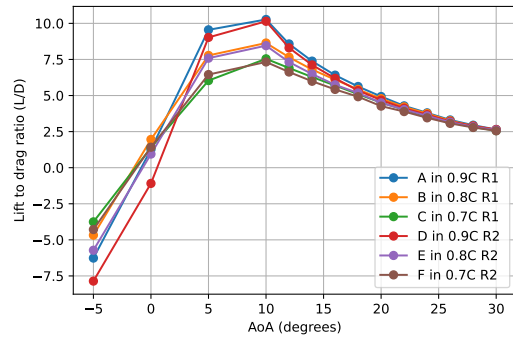
(a) Change in lift coefficient in comparison to clean wing



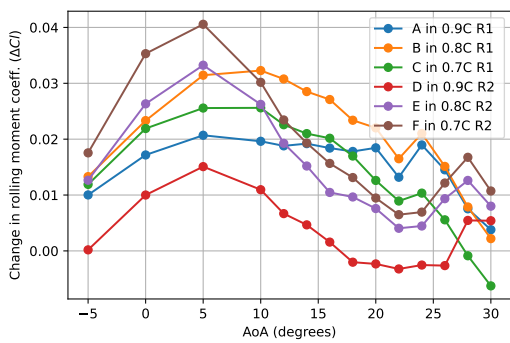
(b) Lift coefficient



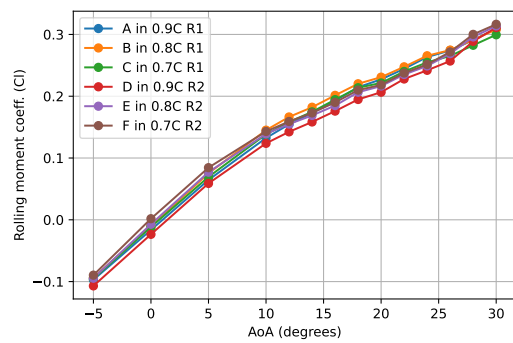
(c) Change in drag coefficient with respect to clean wing



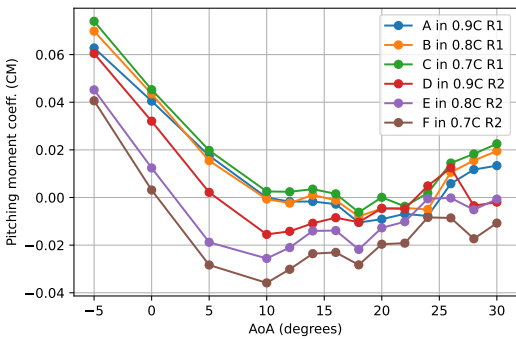
(d) Lift over drag



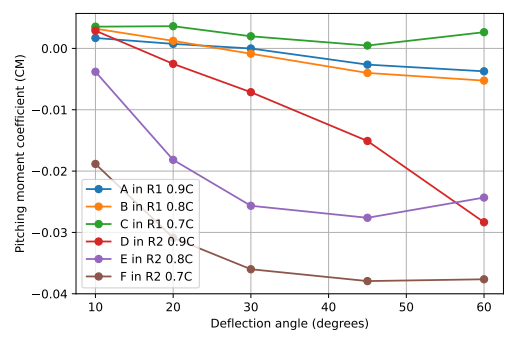
(e) Change in rolling moment coefficient with respect to clean wing



(f) Rolling moment coefficient



(g) Pitching moment coefficient Vs. Angle of attack



(h) Pitching moment coefficient Vs. Deflection angle

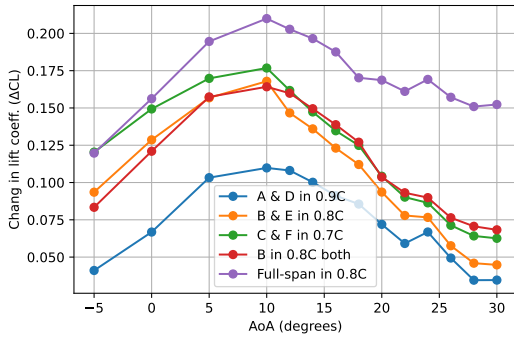
Figure 5.8: Best results of each single-flap configuration for 30° deflection angle

Overall, it is evident from the graphs that flap B is performing best among the single-flap configurations. However, since, some of the graphs show small differences in performance between different configurations a trade-off was also performed taking into account the numerical values, this is discussed in later in this section.

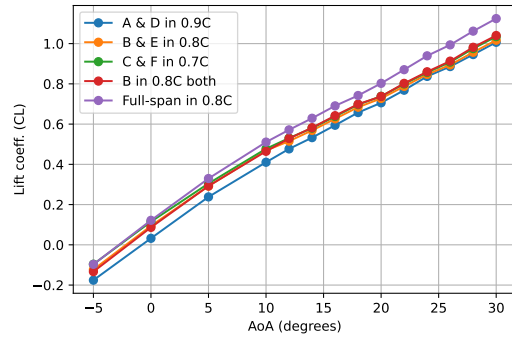
Multi-flap Configurations

Moving on to the multi-flap configurations. Starting with the lift coefficient change, as expected, the full-span flap is performing the best among the multi-flaps, after that C & F are performing best, however, B in both seems to catch up after around 12° angle of attack. A & D are performing significantly worse than the rest in terms of increasing the lift coefficient. Now considering drag, C & F flaps are producing more drag than the rest until angle of attack of about 16° where, full-span starts to produce more drag. As expected A & D are producing the least drag, which also leads to having the highest L/D. The largest

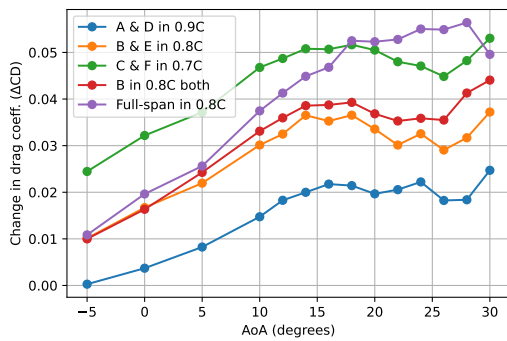
increase in rolling moment is also attributed to the full-span flap. Looking at the pitching moment coefficient versus the angle of attack graph, we observe the pitch break occurring more or less at the same angle of attack for all the configurations with the full-span maintaining more stability afterwards. The change in pitching moment with deflection angle also seems to be the lowest in C&F flaps. Another noteworthy observation is the magnitude of which the pitching moment changes with deflection angle, when comparing to single-flap configuration on region 1, the change is more prominent and cannot be neglected.



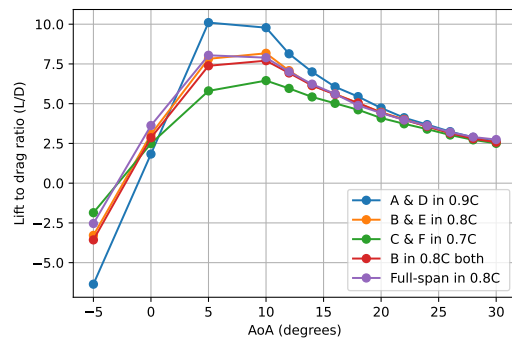
(a) Change in lift coefficient in comparison to clean wing



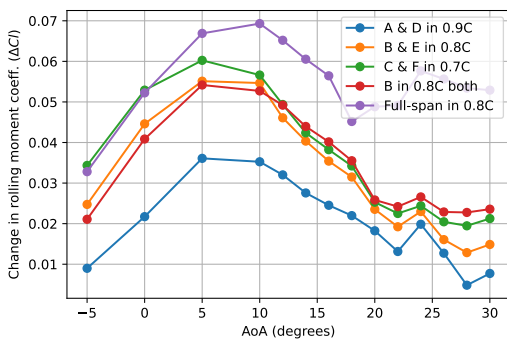
(b) Lift coefficient



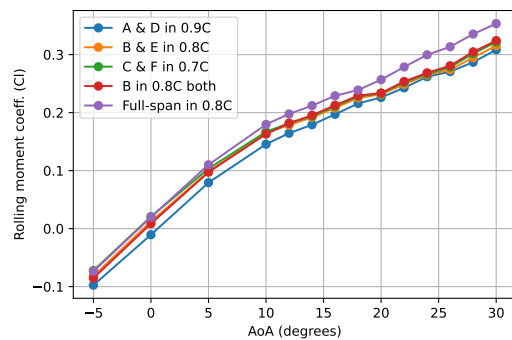
(c) Change in drag coefficient with respect to clean wing



(d) Lift over drag



(e) Change in rolling moment coefficient with respect to clean wing



(f) Rolling moment coefficient

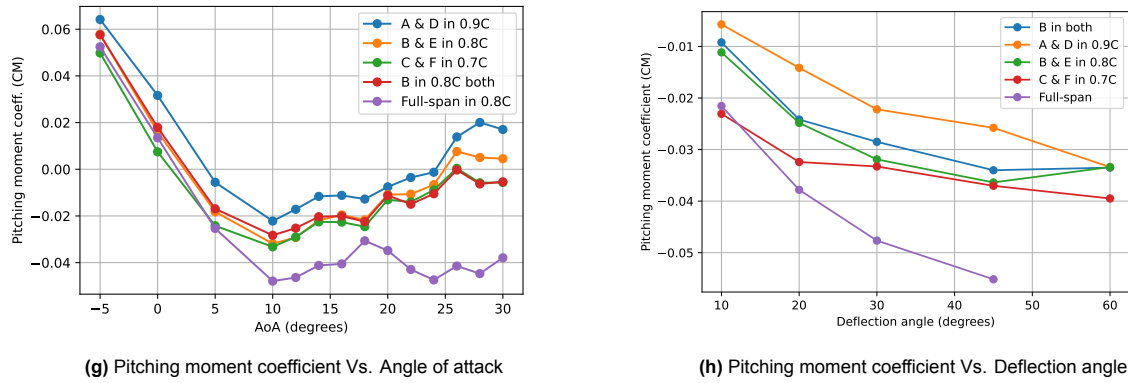


Figure 5.9: Best results of each multi-flap configuration for 30° deflection angle

Overall, C & F flaps are performing the best with regards to the criteria shown in Figure 5.9. However, to make a more accurate comparison a trade-off has been performed using numerical results.

Scoring

Now that the plots are all presented, a scoring is done to make sure the choices of the best flap configurations were supported by the data. The trade-off criteria were

- Lift coefficient (C_L)
- Drag Coefficient (C_D)
- Change in pitching moment coefficient with deflection angle ($\frac{dC_m}{d\delta_f}$)
- Rolling moment coefficient (C_l)

The results for the 30° deflection angle were taken from the data and the highest value for each flap in each criterion was recorded. The best performing flap for each criterion was given a score of 1 and the rest were given a score proportionate to the best performing flap. The scoring table for single-flap configuration is shown in Table 5.1.

Table 5.1: Normalized scores in each criteria for the single-flap configuration

Criteria	ΔC_L	ΔC_D	$dC_m/d\delta_f$	ΔC_l	Total
A in 0.9C R1	0.7	0.6	0.6	0.5	2.4
B in 0.8C R1	1	0.4	0.4	0.8	2.6
C in 0.7C R1	0.8	0.3	1	0.6	2.7
D in 0.9C R2	0.2	1	0.1	0.4	1.7
E in 0.8C R2	0.6	0.4	0.1	0.8	1.9
F in 0.7C R2	0.8	0.3	0.2	1	2.3

Based on the obtained scores by each flap presented in Table 5.1, it was evident that flap B and C were performing best, but since flap C seems to induce pitch up tendency as evident by Figure 5.8, it was decided to choose flap B for further analysis. Another reason for choosing B over C was that B continues to increase lift until the highest tested AoA whereas C starts to lift dump after 26° AoA.

Table 5.2: Normalized scores in each criteria for the multi-flap configuration

Criteria	ΔC_L	ΔC_D	$dC_m/d\delta_f$	ΔC_l	Total
A&D in 0.9C	0.6	1	1	0.5	3.1
B&E in 0.8C	0.9	0.7	0.5	0.8	2.9
C&F in 0.7C	0.9	0.5	0.9	0.9	3.2
B in both 0.8C	0.9	0.6	0.6	0.8	2.9
Full-span in 0.8C	1	0.4	0.4	1	2.8

As it is evident from Table 5.2, C & F flaps and A&D flaps are performing best, since flaps C&F produce much higher lift, it was decided to select them for further analysis.

Conclusion

Based on the presented results and scores, it was decided to choose two flap configurations to use in the future analysis. For the single-flap case, B in R1 0.8C was chosen and for the multi-flap case C&F in 0.7C were selected. Therefore, the flight performance analysis presented in section 5.2 are only based on these two flap configurations.

5.1.4. Results per Design Variable

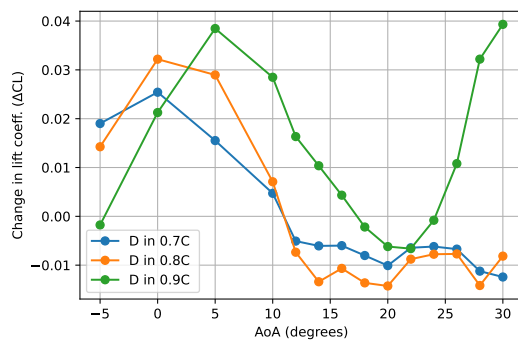
In this subsection the results for each design variable chosen is presented. As mentioned before, during the design of the experiment several design variables were explored which laid the foundation for the different flap designs and their placement on the wing. The design variables were:

1. Chord-wise location of the hinge line
2. Chord length (C)
3. Span (L)
4. Region (R)
5. Deflection angle (δ_f)
6. Number of flaps
7. Angle of attack (α)
8. Free stream velocity (V)

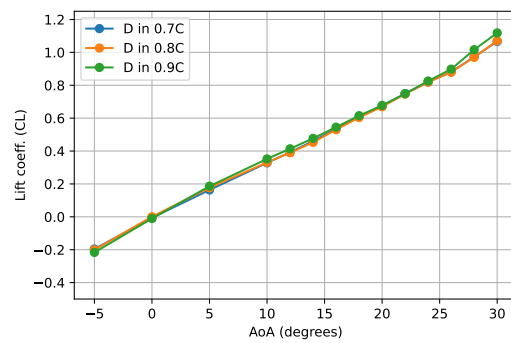
The last two design variables are not independently discussed since the angle of attack is an ever present variable and the free stream velocity was discussed in section 4.2. Additionally, the effect of the deflection angles were shown for each flap in subsection 5.1.1 and subsection 5.1.2.

Chord-wise location of the hinge line

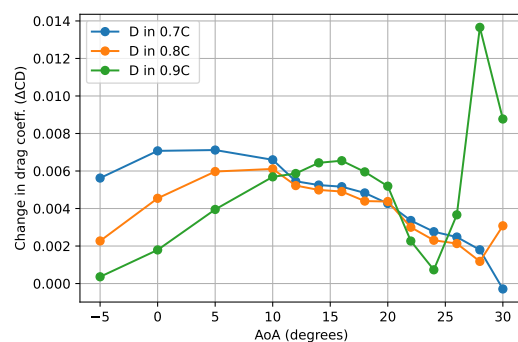
To explore the effect of this variable, flap D was tested on three different chord-wise locations, namely, 70%, 80% and 90% on region 2.



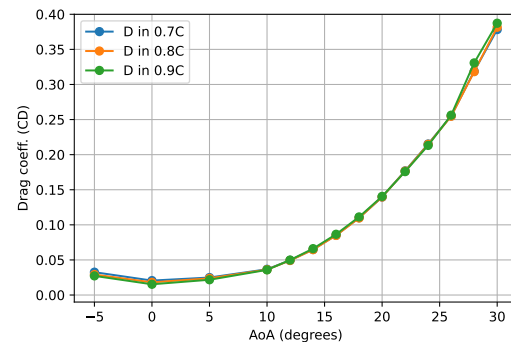
(a) Change in lift coefficient in comparison to clean wing



(b) Lift coefficient



(c) Change in drag coefficient with respect to clean wing



(d) Drag Coefficient

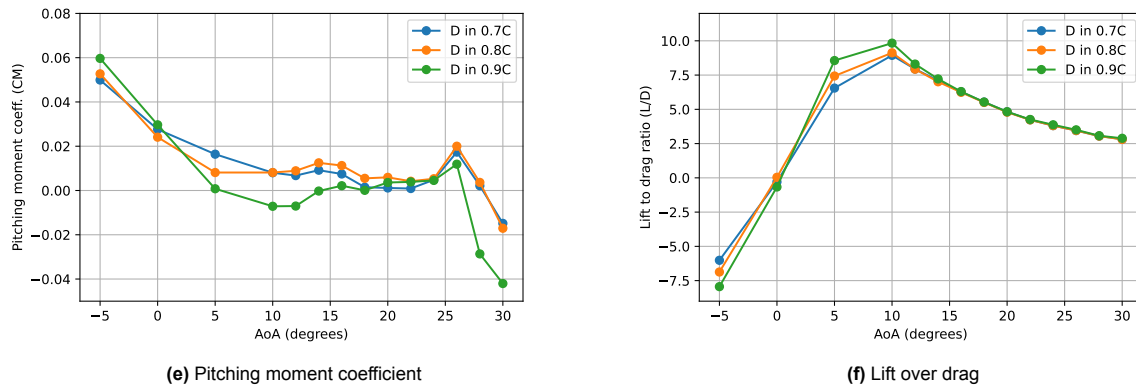
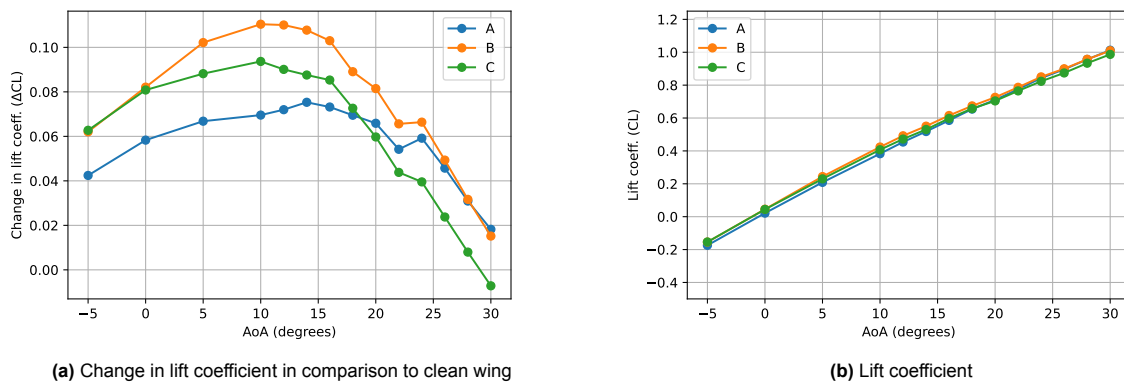


Figure 5.10: Effect of the chord-wise hinge line location on flap performance

Looking at the plots depicted in Figure 5.10, it is seen that the increase in lift coefficient is higher overall for the case where the flap is placed at 0.9C by up to 3 times comparing to the other cases. Note that flap D has a chord length of 0.1C, meaning that in cases where it is placed on 0.7C or 0.8C the separated air behind the flap gets into contact with the wing, causing the flap to act more as a spoiler. This is especially evident after 10° angle of attack. So it is no surprise that the lift to drag ratio is higher for the case where the flap is placed at 0.9C. In terms of stability, D in 0.9C seems to create a more negative pitching moment, this could be due to higher lift generation and since it is placed on region 2, it has a more visible effect on the wing. It can thus be concluded that the split flaps should have a hinge line location such that the flap's trailing edge meets the wing trailing edge.

Chord length

To study the effect of the variation in chord length of the split flaps on the aerodynamic coefficients, three different chord lengths were tested on both regions. For region 1, these were flaps A, B and C with the lengths of 0.1C, 0.2C and 0.3C, respectively and for region 2, these were D, E, F. Firstly the graphs for region 1 are shown in Figure 5.11.



(a) Change in lift coefficient in comparison to clean wing

(b) Lift coefficient

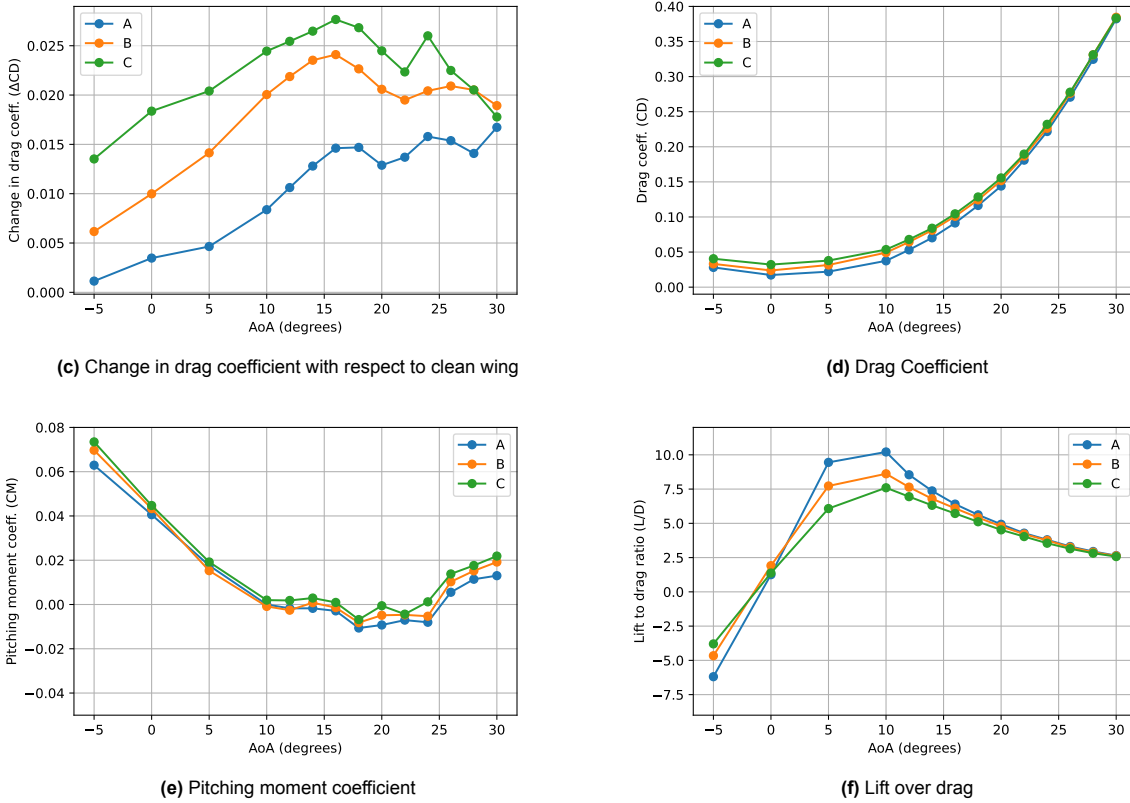
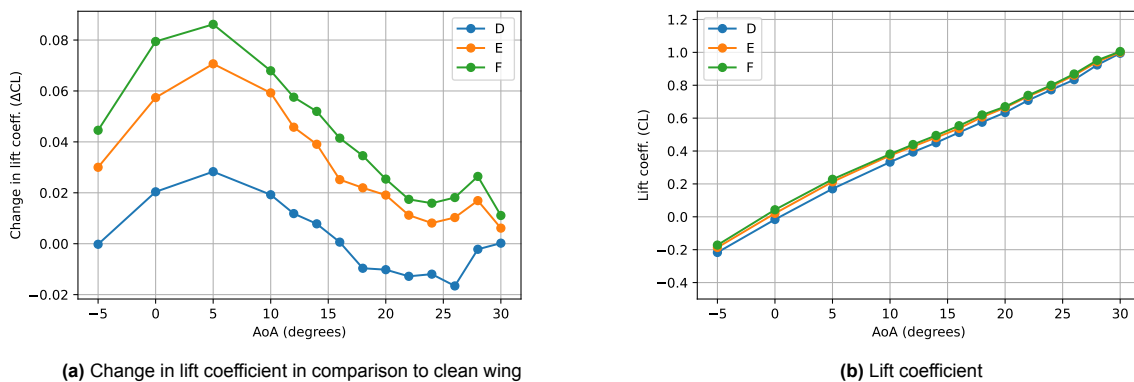


Figure 5.11: Effect of the chord length on flap performance in region 1

It is evident that in terms of increase in lift flap B is performing best with a 70% larger increase in lift comparing to flap A, even though it is not the largest flap. This may seem counter intuitive, it may be due to the placement of the flaps. In region 1 the curvature of the wing may have caused the effective deflection angle of flap C to reduce, making it less efficient in increasing the lift than flap B. However, according to the literature explored during the literature study phase, it was also found that the flaps placed at 20% of the chord length were more efficient in increasing the lift [21]. The results of increase in drag however, are according to the expectations, the larger the chord length the larger the drag increase, showing a 80% difference in drag rise between the largest and the smallest flaps. Overall, the smallest flap, A, has the highest lift to drag ratio which can be attributed mostly to its low drag.

In terms of stability there is not a large difference between the three flaps. This is especially because of the region of placement which has a smaller moment arm to the CG, making the size of the flaps a less significant variable. Next the results for variations in chord length in region 2 are shown in Figure 5.12.



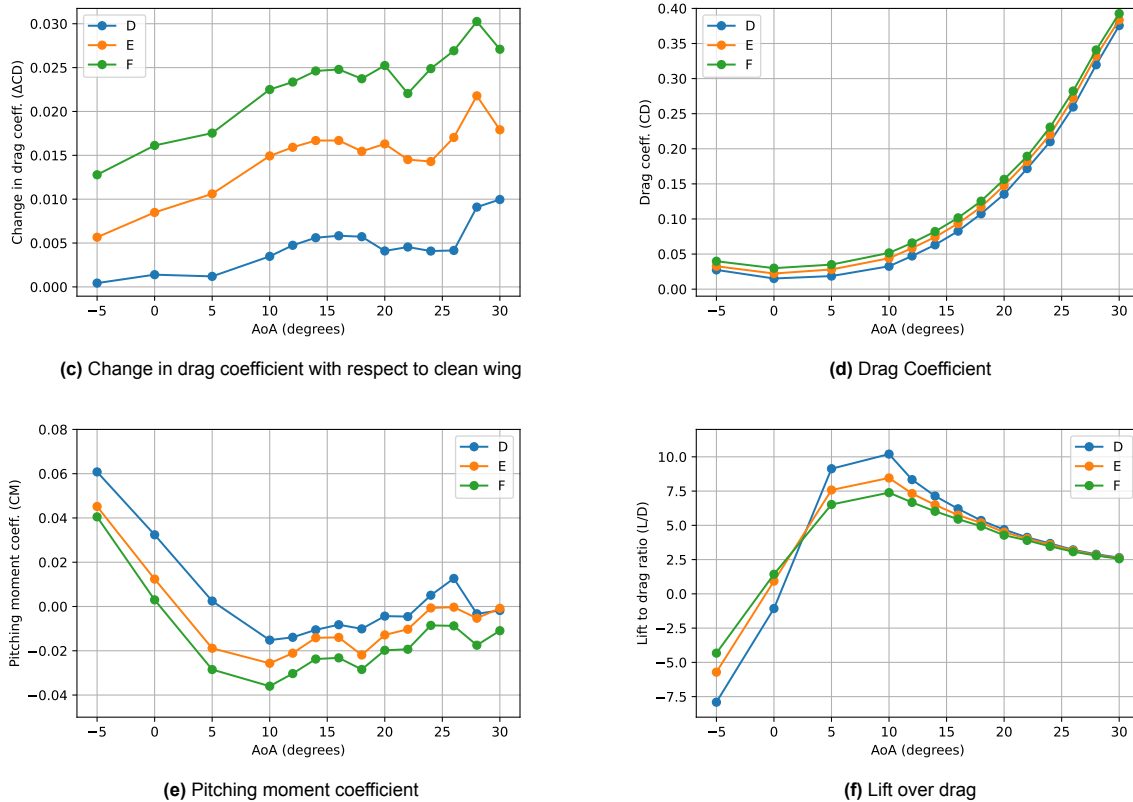


Figure 5.12: Effect of the chord length on flap performance in region 2

Figure 5.12 shows similar results as in region 1, however, this time the increase in lift is 30% higher for flap F with the chord length of 0.3C than that of flap E with 0.2C chord length. Similarly, the increase in drag is also according to the increase in the chord lengths with flap F having up to 5 times higher drag rise comparing to flap D. The lift to drag ratio is also highest for the smallest flap, D. We also notice a larger difference between pitching moment induced by the flaps, which confirms the effect of region of placement. These are placed in region 2 with a larger moment arm to CG and therefore, the difference in flap size and lift produced is more influential on the pitching moment.

Span

To explore the effect of the span length on the performance of the flaps, a second version of flap B was made with the span equal to full length of R1 which is L1 but a chord length equal to 20% of the chord length of region 2, subsequently this was compared with the results of flap E on region 2. This was done to assure that all variables stay similar between the two flaps except for their span length.

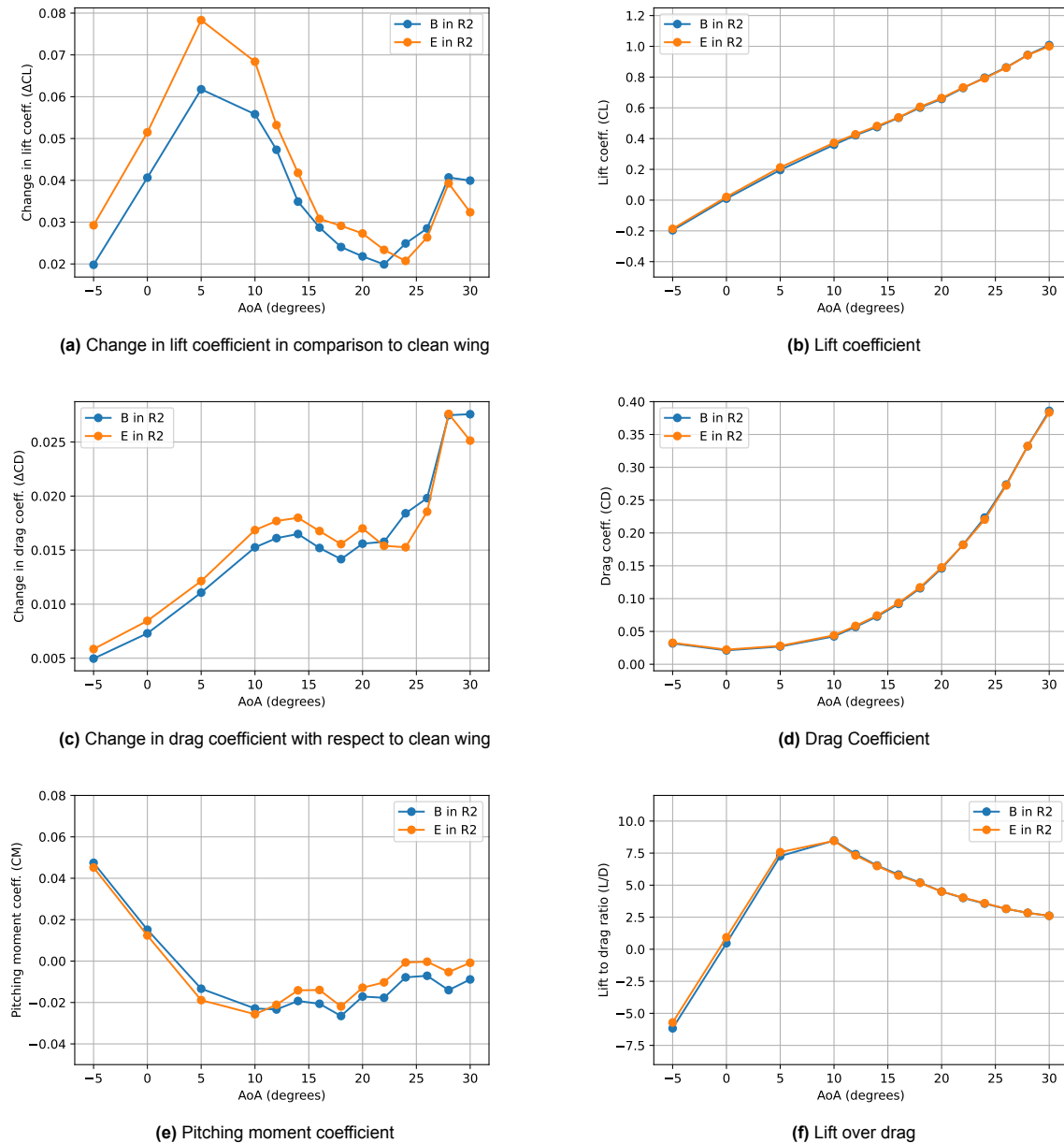


Figure 5.13: Effect of the span length on flap performance

The biggest difference between the two flaps was in lift increase, with E increasing lift by 30% more than flap B, this is not surprising simply because flap E is larger due to its larger span. The difference in drag increase is smaller (about 10%). However, the lift to drag ratio and longitudinal stability are almost identical for the two flaps. It can be concluded that the variation in span length has minimal effect on the flap performance, but it should be noted that due to the limited time of the experiment there was not any tests with a larger variation in the span length. It could be expected to see more differences in performance resulting from a larger increase in span length. It should be noted that the length of the flaps cannot be increased with no limitation due to the required space for control surfaces, engines, landing gear and other subsystems on the wing.

Region

The effect of the region where the flaps were placed on their performance was studied by three sets of comparisons. A and D as the first set, B and E as second and C and F as the third set. To avoid repetition, two graphs for each set are shown in Figure 5.14.

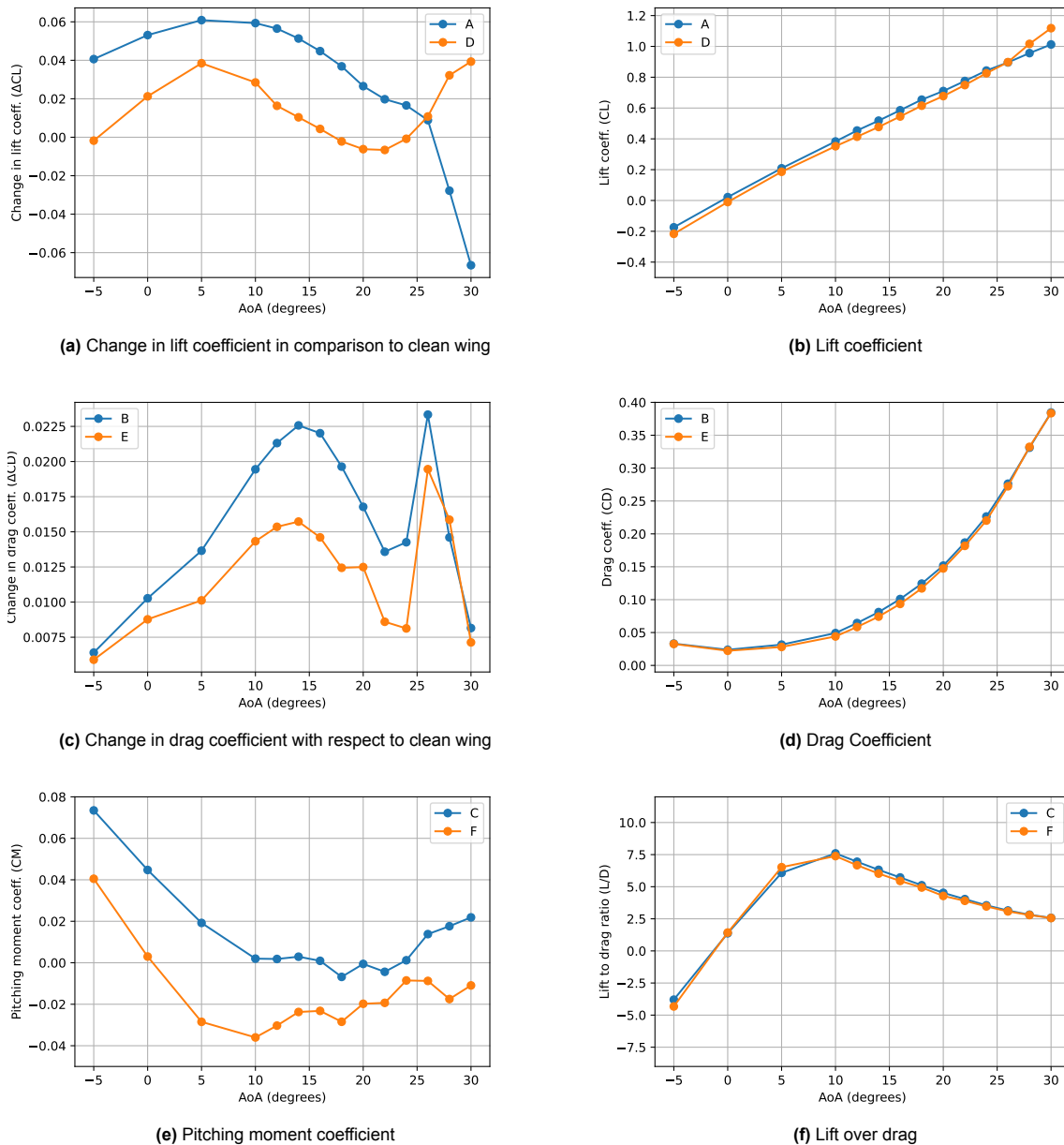


Figure 5.14: Effect of the region of placement on flap performance

It can be seen in Figure 5.14 that the flaps placed on region 1 are performing better than flaps placed in region 2 in most aspects. The increase in lift is significantly higher with flap A increasing the lift by up to 5 times to that of flap D. Even though the drag increase is also up to 50% higher for the flaps in region 1, they still perform better in terms of lift to drag ratio. Same conclusion are reached for the other sets, this means that placing the flap in region 1 results in a better performance. This can be attributed to the fact that there is a downwash near the kink caused by the flow moving from the root to the kink which may reduce the effective angle of attack of the flaps placed on region 2. This confirms what was already discussed, showing that region 2 is more prone to the influence of cross flow and separation. Additionally, placing the flaps on region 2 has a larger effect on the pitching moment due to the larger moment arm to the CG.

For all sets it is observed that the drag rises rapidly at AoA of 26°, this could be due to pitch break occurring around this angle where the flow experiences large separation which causes loss of lift and increase in drag. Flap D however, seems to be producing lift until the highest AoA as opposed to A which becomes ineffective after 26°. It may be that flap A had experienced a decrease in effective angle

of attack under the strong flow and may be considered as an outlier.

Number of Flaps

For determining the effect of the number of flaps on the aerodynamic performance of the wing three cases were tested and compared. To keep all the other variables constant, flap B was chosen to be tested in three configurations. Firstly, it is placed on region 1, secondly, it was placed on both regions, and thirdly the full-span version where the whole wing was covered by flaps B and E. As a reminder two versions of flap B were designed and manufactured to be tested on both regions.

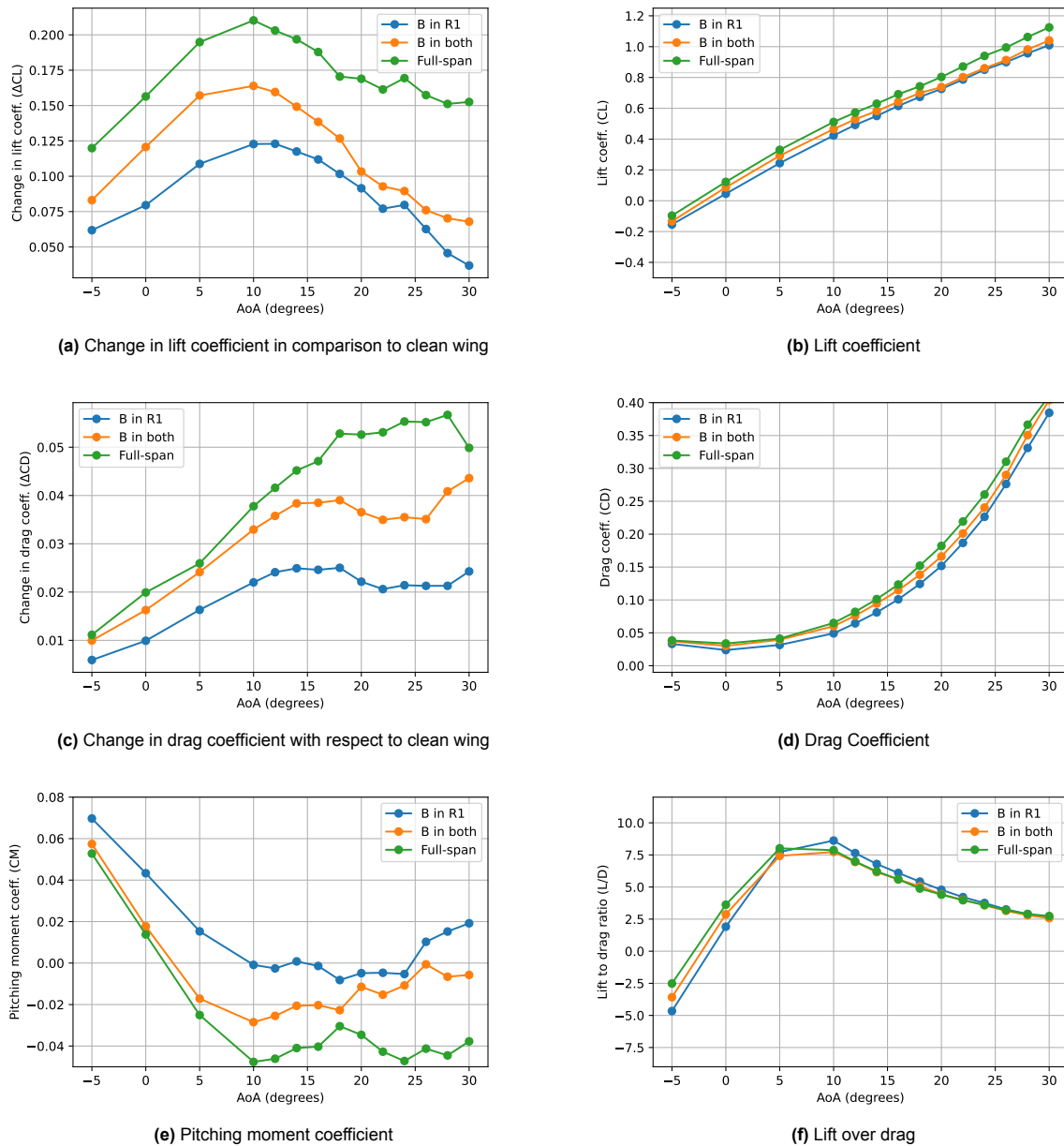


Figure 5.15: Effect of the number of flaps on flap performance

Figure 5.15 shows the effect of number of flaps on the aerodynamic performance of the wing. As expected the full-span flap has the largest increase in lift but also in drag, followed by flap B in both regions. By adding each flap the lift increase goes up by about 30% while the drag increase goes up by 70% and 60% going from one to two flaps and two to three flaps respectively. Thus, when looking at the lift to drag ratio, it is observed that flap B surpasses the other cases after the angle of attack of 6

degrees. This means that even though the lift increase is higher in multi-flap configurations, the drag rise negates this advantage.

Moreover, as expected the higher the number of flaps the larger the produced pitching moment becomes and the more disturbance there is in the trimmed conditions.

5.1.5. Trimming

As established before, two different sets of flap configurations were chosen to be used in further analysis, namely, flap B in 0.8C R1 and flaps C&F in 0.7C on both regions.

During the experiment, it was not possible to use the control surfaces due to defects, therefore to find the trimmed lift coefficient for these flaps, the data of the wind tunnel test conducted by Palermo [9] were used. For this procedure, it was attempted to find the deflection of one or a combination of control surfaces which counteract the pitching moment created by the flaps on the wind tunnel model. Firstly, the aerodynamic center of the half-wing model had to be found. For this a range of possible aerodynamic centers were tested to find which point creates the lowest change in pitching moment with changing the angle of attack.

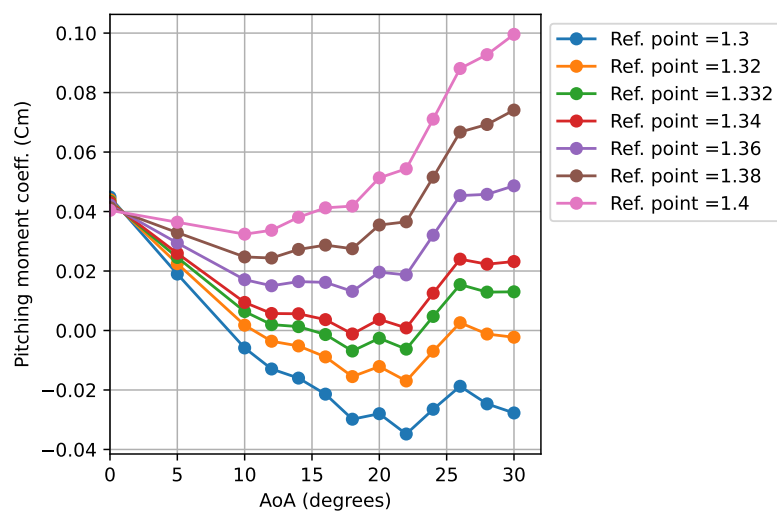


Figure 5.16: Determination of the aerodynamic center

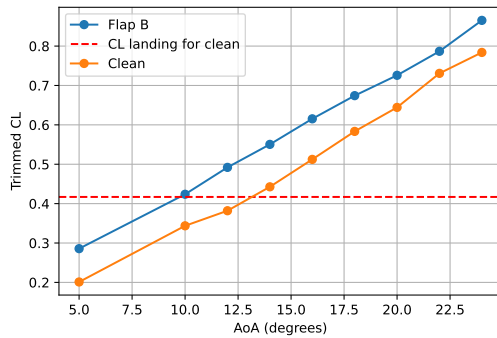
Based on the results shown in Figure 5.16 it is concluded that the aerodynamic center shifts with angle of attack, such that prior to 10° AoA, it is located at $x=1.4$ and shifts forward after that. Therefore it was decided to choose 1.332 m point measured from the nose of the model as the aerodynamic center which is somewhat of an average. Therefore the pitching moment is determined around this point.

Next the trimmed lift coefficients were found for the cases of clean wing, wing with flap B on and wing with flap C&F on. At this point it was assumed that the approach angle of attack for the case with clean wing was 15° . Note that this assumption was used only for the preliminary analysis of the wind tunnel data and later on in the flight performance analysis different assumptions were made which are explained in section 5.2.

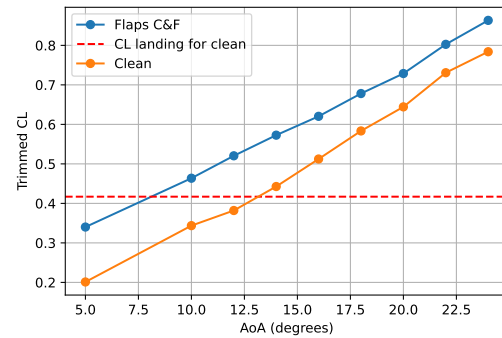
Figure 5.17 shows the comparison of the trimmed lift coefficient for each flap versus the clean wing. The red line shows the trimmed lift coefficient at 15° angle of attack which is taken as the approach angle. We can see that both flap configurations achieve the same lift coefficient at a lower angle of attack. For flap B this value is 11.57° , meaning that using flap B, amounts to a 3.46 degrees reduction in the approach angle of attack and by extension the pitch attitude. Alternatively, using flaps C&F results in an approach angle of attack of 10.49° which is a reduction of 4.51 degrees. These are quite desirable results since such a reduction in approach pitch attitude also yields a lower obscured segment which significantly increases the pilot's vision during landing, more analysis on landing are presented in section 5.2

A few points should be noted. The trimming at this point of the analysis was done rather manually by matching the data acquired from the wind tunnel test of current study, with the data on the behavior of

the control surfaces from the experiments conducted by Palermo [9]. This resulted in some non-linear behavior in lift coefficient trends as seen in Figure 5.17, which is unavoidable since two different sets of data points were being used. Additionally, before using Palermo's data the clean wing results of both experiments were compared to make sure there is sufficient compatibility between mine and Palermo's data set. This was the case up until the angle of attack of 24° , therefore, the trimming was only done up to this point.



(a) Trimmed lift coefficient for flap B Vs. clean wing



(b) Trimmed lift coefficient for flaps C&F Vs. clean wing

Figure 5.17: Trimmed lift coefficient for the two selected flap configurations in comparison to clean wing

After this preliminary analysis which showed promising results for improvements in landing performance of the Flying-V, a more elaborate flight performance analysis was conducted using PHALANX which is explained further in section 5.2.

5.2. Flight Performance

So far, all of the analysis have been done using experimental data and data analysis methods. For this final part of current thesis project a flight performance analysis focusing on the landing phase was implemented. This was done using a flight performance analysis tool developed at the Delft University of Technology by the name of PHALANX as explained in section 2.5 and section 3.2.

The landing analysis were performed with two options. Firstly, to keep the approach speed same as before (75 m/s) and find the reduction in the pitch attitude, obscured segment and pilot's eye altitude by extending the flaps. Second option was to also change the approach speed for the cases with extended flaps. The results for the single-flap configuration are discussed in subsection 5.2.1, followed by the results of the double-flap configuration in subsection 5.2.2.

5.2.1. Landing Analysis for Wing with Single Flap configuration

In this subsection the results of landing analysis performed on the wing with Flap B are shown and compared to clean wing.

Approach speed unchanged

The results for the case with unchanged approach speed has been determined for three center of gravity locations as specified in Table 2.4

Assuming extended flaps two sets of analysis were performed, one for each flap mechanism. Firstly, for flap B the reduction in pitch attitude for aft center of gravity, was 2.91° in comparison to clean wing. This reduction was 2.18° degrees for mid center of gravity and 2.55° for forward center of gravity.

Approach speed reduced

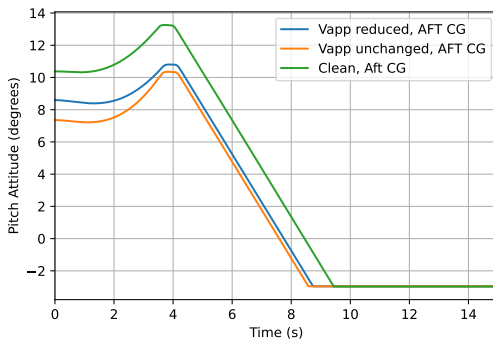
Incorporating flaps in the design of the Flying-V provides an additional benefit in reducing the approach speed. According to CS25.125[44] regulations, the approach speed must be at least 1.23 times larger than the stall speed in landing configuration.

$$V_{app} \geq 1.23V_{Stall} \quad (5.1)$$

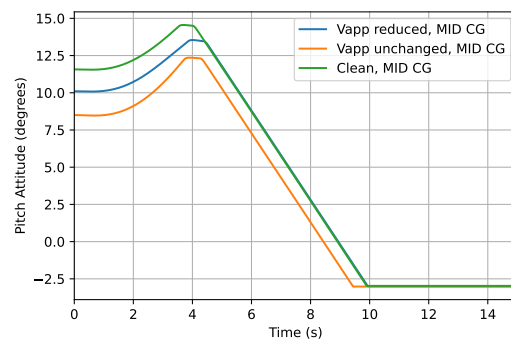
For calculating the stall speed in the Flying-V analysis the assumption was made that the $C_{L,max}$ is achieved at the angle of attack of 18° . This assumption was made by Cappuyns [41] in his thesis and also used by de Zoeten [14], the reason being that the pitch break was observed to happen around 20 degrees angle of attack and a margin was assumed to avoid going into the pitch break while flying on maximum lift coefficient.

Using these assumptions, the maximum lift coefficient for wing with flap B on was found to be 1.037 which resulted in a stall speed of 58.16 m/s using Equation 5.2, for MLW. Subsequently, the approach speed must be at least 71.54 m/s. Having a lower V_{app} resulted in a lower approach attitude as well as a slightly higher flight path angle at touch down. The landing analysis were done again accounting for this lower approach speed. The results for both approach speed are presented in Figure 5.18 for the aircraft trimmed at the three CG locations.

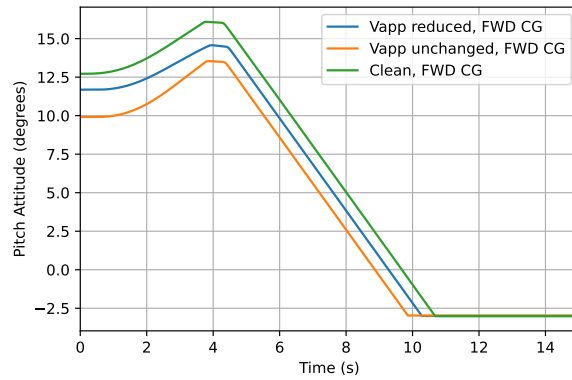
$$L_f = \frac{1}{2}\rho V_{Stall}^2 S C_{L,max} \quad L = MLW \quad (5.2)$$



(a) Wing with flap B Vs. clean wing for aircraft trimmed at aft CG



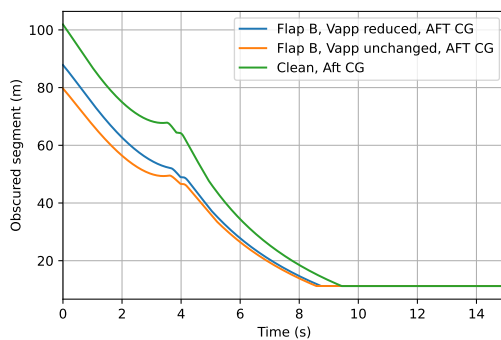
(b) Wing with flap B Vs. clean wing for aircraft trimmed at mid CG



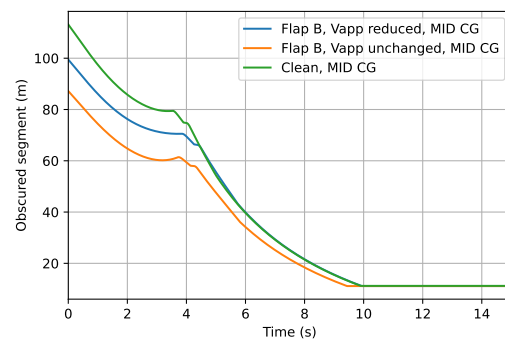
(c) Wing with flap B Vs. clean wing for aircraft trimmed at forward CG

Figure 5.18: Pitch attitude at landing for wing with flap B with unchanged and reduced approach speed versus clean wing for aircraft trimmed at three center of gravity locations

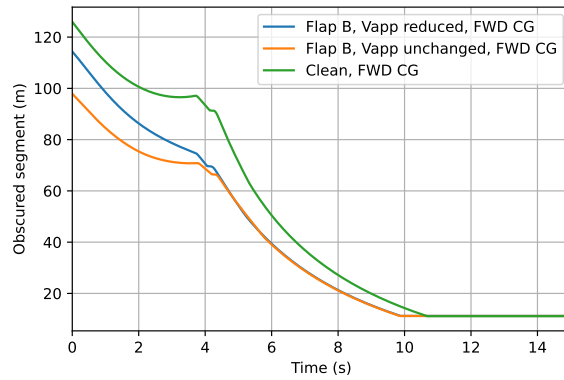
It is observed that reducing the approach speed results in an increase in approach pitch attitude, and a slight increase in touchdown attitude, however, the angle is still larger than the case of clean wing. The greatest reduction is seen when the aircraft is trimmed at aft cg. Another goal for these analyses was determining the reduction in obscured segment during landing. Obscured segment is defined as the horizontal distance to the closest point on the ground which pilot can see, therefore a lower obscured segment improves the pilot's vision during landing. Figure 5.19 shows the obscured segment for the clean wing and wing with flap B for the three center of gravity locations.



(a) Wing with flap B Vs. Clean wing with aircraft trimmed at aft CG



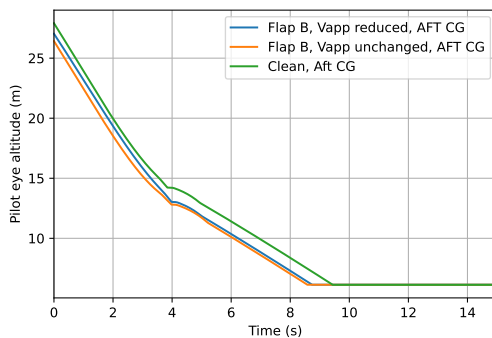
(b) Wing with flap B Vs. Clean wing with aircraft trimmed at mid CG



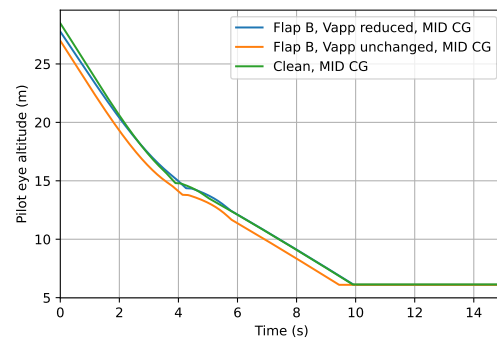
(c) Wing with flap B Vs. Clean wing with aircraft trimmed at forward CG

Figure 5.19: Obscured segment for wing with flap B with unchanged and reduced approach speed versus clean wing for aircraft trimmed at three center of gravity locations

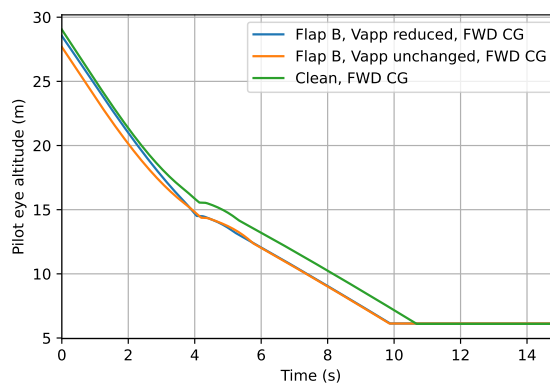
As seen in Figure 5.19, there is a reduction in obscured segment for all three center of gravity locations where the largest difference is observed for the forward center of gravity. This is quite a desirable result as it greatly improves the landing experience for the pilot. To assess the pilot's vision even further, another criterion could be measured, namely, the pilot eye altitude. As observed in Figure 5.20, there is a decrease in the altitude of the pilot's eye. This in combination with the lower obscured segment provides a better vision for the pilot during landing which is significantly important.



(a) Wing with flap B Vs. Clean wing with aircraft trimmed at aft CG



(b) Wing with flap B Vs. Clean wing with aircraft trimmed at mid CG



(c) Wing with flap B Vs. Clean wing with aircraft trimmed at forward CG

Figure 5.20: Pilot eye altitude for wing with flap B with unchanged and reduced approach speed versus clean wing for aircraft trimmed at three center of gravity locations

The influence of reducing the approach speed on the pilot eye altitude seems to be minimal as shown in Figure 5.20. However, there is still a reduction in comparison to clean wing for both velocities.

Overall, it can be concluded that incorporating flap B on the Flying-V has significant benefits for the landing phase in terms of both better compliance with safety requirements as well the pilot experience. In addition to the discussed parameters, other relevant landing characteristics are summarized in Table 5.3 for aft CG, Table 5.4 for mid CG and Table 5.5 for forward CG. Note that the values reported for the obscured segment and the pilot's eye altitude are the ones at the beginning of the landing maneuver.

Table 5.3: The landing performance comparison between clean wing and wing with single-flaps for aft CG

Landing Characteristics	V_{app} Unchanged		V_{app} reduced
	Clean Wing	Flap B	Flap B
V_{app} (m/s)	74.5	74.5	71.5
$V_{touchdown}$ (m/s)	74.0	74.4	71.6
$\theta_{touchdown}$ (deg)	13.2	10.3	10.8
Obscured Segment (m)	102	80	88
Pilot's eye altitude (m)	28	26	27
Total landing distance (m)	1212	1182	1133

Table 5.4: The landing performance comparison between clean wing and wing with single-flaps for mid CG

Landing Characteristics	V_{app} Unchanged		V_{app} reduced
	Clean Wing	Flap B	Flap B
V_{app} (m/s)	74.5	74.5	71.5
$V_{touchdown}$ (m/s)	74.0	74.3	71.5
$\theta_{touchdown}$ (deg)	14.5	12.3	12.4
Obscured Segment (m)	113	87	100
Pilot's eye altitude (m)	28	27	28
Total landing distance (m)	1227	1218	1147

Table 5.5: The landing performance comparison between clean wing and wing with single-flaps for forward CG

Landing Characteristics	V_{app} Unchanged		V_{app} reduced
	Clean Wing	Flap B	Flap B
V_{app} (m/s)	74.5	74.5	71.5
$V_{touchdown}$ (m/s)	74.0	74.2	71.3
$\theta_{touchdown}$ (deg)	16.0	13.5	14.5
Obscured Segment (m)	126	98	114
Pilot's eye altitude (m)	29	28	29
Total landing distance (m)	1290	1256	1224

5.2.2. Landing Analysis for Wing with Double Flap Configuration

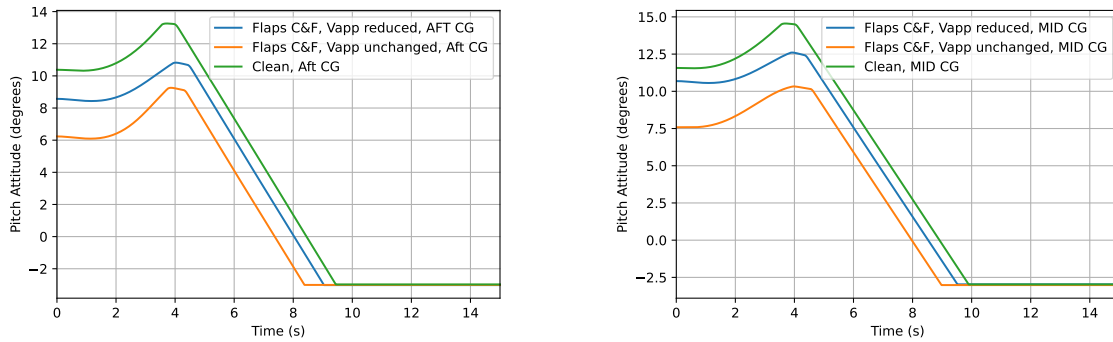
Finally, the results for flaps C&F are shown in this section. Similar to flap B, the analysis were done for three trimmed CGs and two different approach speeds. There was however, one important difference for this flap, with MLW it was not possible to trim the aircraft for forward CG, so, the trim point was found for a lower landing mass. Therefore, the results for this case are shown separately.

Approach speed unchanged

The approach speed for this case was remained as 74.51 m/s. The aircraft was then trimmed for aft and mid center of gravity.

Approach speed reduced

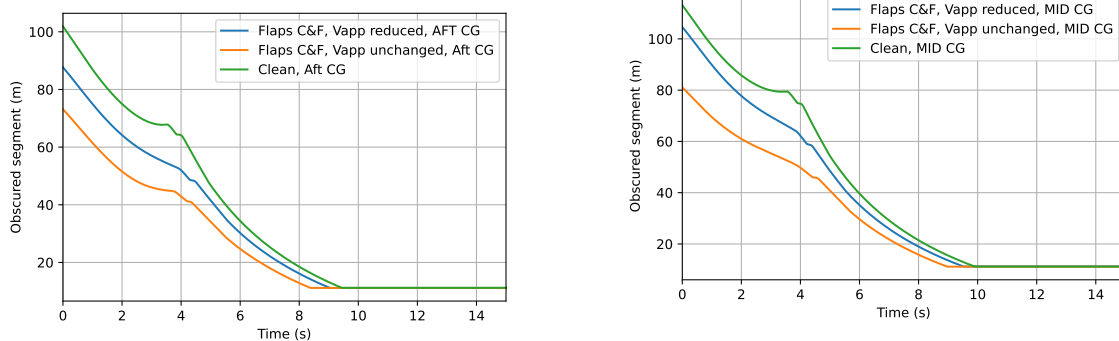
For the case with flaps C&F, a similar process as for flap B was followed to find the reduced approach speed. The maximum lift coefficient was 1.071 for this case which resulted in a stall speed of 57 m/s and an approach speed of 70 m/s. The results are shown for the aft and mid CGs in Figure 5.21.



(a) Wing with flaps C&F Vs. clean wing for aircraft trimmed at aft CG (b) Wing with flaps C&F Vs. clean wing for aircraft trimmed at mid CG

Figure 5.21: Pitch attitude at landing for wing with flaps C&F with unchanged and reduced approach speed versus clean wing for aircraft trimmed at two center of gravity locations

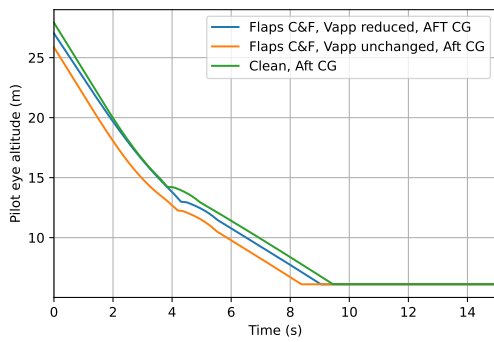
As observed in Figure 5.21, the reduction in pitch attitude at touchdown for aft CG is 4° in comparison to the clean wing, whereas for mid CG, this number is 4.3° . By lowering the approach speed the pitch attitude was increased by about 2° compared to the case with unchanged V_{app} .



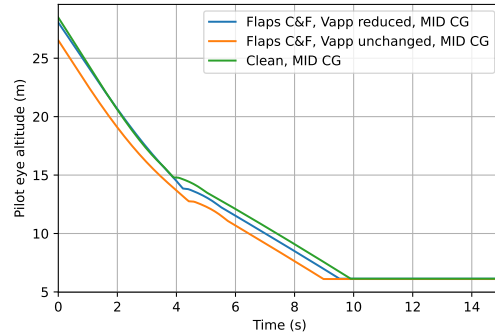
(a) Wing with flaps C&F Vs. Clean wing with aircraft trimmed at aft CG (b) Wing with flaps C&F Vs. Clean wing with aircraft trimmed at mid CG

Figure 5.22: Obscured segment for wing with flaps C&F with unchanged and reduced approach speed versus clean wing for aircraft trimmed at two center of gravity locations

Figure 5.22 shows a reduction in obscure segment for wings with flaps on for both speeds in comparison to clean wing. There is a higher reduction for the case with higher V_{app} which is expected since the lower approach speed has to be compensated with higher pitch attitude, reducing the pilot vision in turn. Lastly, the pilot eye altitude is analyzed.



(a) Wing with flaps C&F Vs. Clean wing with aircraft trimmed at aft CG



(b) Wing with flaps C&F Vs. Clean wing with aircraft trimmed at mid CG

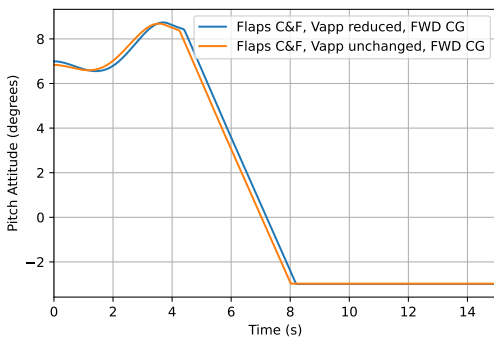
Figure 5.23: Pilot eye altitude for wing with flaps C&F with unchanged and reduced approach speed versus clean wing for aircraft trimmed at two center of gravity locations

As observed in Figure 5.23, the pilot eye’s altitude is reduced by using the flaps, however, this reduction is quite small for lower approach speed.

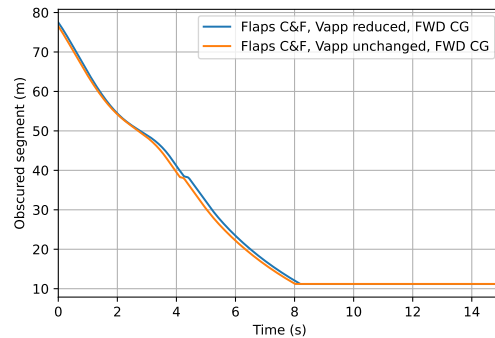
Landing mass reduced

Lastly, as mentioned, the aircraft was not trimmable at forward CG with maximum landing mass. Therefore, the mass was reduced to maximum number for which the aircraft could be trimmed. Both approach speeds of 74.51 m/s and 70 m/s are considered. Please note that reduction in mass could reduce the stall and therefore the approach speed further, which in turn would change the mass at which the aircraft is trimmed for at forward CG resulting in a loop. It was decided to keep the V_{app} as 70 m/s to keep the differences at minimal with the cases where the aircraft was trimmed at aft and mid CG.

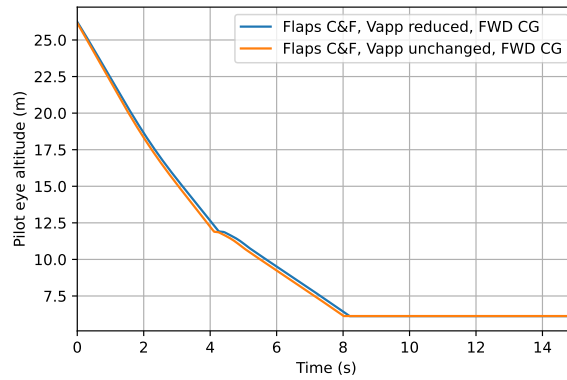
The mass for landing at V_{app} of 74.51 m/s was 172500 kg which is a reduction 20500 kg relative to MLM, that is about 7% of the MTOW. For the reduced approach speed of 70 m/s, the landing mass was 153900 kg which is a reduction of about 39100 kg and 14% of the MTOW [39]. As such, for both cases there needs to a large reduction in mass to make the aircraft trimmable at FWD CG. This is not a feasible compromise, therefore, it is recommended to not trim the aircraft for FWD CG at landing if the double-flap configuration is used. Nonetheless, this condition has been analyzed and the results are shown in Figure 5.24.



(a) Pitch attitude for wing with flap C&F for both V_{app} aircraft trimmed at forward CG



(b) Obscured segment for wing with flap C&F for both V_{app} aircraft trimmed at forward CG



(c) Pilot eye altitude for wing with flap C&F for both V_{app} aircraft trimmed at forward CG

Figure 5.24: Landing performance for wing with flaps C&F with unchanged and reduced approach speed and lower MLM for aircraft trimmed at forward CG location

It is seen in Figure 5.24 that the differences between the two approach speed for this case are quite small, therefore the reduction in mass seem to have a much larger effect on landing performance than reduction in V_{app} . Summary of the results are shown in Table 5.6 for aft CG, Table 5.7 for mid CG and Table 5.8 for forwards CG. Note that the values reported for the obscured segment and the pilot's eye altitude are the ones at the beginning of the landing maneuver.

Table 5.6: The landing performance comparison between clean wing and wing with double-flaps for aft CG

Landing Characteristics	V_{app} Unchanged		V_{app} reduced
	Clean Wing	Flaps C&F	Flaps C&F
V_{app} (m/s)	74.5	74.5	70
$V_{touchdown}$ (m/s)	74.0	75.4	70.7
$\theta_{touchdown}$ (deg)	13.2	9.2	10.7
Obscured Segment (m)	102	73	88
Pilot's eye altitude (m)	28	26	27
Total landing distance (m)	1212	1198	1146

Table 5.7: The landing performance comparison between clean wing and wing with double-flaps for mid CG

Landing Characteristics	V_{app} Unchanged		V_{app} reduced
	Clean Wing	Flaps C&F	Flaps C&F
V_{app} (m/s)	74.5	74.5	70
$V_{touchdown}$ (m/s)	74.0	75.3	70.6
$\theta_{touchdown}$ (deg)	14.5	10.2	12.5
Obscured Segment (m)	113	81	104
Pilot's eye altitude (m)	28	26	28
Total landing distance (m)	1227	1219	1161

Table 5.8: The landing performance comparison between clean wing and wing with double-flaps for forward CG

Landing Characteristics	V_{app} Unchanged		V_{app} reduced
	Clean Wing	Flaps C&F	Flaps C&F
V_{app} (m/s)	74.5	74.5	70
$V_{touchdown}$ (m/s)	74.0	75.6	71.2
$\theta_{touchdown}$ (deg)	16.0	8.5	8.5
Obscured Segment (m)	126	77	77
Pilot's eye altitude (m)	29	26	26
Total landing distance (m)	1290	1144	1059

Outcome

Both flap configurations show promising results in improving landing performance, by reducing the pitch attitude, obscured segment and the pilot's eye altitude. The improvements in performance are not significantly different between the two flap configurations, and given the fact that flap B is a single flap set-up and keeps the aircraft trimmable for all three center of gravity locations, it is recommended to use flap B in further design of the Flying-V. However, flaps C&F are also perfectly feasible to be used, should there be a decision in their favor.

5.2.3. Effect on the Landing Gear

The reduction in pitch attitude can have an impact on the landing gear length. The design of the landing gear for the Flying-V depends on various factors such as roll angle, the location of the landing gear and wing tip clearance in addition to the pitch attitude. With a preliminary estimation, based on a simple 2D relation shown in Equation 5.3, assuming the main landing gear location to be at 25 m from the tip in longitudinal direction [14], and a reduction of 3° in pitch attitude at landing using flaps, a reduction of 1.3 m in landing gear length is achieved.

$$\Delta L_{MLG} = 25 \cdot \sin(3) = 1.3 \quad (5.3)$$

Note that this is a rough estimation and in reality it is expected that the landing gear length reduction would be less than 1.3 m. However, this goes to show that a great difference can be achieved.

6

Conclusion and Recommendations

This chapter presents conclusions of the study of High Lift Split Flaps on the Flying-V in section 6.1. Afterwards, based on the knowledge gathered during this study and the outcomes, a few recommendations are presented in section 6.2 for future studies.

6.1. Conclusions

The Flying-V, a novel aircraft concept under development at the faculty of Aerospace Engineering at TU Delft, has shown promising results in increasing efficiency by 20% in comparison to a conventional twin-isle transport aircraft. However, improvements in landing performance are required, in particular pilot's vision. For this the pitch attitude at landing must be reduced. One possible solution is the use of high lift devices. Therefore, this thesis project was started to study the increase in the maximum lift coefficient of trimmed configuration by use of split flaps. This was done by means of a wind tunnel experiment, followed by flight performance analysis using PHALANX.

Verification and Validation have been performed to ensure the obtained results were in agreement with previous studies and that the model applied was feasible. The reproducibility of the data in short and long term were checked by comparing the repeated measurements throughout the experiment, and comparison with the results of previous studies respectively. In short-term a maximum difference of 0.1 in lift coefficient, 0.02 in drag coefficient and 0.04 in pitching moment coefficient were found. Whereas these numbers were 0.06, 0.03 and 0.02 in long-term comparisons respectively. Furthermore, the absence of systemic error was confirmed based on obtaining a P-value of 0.99, when comparing the measurements with and without removing the bias. Lastly, the flight performance model was verified by comparing the outcome of the model using data obtained during previous studies and the current studies on the clean wing. It resulted in great similarity in the landing performance using the two data set. These showed that the data and the model used during these studies were valid and verified. After this, the three research questions could be answered.

"What are the effects of changing the split flap's chord length, deflection angle, location of the hinge line, span, region of placement, as well as the number of flaps on the aerodynamic coefficients of the half-wing model?"

The effect of various design variables on the aerodynamic performance of the split flaps was studied during the wind tunnel test campaign which are as following:

- **Chord-wise location of the hinge line:** Placing the flaps in a chord-wise location such that the trailing edges of the flap and the wing met, improved the lift increase up to 3 times when comparing to the cases where the flap's TE stopped before the wing's TE. This can be attributed to the fact that the flap starts to act as a spoiler and causes lift dumping if placed in such position which also causes a larger drag rise for most of the angle of attack range. Placing the flap in a position where the trailing edges met, also contributed to maintaining a better longitudinal stability.
- **Chord length:** Regarding the effect of chord length on the lift improvement there was a distinction based on the region of placement of the flaps such that, in region 1, the region closer to the root,

the flap with a chord length equal to 20% of the local chord performed better than the ones with chord lengths of 10% and 30% of the local chord, improving the lift up to 70%. In terms of drag rise the flaps were also behaving based on their size, where the largest had a 80% increase in drag in comparison to smallest one. Regarding longitudinal stability there was not a significant difference between the three flaps in region 1. In region 2, which is the region closer to the kink, the largest flap with the longest chord length, was performing better in terms of lift, having 30% larger lift increase than the second largest flap. Moreover, this flap, had a maximum of 5 times larger drag rise in comparison to the smallest flap. There was a more visible difference in longitudinal stability, with the pitching moment coefficient assuming more negative values by increasing the chord length.

- **Span:** In terms of span length no significant differences was observed in flap performance.
- **Number of flaps:** The effect of number of flaps was such that by adding the flap numbers, the increase in lift was improved causing a 30% rise in lift by adding each flap. This however, increased drag such that by each addition of flap the drag rise would go up by 70% and 60% from one to two flaps and from two to three flaps, respectively. The pitching moment coefficient assumed more negative values with increasing the number of flaps, disturbing the trimmed condition more.
- **Region of placement** The effect of the region of placement was assessed such that the flaps placed on region 1 were performing significantly better than the ones placed on region 2 increasing the lift by up to 5 times more. The difference in drag was about 50% between the two regions. Additionally, the effect on the pitching moment coefficient by the flaps on region 1 was almost zero, meaning that the aircraft's trimmed condition was not disturbed by deploying the flaps. This was an important distinction of region 1.

Note that deflection angle was not independently discussed since a 30° angle was fixed for further analysis. Overall, the conclusion from studying the design variables was that the flaps placed on region 1 were doing significantly better than the ones on region 2. Moreover, the multi-flap configurations did not provide significant additional benefits to the single-flap configurations.

"What is the effect of the different configurations of the split flaps on lift, drag, pitching moment and rolling moment coefficients?"

For single flap options, the highest increase in lift belonged to flap B, the second largest flap on region 1, followed by flap C, the largest flap on region 1 where, B scored 0.2 higher. Regarding drag flap D, the smallest flap, was producing the least amount of drag and flap C the highest, resulting in 0.7 difference in their score. Furthermore, the flaps placed on region 1 were performing significantly better than the ones on region 2 in terms of change in pitching moment by changing their deflection angle. Lastly, flap F, the largest flap on region 2 performed the best in terms of producing rolling moment coefficient.

In multi-flap configurations, the highest increase in lift was achieved by the full-span configuration, followed by C&F, where both flaps were placed at 70% of the chord, the lowest performing option in multi-flaps was A&D which consisted of the smallest flaps placed at 90% of the chord. C&F scored 0.3 more than A&D. A&D had also the least drag rise, which resulted in 0.6 higher score than the full-span flap. The least moment produced was achieved by deploying flaps A&D and C&F. Furthermore, the full-span flap produced much larger rolling moment coefficient than flap A&D.

"What is the reduction in landing pitch attitude, obscured segment and pilot's eye altitude that can be achieved by using split flaps?"

After selecting the top two best performing designs among the single and multi-flap configurations, namely, a single flap configuration placed at 80% of the chord on the region closer to the root (Flap B) and a double-flap configuration placed at 70% of the chord on both regions (Flaps C&F), a landing analysis was conducted. The objective of the landing analysis using PHALANX, a flight performance analysis tool developed at TU Delft, was to study the effect of the flaps on the full-scale aircraft. There is about 3° reduction in pitch attitude by using the single-flap configuration as well as a 20 to 30 m reduction in obscured segment and 1 m reduction in pilot's eye altitude. This is a quite desirable outcome and a promising means of improving landing performance of the Flying-V.

The double-flap configuration was found to cause the aircraft to be untrimmable for forward CG for maximum landing mass, in addition to not providing any significant improvement over the single-flap configuration and therefore the single-flap option was chosen as the best flap design. It is thus concluded that all research questions outlined at the beginning of this thesis project have been answered.

6.2. Recommendations

Initially, it was planned to conduct two wind tunnel test campaigns, but due to scheduling issues it was only possible to have one campaign. Thus added design variables such as taper, sweep, larger range of deflection angles, etc, for a more optimized version were not possible to test. Furthermore, the control surface deflections were kept at 0° whereas they could have been deflected to study their correlation with flap performance.

Therefore, it is recommended to do a more in-depth research and possibly further wind tunnel tests by incorporating all these design variables to come up with a more optimized flap design. Additionally, testing the wing with flaps on, and using flow visualization methods as was done in previous studies on the clean wing, is of high value and could be incorporated in future wind tunnel tests. However, it should be noted that, despite having only one wind tunnel campaign, many configurations were tested due to great time management and the desired outcome was achieved.

As there are more wind tunnel models of the Flying-V being developed, it will definitely be valuable to test some flap configurations on other models as well. For instance, if there is a full span model available, testing a flap at exactly the midsection could be potentially beneficial.

The flap design and placement could also be taken out by means of simulations, instead of wind tunnel tests. Though challenging, CFD analysis could be helpful in optimizing the flap design.

Additionally, since this research was focusing purely on the aerodynamic performance of the split flaps without considering the structural aspect, it is recommended to conduct further research on the structural design of the flaps.

Moreover, the set-up for testing the half-wing model at the Open Jet Facility is quite labor intensive and requires many assembly parts, making it prone to errors and discrepancies between different campaigns. Therefore it is recommended to make a more permanent and easy to assemble facility for testing the half-wing model of the Flying-V.

Another valuable study is an elaborate evaluation of the effect of the pitch attitude reduction achieved by using flaps on the landing gear length, positioning and load distribution. The Flying-V landing gear design depends on various factors such as the maximum roll angle and lateral position in addition to the longitudinal position and pitch angle. Therefore, for the scope of this thesis it was decided to use a simple 2D analysis.

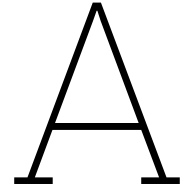
A more general recommendation for the Flying-V studies is looking more into incorporating the data obtained from the wind tunnel tests on the half-wing model as well as the data from the Sub-scaled flight tests with the analytical studies on the full-scale aircraft. There is a large gap in the two methods of studying the Flying-V in the past few years, and it is of great value to integrate them better.

References

- [1] J. D. Anderson, *The Airplane: A History of Its Technology*. Reston, VA: American Institute of Aeronautics and Astronautics (AIAA), (2002).
- [2] R. Martínez-Val, J. F. Palacin, and E. Perez, "The evolution of jet airliners explained through the range equation," *Proceedings of the Institution of Mechanical Engineers, Part G: Journal of Aerospace Engineering*, vol. 222, 6 2008, ISSN: 09544100. DOI: 10.1243/09544100JAER0338.
- [3] Y. Vigneron, "Commercial aircraft for the 21st century: A380 and beyond," 2003. DOI: 10.2514/6.2003-2886.
- [4] R. Martínez-Val, E. Pérez, P. Alfaro, and J. Pérez, "Conceptual design of a medium size flying wing," *Proceedings of the Institution of Mechanical Engineers, Part G: Journal of Aerospace Engineering*, vol. 221, 1 2007, ISSN: 09544100. DOI: 10.1243/09544100JAER090.
- [5] A. L. Bolsunovsky *et al.*, "Flying wing - problems and decisions," *Aircraft Design*, vol. 4, 4 2001, ISSN: 13698869. DOI: 10.1016/S1369-8869(01)00005-2.
- [6] J. Benad, "The flying v - a new aircraft configuration for commercial passenger transport," *Deutscher Luft- und Raumfahrtkongress, 2015*.
- [7] J. B. R. Vos, "Design of a flying v subsonic transport," *ICAS 2022, 2022*.
- [8] F. Faggiano, "Aerodynamic design optimization of a flying v aircraft," M.S. thesis, Delft University of Technology, Delft, (2016).
- [9] M. Palermo, "The longitudinal static stability and control characteristics of a flying v scaled model," M.S. thesis, Delft University of Technology, Delft, (2019).
- [10] C. H. Wolowicz, J. S. Bowman, and W. P. Gilbert, *Similitude requirements and scaling relationships as applied too model testing*, (1979).
- [11] G. Bourget, "The effect of landing gear implementation on flying v aerodynamics, stability and controllability," M.S. thesis, Delft University of Technology, Delft, (2020).
- [12] A. Santosh, "Influence of ground effect on the flying v aircraft," M.S. thesis, Delft University of Technology, Delft, (2020).
- [13] O. Erdinçler, "Aerodynamic and performance analysis of ground spoilers," M.S. thesis, Delft University of Technology, Delft, (2021).
- [14] G. J. de Zoeten, C. Varriale, and R. Vos, "Flight performance evaluation of the flying-v," 2022. DOI: 10.2514/6.2023-3484.
- [15] R. Viet, "Analysis of the flight characteristics of a highly swept cranked flying wing by means of an experimental test," M.S. thesis, Delft University of Technology, Delft, (2019).
- [16] Roelof Vos, Saeed Farokhi, *Introduction to Transonic Aerodynamic*. The Netherlands, USA: Springer, (2014).
- [17] A. Rizzi, M. Tomac, and A. Jirásek, "Hybrid rans-les simulations of f-16xl aircraft in low-speed high-alpha flight," 2015. DOI: 10.2514/6.2015-2874.
- [18] A. Rizzi and J. M. Luckring, "What was learned in predicting slender airframe aerodynamics with the f-16xl aircraft," vol. 54, 2017. DOI: 10.2514/1.C033569.
- [19] S. Hitzel, "Vortex flows of the f-16xl configuration-cawapi-ii free-flight simulations," 2014. DOI: 10.2514/6.2014-0758.
- [20] R. G. J. Frey F. Sell and H. Pfifer, "Aerodynamic design and wind tunnel test of a laminar wing with split flap for a fuel cell powered aircraft," *Deutscher Luft und Raumfahrtkongress 2022, 2022*.
- [21] C. J. Wenzinger, "Wind-tunnel investigation of ordinary and split flaps on airfoils of different profile," *NACA*, 1936.

- [22] C. J. Wenzinger, "The effects of full-span and partial-span split flaps on the aerodynamic characteristics of a tapered wing," *National Advisory Committee for Aeronautics*, 1934.
- [23] A. V. Daniel Dougherty and H. Hefazi, "High lift flap system for a tailless transport aircraft," *51st AIAA Aerospace Sciences Meeting*, 2013.
- [24] I. Abbott and H. Greenberg, "Tests in the variable-density wind tunnel of the naca 23012 airfoil with plain and split flaps," *National Advisory Committee for Aeronautics*, vol. NACA-TR-66, 661 1939.
- [25] J. P. Jewel B. Barlow William H. Rae, *Low-Speed Wind Tunnel Testing*, 3rd ed. Canada: Wiley-Merscience Publication, (1999).
- [26] Faculty of Aerospace Engineering. "Open jet facility." (), [Online]. Available: <https://www.tudelft.nl/en/ae/organisation/departments/flow-physics-and-technology/facilities/low-speed-wind-tunnels/open-jet-facility> (visited on 04/06/2023).
- [27] M. Costes, A. Gravelle, J. Philippe, S. Vogel, and H. Triebstein, "Investigation of unsteady subsonic spoiler and flap aerodynamics," *Journal of Aircraft*, vol. 24, 9 1987, ISSN: 00218669. DOI: 10.2514/3.45488.
- [28] E. N. Jacobs and A. Sherman, "Airfoil section characteristics as affected by variations of the reynolds number," *Tech. rep., Washington. D.C: National Advisory Committee for Aeronautics*, 586 1939.
- [29] J. van Uitert, "Experimental investigation into the effect of aerodynamic add-ons on the aerodynamic characteristics of the flying v," M.S. thesis, Delft University of Technology, Delft, (2021).
- [30] W. E. Milholen, N. Chokani, and R. J. McGhee, "Development of semispan model test techniques," *Journal of Aircraft*, vol. 33, 6 1996, ISSN: 15333868. DOI: 10.2514/3.47065.
- [31] S. Eder, K. Hufnagel, and C. Tropea, "Semi-span testing in wind tunnels," vol. 2, 2006.
- [32] G. M. Gatlin and R. J. McGhee, "Study of semi-span model testing techniques," 1996. DOI: 10.2514/6.1996-2388.
- [33] S. N. Skinner and H. Zare-Behtash, "Semi-span wind tunnel testing without conventional peniche," *Experiments in Fluids*, vol. 58, 12 2017, ISSN: 07234864. DOI: 10.1007/s00348-017-2442-7.
- [34] F. M. D. et al., *A Modern Introduction to Probability and Statistics: Undesratingd why and how*. (2005).
- [35] D. C. Montgomery, *Design and Analysis of Experiments - Douglas C. Montgomery - Google Kitaplar*. (2017).
- [36] A. R. Garcia, "Aerodynamic model identification of the flying v using wind tunnel data," M.S. thesis, Delft University of Technology, Delft, (2019).
- [37] N. Johnson, "Effect of winglet integration and rudder deflection on flying-v aerodynamic characteristics," M.S. thesis, Delft University of Technology, Delft, (2021).
- [38] S. Nolet, "Improving the flying v directional control power by the implementation of split flaps," M.S. thesis, Delft University of Technology, Delft, (2019).
- [39] W. J. Oosterom and R. Vos, "Conceptual design of a flying-v aircraft family," 2022. DOI: 10.2514/6.2022-3200.
- [40] M. Claeys, "Flying v and reference aircraft structural analysis and mass comparis," M.S. thesis, Delft University of Technology, Delft, (2018).
- [41] T. Cappuyns, "Handling qualities of a flying v configuration," 2019. DOI: MScthesis.
- [42] B. R. Pascual and R. Vos, "The effect of engine location on the aerodynamic efficiency of a flying-v aircraft," vol. 1 PartF, 2020. DOI: 10.2514/6.2020-1954.
- [43] AIRBUS, "A330-flight deck and systems briefing for pilots," *Course Handout*, 4 1999.
- [44] *Certification specifications and acceptable means of compliance for large aeroplanes cs-25*, (2018).
- [45] H. Y. Ratcliffe, "Elements of airplane performance. g. j. j. ruijgrok. delft university press, stevinweg 1, 2628 cn delft, the netherlands. 1990. 452 pp. illustrated. dfls 90.00.," *The Aeronautical Journal*, vol. 95, 950 1991, ISSN: 0001-9240. DOI: 10.1017/s0001924000024349.

- [46] F. A. Administration, "Airplane flying handbook," *U.S. Department of Transportation*, 2016.
- [47] S. A. van Empelen and R. Vos, "Effect of engine integration on a 4.6%-scale flying-v subsonic transport," 2021. DOI: 10.2514/6.2021-0939.
- [48] D. A. V. Ginneken, M. Voskuijl, M. J. V. Tooren, and A. Frediani, "Automated control surface design and sizing for the prandtl plane," 2010. DOI: 10.2514/6.2010-3060.
- [49] M. Voskuijl, J. de Klerk, and D. van Ginneken, "Flight mechanics modeling of the prandtlplane for conceptual and preliminary design," in 2012, vol. 66. DOI: 10.1007/978-1-4614-2435-2_19.
- [50] C. Varriale, K. Hameeteman, M. Voskuijl, and L. L. Veldhuis, "A thrust-elevator interaction criterion for aircraft optimal longitudinal control," 2019. DOI: 10.2514/6.2019-3001.
- [51] C. Varriale and M. Voskuijl, "A control allocation approach to induce the center of pressure position and shape the aircraft transient response," *Aerospace Science and Technology*, vol. 119, 2021, ISSN: 12709638. DOI: 10.1016/j.ast.2021.107092.
- [52] C. Varriale and M. Voskuijl, "A trim problem formulation for maximum control authority using the attainable moment set geometry," *CEAS Aeronautical Journal*, vol. 13, 1 2022, ISSN: 18695590. DOI: 10.1007/s13272-021-00560-4.
- [53] M. Cavcar, "The international standard atmosphere (isa)," *Anadolu University, Turkey*, 2000.
- [54] C. Varriale, "Flight mechanics and performance of direct lift control: Applying control allocation methods to a staggered box-wing aircraft configuration," 2022, ISBN: 1978-94-6366-510-0.
- [55] D. P. Raymer, "Aircraft design: A conceptual approach[book]," *Washington, DC: American Institute of Aeronautics and Astronautics, Inc, 1992.*, 1992.
- [56] E. Torenbeek, *Advanced Aircraft Design*. 2013. DOI: 10.1002/9781118568101.
- [57] R. Feagin and W. Morrison, "Delta method, an empirical drag buildup technique," *NASA CR-151971, Dec*, December 1978.
- [58] J. A. Vargas and R. Vos, "Development of a wave drag prediction tool for the conceptual design phase," 2016. DOI: 10.2514/6.2016-1279.



Test Matrix

In this appendix the test matrices used during wind tunnel experiment are shown. Table A.1 shows the initial test matrix and Table A.2 shows the extra measurements that were possible due to extra time during the second week of the campaign.

Table A.1: Test matrix used during the wind tunnel experiment

Design Variable	Chord length	Span	Deflection angle	Location of the hinge line	Number of flaps	AoA	Free stream velocity	Flap name
	clean					[-5 to 30]		
1	0.1c	L1	10	0.7C	R2	[-5 to 30]	[0,20]	a
2	0.1c	L1	10	0.8C	R2	[-5 to 30]	[0,20]	a
3	0.1c	L1	10	0.9C	R2	[-5 to 30]	[0,20]	a
4	0.1c	L1	20	0.7C	R2	[-5 to 30]	[0,20]	a
5	0.1c	L1	20	0.8C	R2	[-5 to 30]	[0,20]	a
6	0.1c	L1	20	0.9C	R2	[-5 to 30]	[0,20]	a
7	0.1c	L1	30	0.7C	R2	[-5 to 30]	[0,20]	a
	clean					[-5 to 30]		
8	0.1c	L1	30	0.8C	R2	[-5 to 30]	[0,20]	a
9	0.1c	L1	30	0.9C	R2	[-5 to 30]	[0,20]	a
10	0.1c	L1	45	0.7C	R2	[-5 to 30]	[0, 20, 25, 30]	a
11	0.1c	L1	45	0.8C	R2	[-5 to 30]	[0, 20]	a
12	0.1c	L1	45	0.9C	R2	[-5 to 30]	[0, 20]	a
13	0.1c	L1	60	0.7C	R2	[-5 to 30]	[0, 20]	a
14	0.1c	L1	60	0.8C	R2	[-5 to 30]	[0, 20]	a
	clean					[-5 to 30]		
15	0.1c	L1	60	0.9C	R2	[-5 to 30]	[0,20]	a
16	0.1c	L2	10	0.7C	R2	[-5 to 30]	[0,20]	d
17	0.1c	L2	10	0.8C	R2	[-5 to 30]	[0,20]	d
18	0.1c	L2	10	0.9C	R2	[-5 to 30]	[0,20]	d
19	0.1c	L2	20	0.7C	R2	[-5 to 30]	[0,20]	d
20	0.1c	L2	20	0.8C	R2	[-5 to 30]	[0,20]	d
21	0.1c	L2	20	0.9C	R2	[-5 to 30]	[0,20]	d
	clean					[-5 to 30]		
22	0.1c	L2	30	0.7C	R2	[-5 to 30]	[0,20]	d
23	0.1c	L2	30	0.8C	R2	[-5 to 30]	[0,20]	d
24	0.1c	L2	30	0.9C	R2	[-5 to 30]	[0,20]	d
25	0.1c	L2	45	0.7C	R2	[-5 to 30]	[0, 20, 25, 30]	d
26	0.1c	L2	45	0.8C	R2	[-5 to 30]	[0,20]	d
27	0.1c	L2	45	0.9C	R2	[-5 to 30]	[0,20]	d

Table A.1 Test matrix used during the wind tunnel experiment

Design Variable	Chord length	Span	Deflection angle	Location of the hinge line	Number of flaps	AoA	Free stream velocity	Flap name
28	0.1c clean	L2	60	0.7C	R2	[-5 to 30] [-5 to 30]	[0,20]	d
29	0.1c	L2	60	0.8C	R2	[-5 to 30]	[0,20]	d
30	0.1c	L2	60	0.9C	R2	[-5 to 30]	[0,20]	d
31	0.2c	L1	10	0.8C	R1	[-5 to 30]	[0,20]	b
32	0.2c	L1	20	0.8C	R1	[-5 to 30]	[0,20]	b
33	0.2c	L1	30	0.8C	R1	[-5 to 30]	[0,20]	b
34	0.2c	L1	45	0.8C	R1	[-5 to 30]	[0, 20, 25, 30]	b
35	0.2c clean	L1	60	0.8C	R1	[-5 to 30] [-5 to 30]	[0,20]	b
36	0.2c	L1	60	0.8C	both	[-5 to 30]	[0,20]	b
37	0.2c	L1	10	0.8C	both	[-5 to 30]	[0,20]	b
38	0.2c	L1	20	0.8C	both	[-5 to 30]	[0,20]	b
39	0.2c	L1	30	0.8C	both	[-5 to 30]	[0,20]	b
40	0.2c	L1	45	0.8C	both	[-5 to 30]	[0,20]	b
41	0.2c	L1	45	0.8C	R2	[-5 to 30]	[0, 20, 25, 30]	b
42	0.2c clean	L1	10	0.8C	R2	[-5 to 30] [-5 to 30]	[0,20]	b
43	0.2c	L1	20	0.8C	R2	[-5 to 30]	[0,20]	b
44	0.2c	L1	30	0.8C	R2	[-5 to 30]	[0,20]	b
45	0.2c	L1	60	0.8C	R2	[-5 to 30]	[0,20]	b
46	0.2c	L2	60	0.8C	R2	[-5 to 30]	[0,20]	e
47	0.2c	L2	10	0.8C	R2	[-5 to 30]	[0,20]	e
48	0.2c	L2	20	0.8C	R2	[-5 to 30]	[0,20]	e
49	0.2c clean	L2	30	0.8C	R2	[-5 to 30] [-5 to 30]	[0,20]	e
50	0.2c	L2	45	0.8C	R2	[-5 to 30]	[0, 20, 25, 30]	e
51	0.3c	L1	10	0.7C	R1	[-5 to 30]	[0,20]	c
52	0.3c	L1	20	0.7C	R1	[-5 to 30]	[0,20]	c
53	0.3c	L1	30	0.7C	R1	[-5 to 30]	[0,20]	c
54	0.3c	L1	45	0.7C	R1	[-5 to 30]	[0, 20, 25, 30]	c
55	0.3c	L1	60	0.7C	R1	[-5 to 30]	[0,20]	c
56	0.3c	L2	10	0.7C	R2	[-5 to 30]	[0,20]	f
57	0.3c	L2	20	0.7C	R2	[-5 to 30]	[0,20]	f
58	0.3c	L2	30	0.7C	R2	[-5 to 30]	[0,20]	f
59	0.3c	L2	45	0.7C	R2	[-5 to 30]	[0, 20, 25, 30]	f
60	0.3c	L2	60	0.7C	R2	[-5 to 30]	[0,20]	f

Table A.2: Extra measurements taken during wind tunnel test

Design Variable	Chord length	Span	Deflection angle	Location of the hinge line	Number of flaps	AoA	Free stream velocity	Flap name
1	clean					[-5 to 30]		
2	0.1c	L1	10	0.9C	R1	[-5 to 30]	[0,20]	a
3	0.1c	L1	20	0.9C	R1	[-5 to 30]	[0,20]	a
4	0.1c	L1	30	0.9C	R1	[-5 to 30]	[0,20]	a
5	0.1c	L1	45	0.9C	R1	[-5 to 30]	[0, 20]	a
6	0.1c	L1	60	0.9C	R1	[-5 to 30]	[0,20]	a
	clean					[-5 to 30]		
7	0.2c	L1 and L2	10	0.8C	both	[-5 to 30]	[0,20]	B&E
8	0.2c	L1 and L2	20	0.8C	both	[-5 to 30]	[0,20]	B&E
9	0.2c	L1 and L2	30	0.8C	both	[-5 to 30]	[0,20]	B&E
10	0.2c	L1 and L2	45	0.8C	both	[-5 to 30]	[0,20]	B&E
11	0.2c	L1 and L2	60	0.8C	both	[-5 to 30]	[0,20]	B&E
12	0.1c	L1 and L2	10	0.9C	both	[-5 to 30]	[0,20]	A&D
13	0.1c	L1 and L2	20	0.9C	both	[-5 to 30]	[0,20]	A&D
14	0.1c	L1 and L2	30	0.9C	both	[-5 to 30]	[0,20]	A&D
15	0.1c	L1 and L2	45	0.9C	both	[-5 to 30]	[0,20]	A&D
16	0.1c	L1 and L2	60	0.9C	both	[-5 to 30]	[0,20]	A&D
17	0.3c	L1 and L2	10	0.7C	both	[-5 to 30]	[0,20]	C&F
18	0.3c	L1 and L2	20	0.7C	both	[-5 to 30]	[0,20]	C&F
19	0.3c	L1 and L2	30	0.7C	both	[-5 to 30]	[0,20]	C&F
20	0.3c	L1 and L2	45	0.7C	both	[-5 to 30]	[0,20]	C&F
21	0.3c	L1 and L2	60	0.7C	both	[-5 to 30]	[0,20]	C&F
21	Full-span		20	0.8C		[-5 to 30]	[0,20]	Bs&E
22			30	0.8C		[-5 to 30]	[0,20]	Bs&E
23			45	0.8C		[-5 to 30]	[0,20]	Bs&E
24			10	0.8C		[-5 to 30]	[0,20]	Bs&E

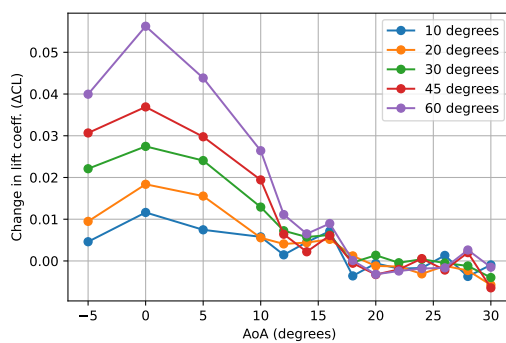
B

Additional Wind Tunnel Test Results

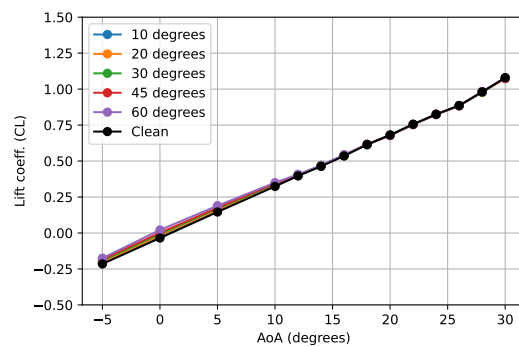
This appendix presents the remainder of the wind tunnel tests results on different flaps.

B.1. Flap A

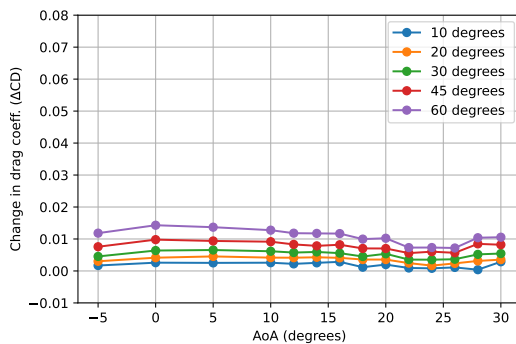
First, the results for the case where flap A was placed on 70% of the chord are shown in Figure B.1. Increase in lift coefficient is about 0.06 at its highest point and for the most part, there seems to be minimal increase in lift. After the angle of attack of 16° no increase is observed and even lift dumping occurs. Increase in drag is as expected quite low. Increase in rolling moment is 0.03 at the highest point. This flap also seems to have minimal effect on the pitching moment behavior of the wing and the change in deflection angle produces a very small increase in pitching moment.



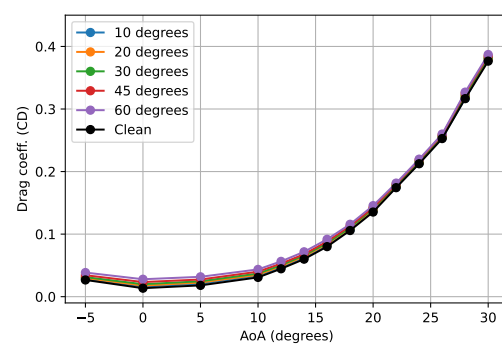
(a) Change in lift coefficient in comparison to clean wing



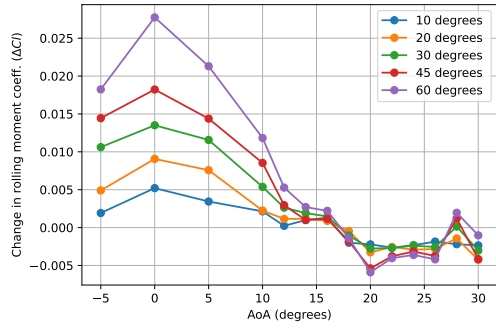
(b) Lift coefficient



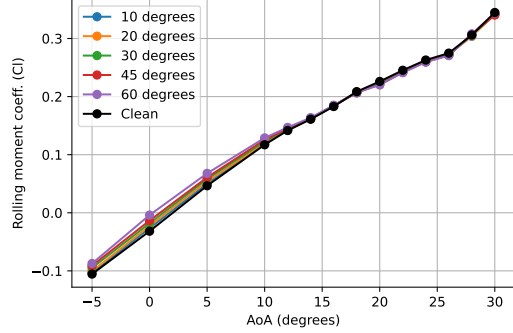
(c) Change in drag coefficient with respect to clean wing



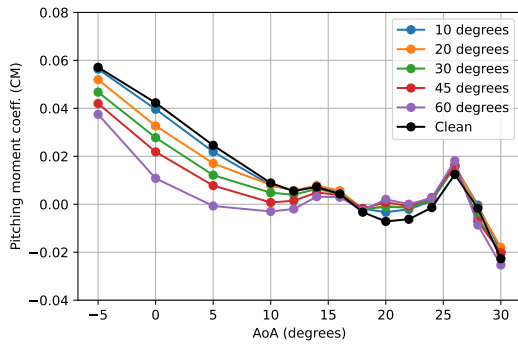
(d) Drag coefficient



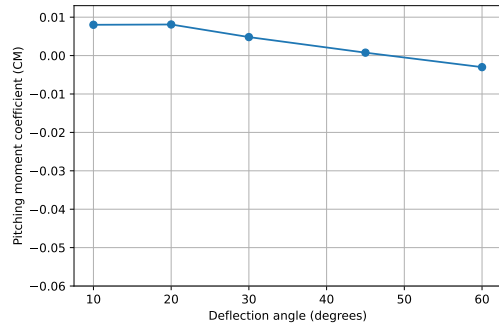
(e) Change in rolling moment coefficient with respect to clean wing



(f) Rolling moment coefficient



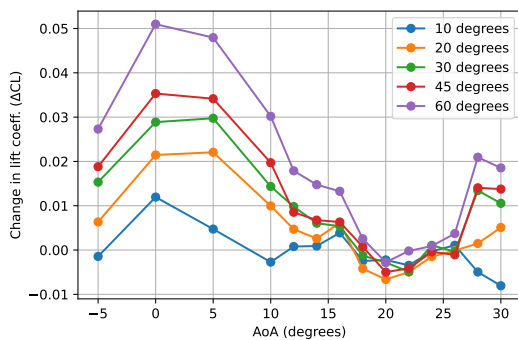
(g) Pitching moment coefficient Vs. Angle of attack



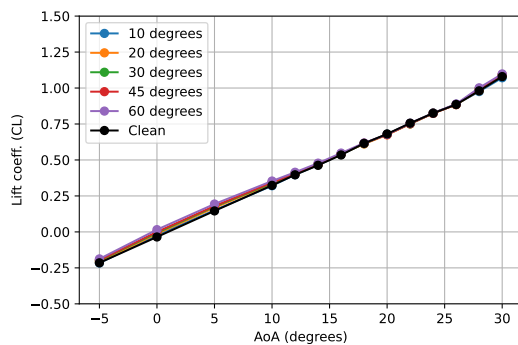
(h) Pitching moment coefficient Vs. Deflection angle

Figure B.1: Results of Flap A in Region 2 at 70% of the chord

Figure B.2 shows the results for the case where flap A was placed on 80% of the chord. In terms of the lift increase, it behaves poorly, with the highest lift coefficient increase of 0.05 at 60° deflection angle. Additionally, there are also instances where the lift is even decreased, particularly after the angle of attack of 18°. This can be due to the fact that the trailing edges of flaps and the wing do not overlap and therefore in higher angles of attack the flap is acting closer to a spoiler by causing the air to separate on the wing causing a lift dumping behavior. The drag rise stays quite constant throughout the angles of attack and rises a bit after the pitch break occurs at 24° AoA. The change in pitching moment with changing the deflection angles is also quite small.



(a) Change in lift coefficient in comparison to clean wing



(b) Lift coefficient

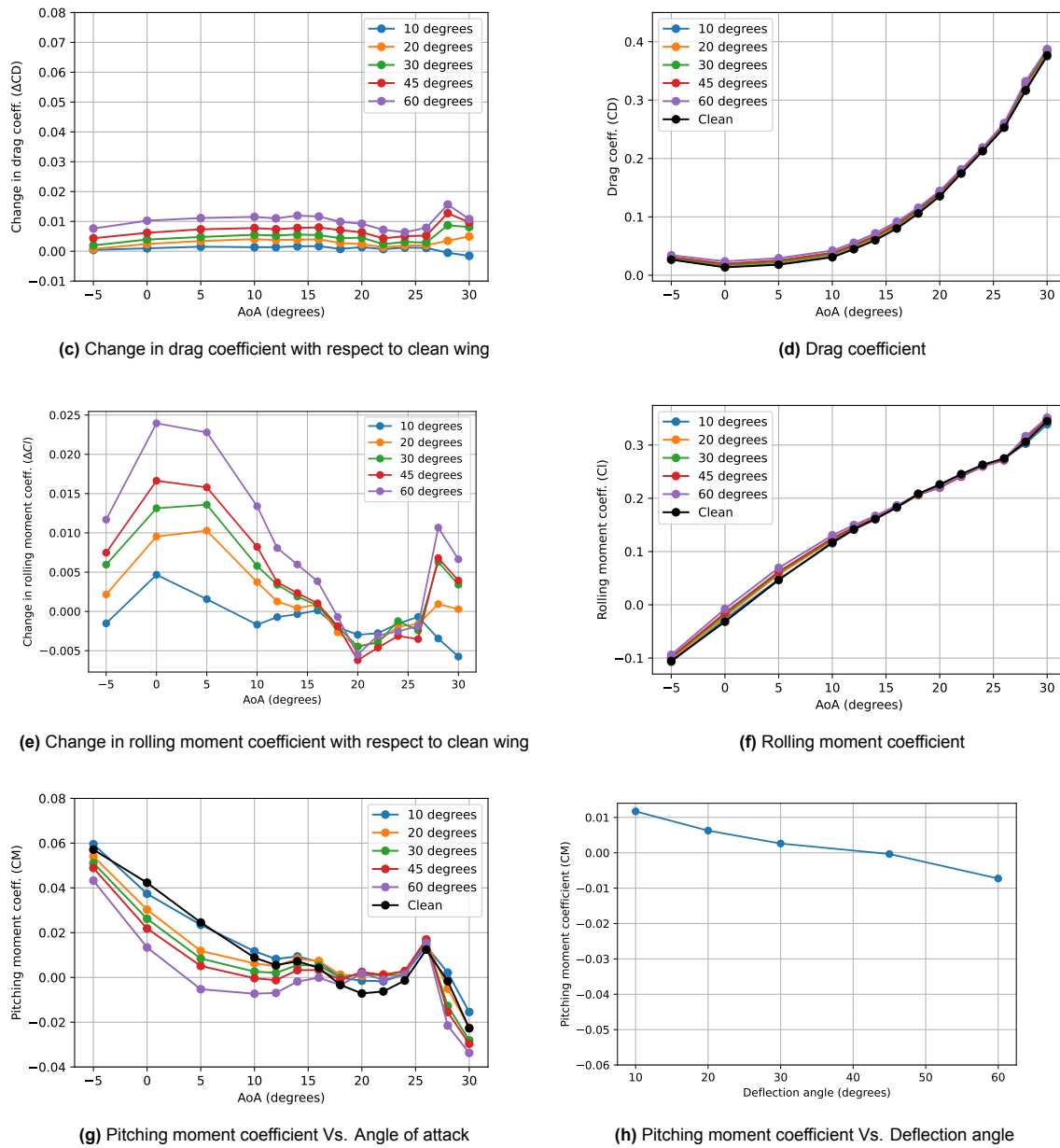
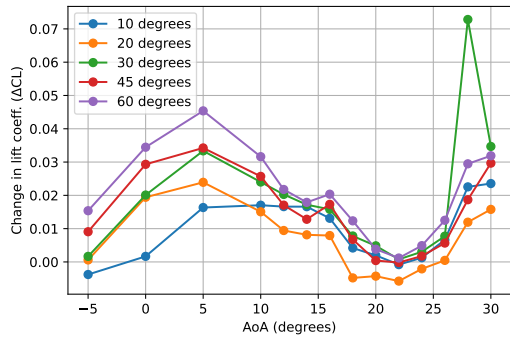
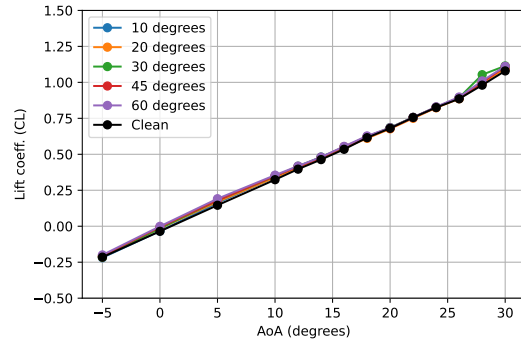


Figure B.2: Results of Flap A in Region 2 at 80% of the chord

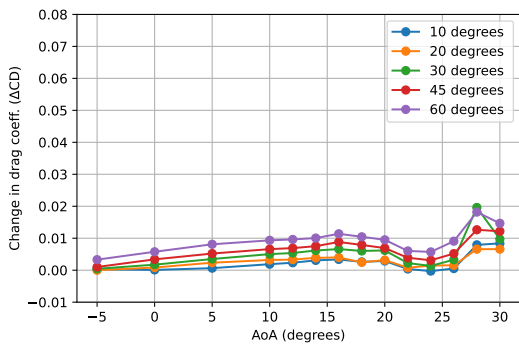
Lastly, flap A was placed on 90% of the chord in region 2. As shown in Figure B.3 there is a better performance in terms of increase in lift coefficient when comparing to the other cases in region 2. There is a slight lift increase up until about 18° angle of attack. The drag rise is less than the previous cases which is expected as in the previous cases there is a gap between the trailing edge of the flap and the wing, meaning the air which is separated from the flap is still in contact with the wing causing more turbulence and drag rise. This is not the case when the trailing edge of the flap and the wing meet. Increase in rolling moment is less than the previous cases. Lastly, the pitching moment behavior follows the clean wing, with a pitch break occurring around 24° . The change in pitching moment coefficient with deflection angle also seems to be quite small.



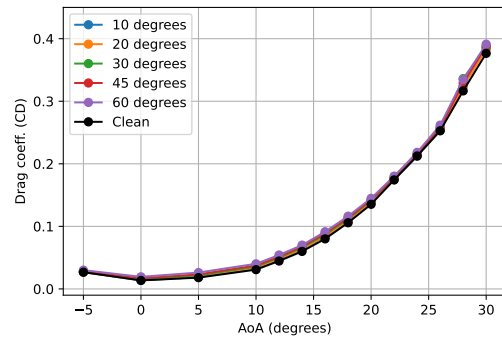
(a) Change in lift coefficient in comparison to clean wing



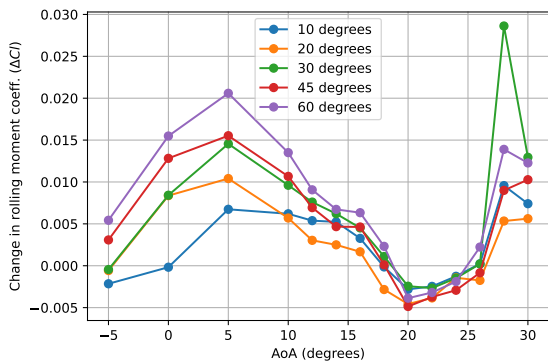
(b) Lift coefficient



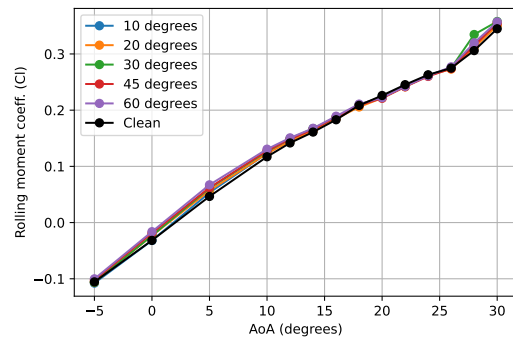
(c) Change in drag coefficient with respect to clean wing



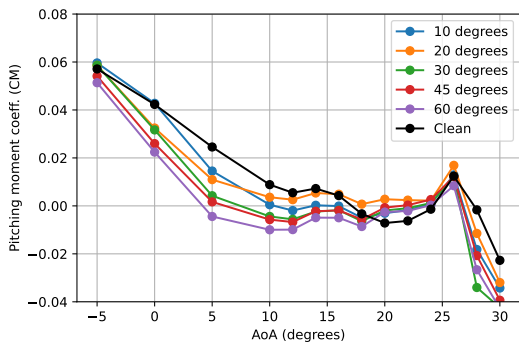
(d) Drag coefficient



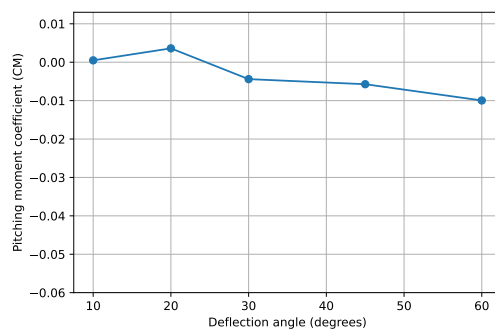
(e) Change in rolling moment coefficient with respect to clean wing



(f) Rolling moment coefficient



(g) Pitching moment coefficient Vs. Angle of attack

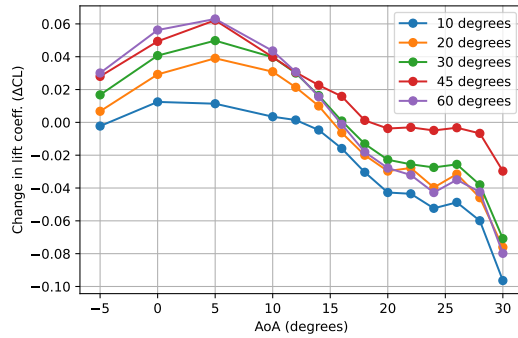


(h) Pitching moment coefficient Vs. Deflection angle

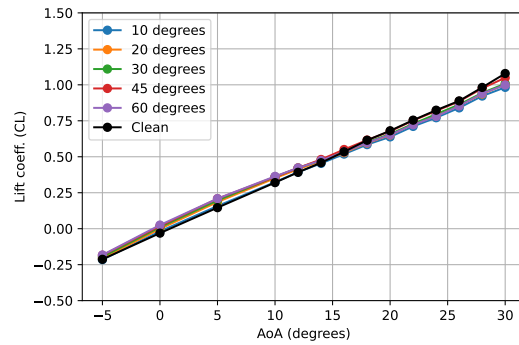
Figure B.3: Results of Flap A in Region 2 90% of the chord

B.2. Flap B in R2

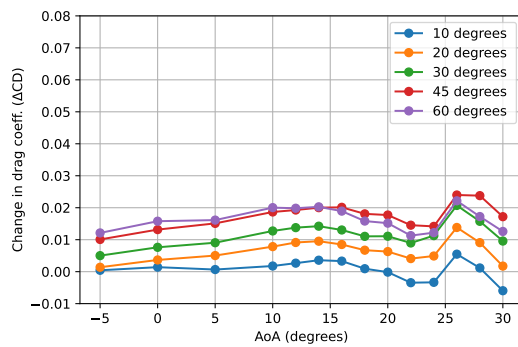
In this case the second version of flap B is used where the chord length is 20% of the kink chord instead of the root chord, since the tests are being done in region 2. As seen in Figure B.4 an important observation is the significant reduction in the lift increase in comparison to when it was in region 1. There is not a big difference in drag rise. Rolling moment coefficient is less for smaller deflection angles in comparison to previous case. Additionally, the wing is quite stable with minimal variations in pitching moment coefficient with changing the angle of attack or the deflection angle.



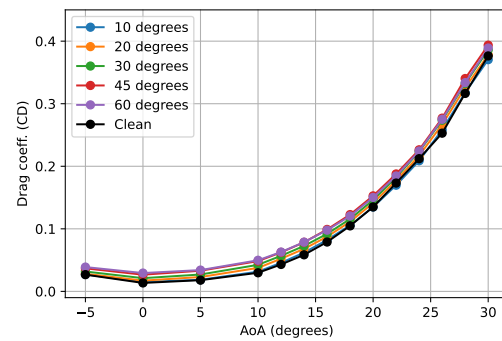
(a) Change in lift coefficient in comparison to clean wing



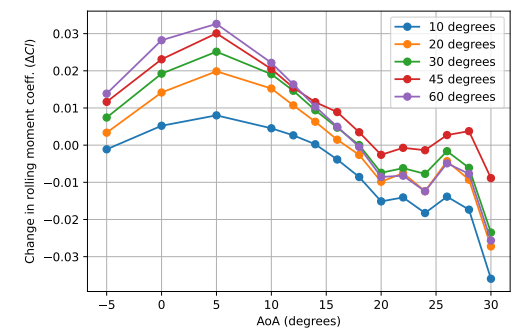
(b) Lift coefficient



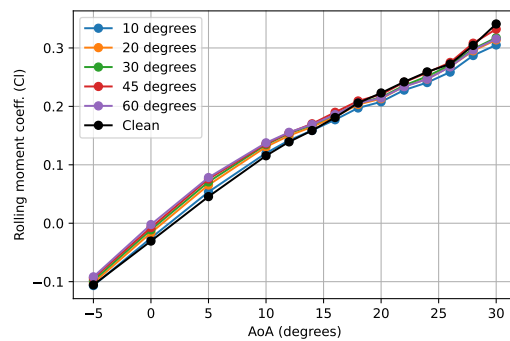
(c) Change in drag coefficient with respect to clean wing



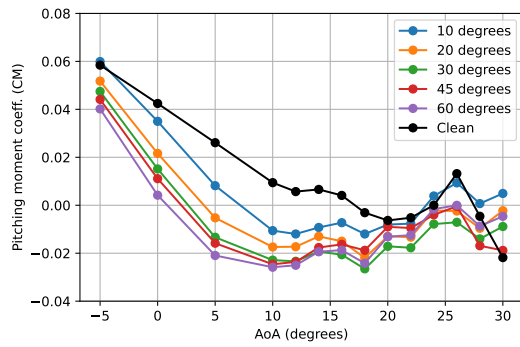
(d) Drag coefficient



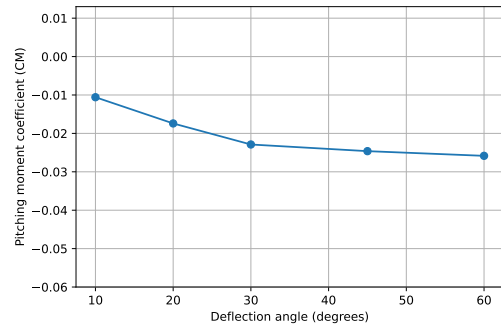
(e) Change in rolling moment coefficient with respect to clean wing



(f) Rolling moment coefficient



(g) Pitching moment coefficient Vs. Angle of attack

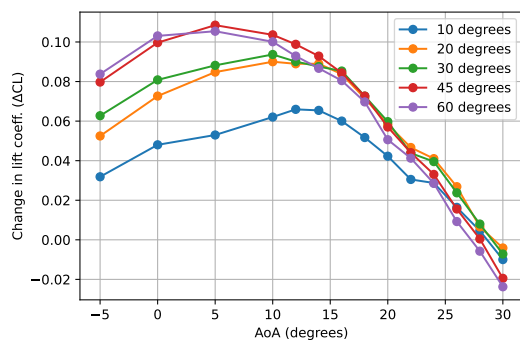


(h) Pitching moment coefficient Vs. Deflection angle

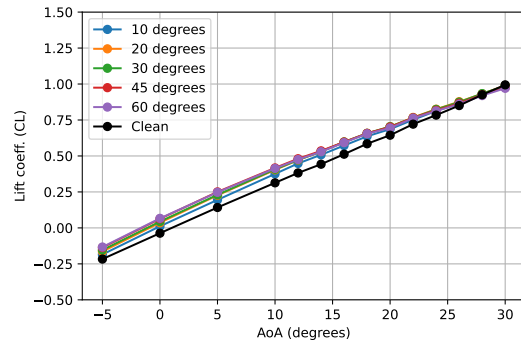
Figure B.4: Results of Flap B in Region 2 at 80% of the chord

B.3. Flap C

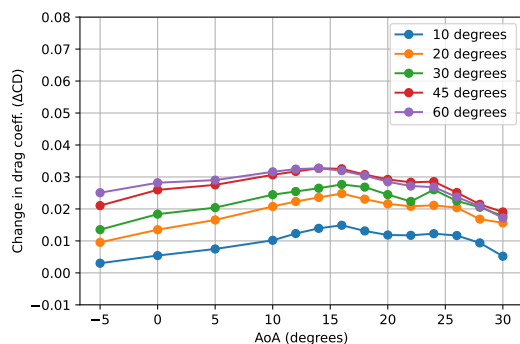
This configuration refers to the flap with span of L1 and chord length of 30% of the root chord. It has been tested for only one position, namely 70% of chord in region 1. The results are shown in Figure B.5. The increase in lift coefficient is significant with a 0.12 maximum, there seems to be small differences between different deflection angles, this could be due to the large size of the flap. The increase in drag is higher than A and B which is not surprising. At the highest point, rolling moment coefficient is increased by about 0.03. There seems to be minimal influence on the pitching moment coefficient with the flap on, with pitch break occurring around 22° angle of attack as before. Change in pitching moment coefficient with deflection angle is also small, however, there seem to be a slight pitch up tendency.



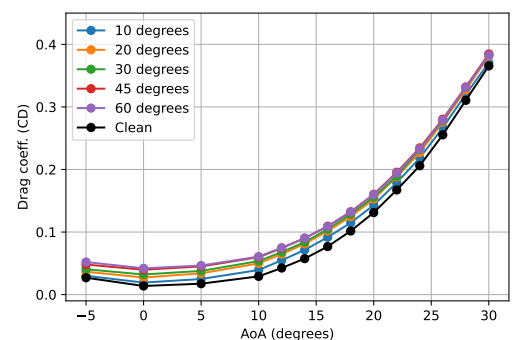
(a) Change in lift coefficient in comparison to clean wing



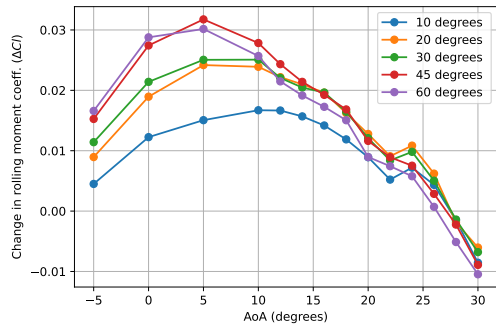
(b) Lift coefficient



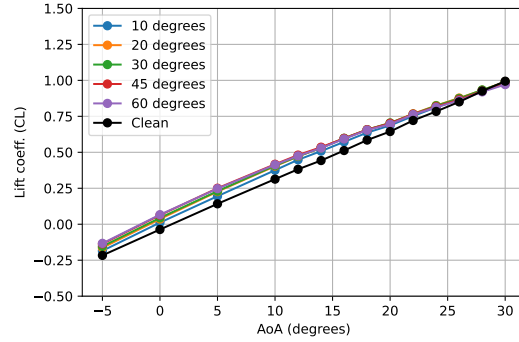
(c) Change in drag coefficient with respect to clean wing



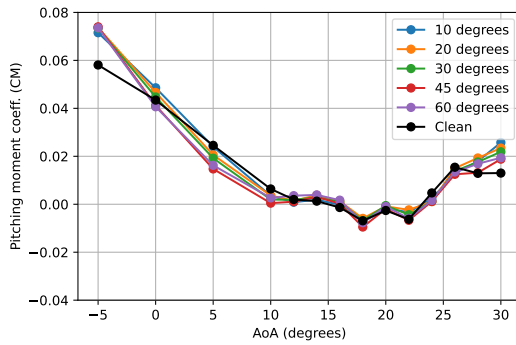
(d) Drag coefficient



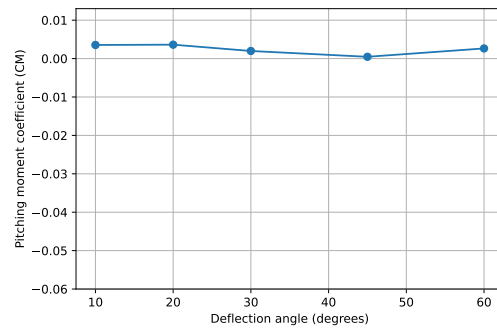
(e) Change in rolling moment coefficient with respect to clean wing



(f) Rolling moment coefficient



(g) Pitching moment coefficient Vs. Angle of attack

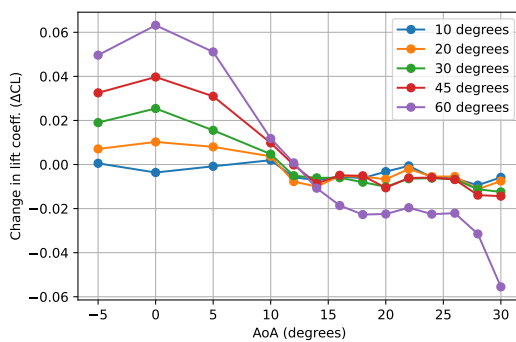


(h) Pitching moment coefficient Vs. Deflection angle

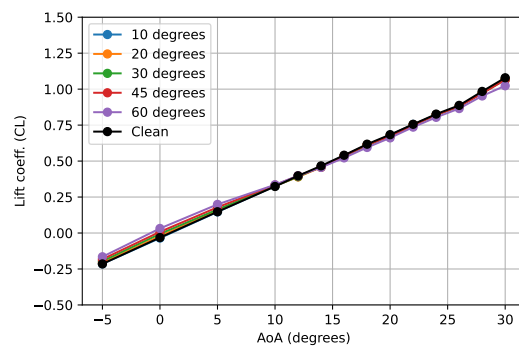
Figure B.5: Results of Flap C in Region 1 at 70% of the chord

B.4. Flap D

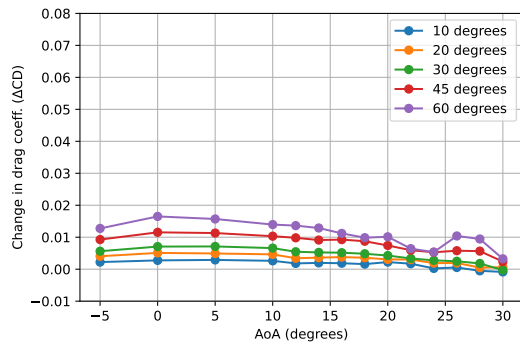
This flap has a span equal to L2 and chord-length of 10% of the local chord in region 2. This flap was tested in three chord wise locations in region 2, namely, 70%, 80% and 90%. Figure B.6 shows the results for the first location. By looking at the lift coefficient graph, it is evident that this flap is performing poorly, such that the flap starts to cause lift reduction after AoA of 12°. Not surprisingly, the drag rise is also quite insignificant. There is however, a relatively high increase in rolling moment coefficient. The pitching moment coefficient seems to follow the clean wing and there is also a small change of pitching moment coefficient with deflection angle however, much larger than the flaps on region 1.



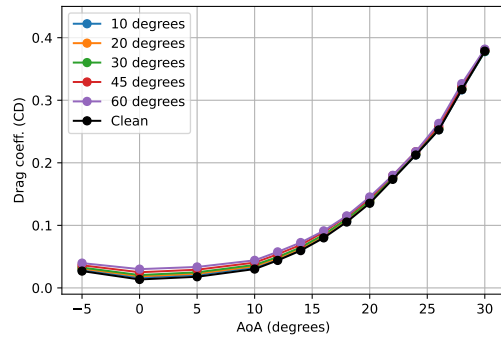
(a) Change in lift coefficient in comparison to clean wing



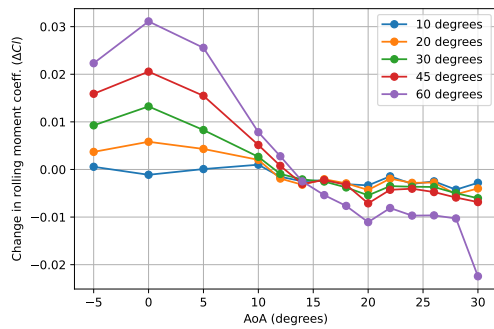
(b) Lift coefficient



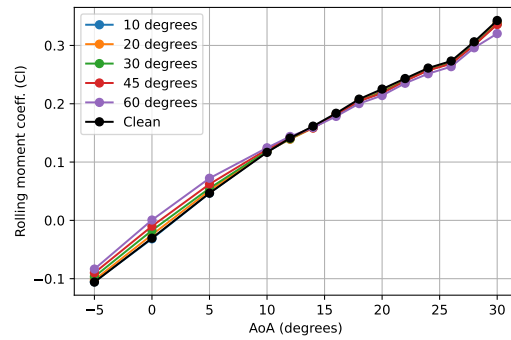
(c) Change in drag coefficient with respect to clean wing



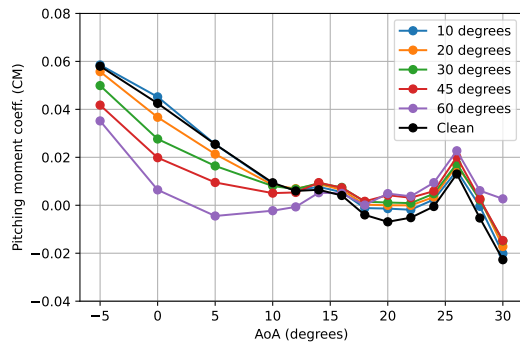
(d) Drag coefficient



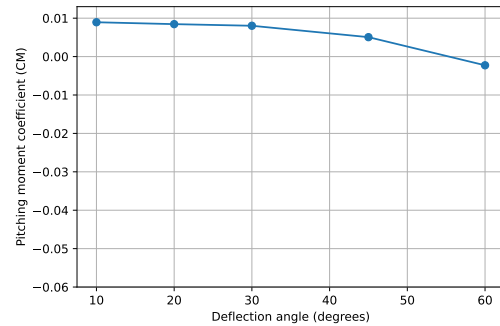
(e) Change in rolling moment coefficient with respect to clean wing



(f) Rolling moment coefficient



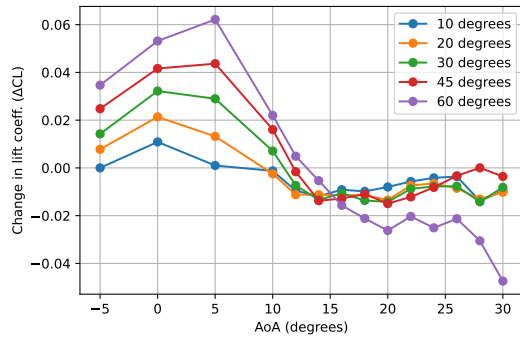
(g) Pitching moment coefficient Vs. Angle of attack



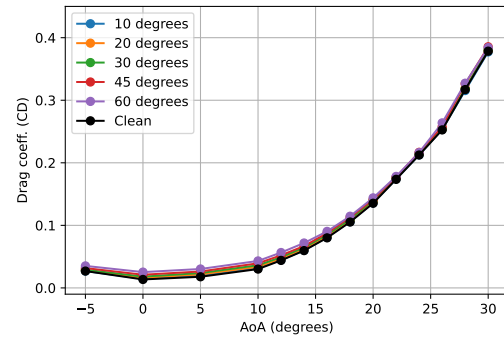
(h) Pitching moment coefficient Vs. Deflection angle

Figure B.6: Results of Flap D in Region 2 at 70% of the chord

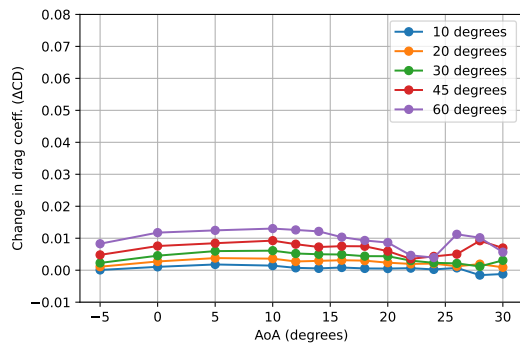
Next the results for when flap D in is 80% of the chord are shown. The results are not much different with the case where it was placed at 70% of the chord. There is a slightly higher lift increase in comparison to previous case, however, there is still reduction in lift after around 12° The rest of the plots are quite comparable.



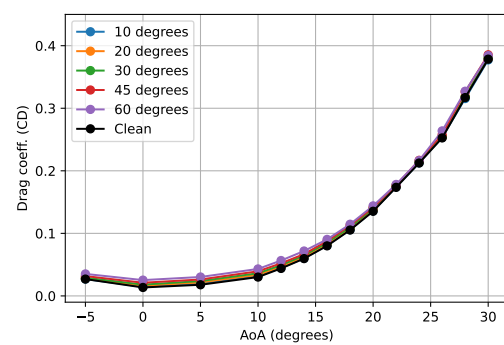
(a) Change in lift coefficient in comparison to clean wing



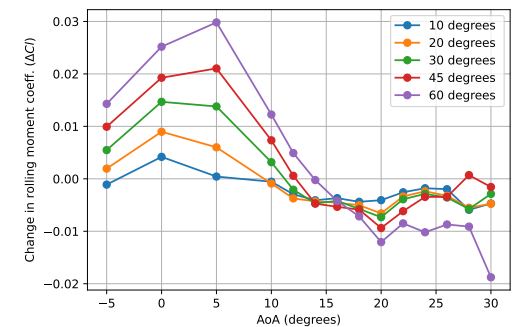
(b) Lift coefficient



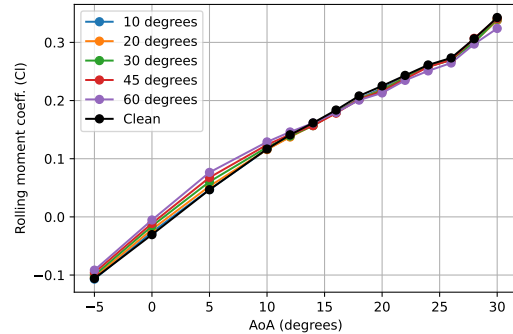
(c) Change in drag coefficient with respect to clean wing



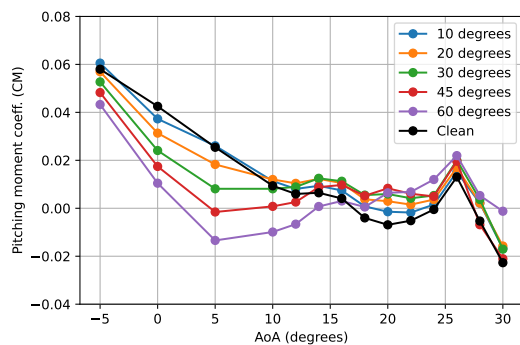
(d) Drag coefficient



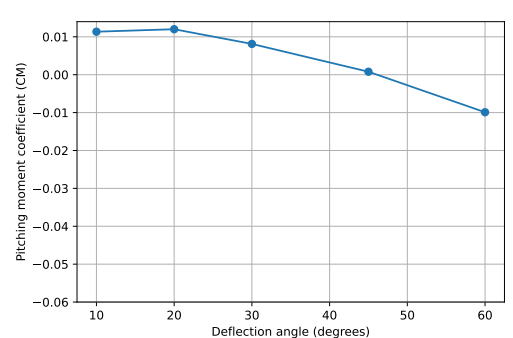
(e) Change in rolling moment coefficient with respect to clean wing



(f) Rolling moment coefficient



(g) Pitching moment coefficient Vs. Angle of attack

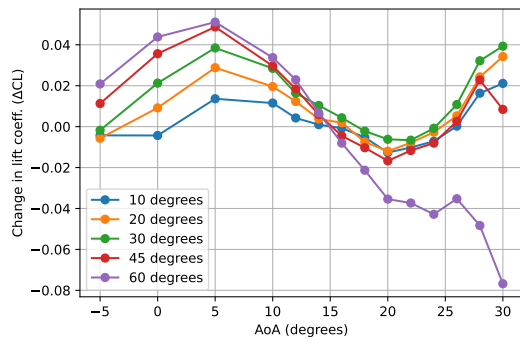


(h) Pitching moment coefficient Vs. Deflection angle

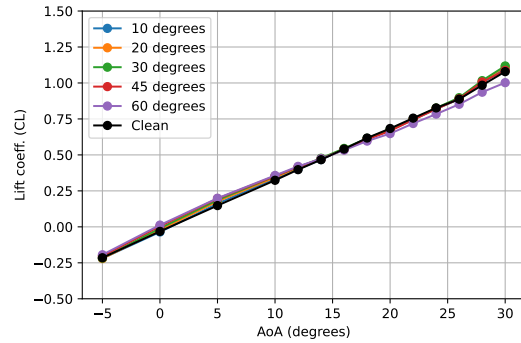
Figure B.7: Results of Flap D Region 2 at 80% of the chord

Lastly, flap D was placed in 90% of the chord. This case performed comparable to the other two

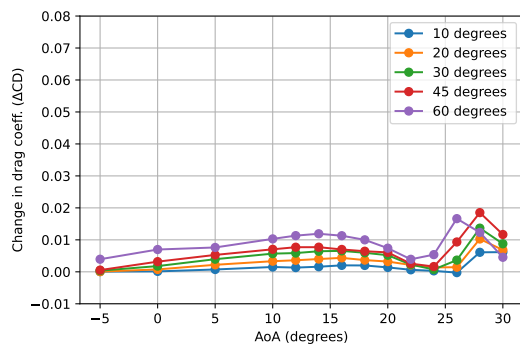
cases in all criteria besides lift increase. The lift increase continues until the AoA of 14° and even reaches 0.075 at the highest point.



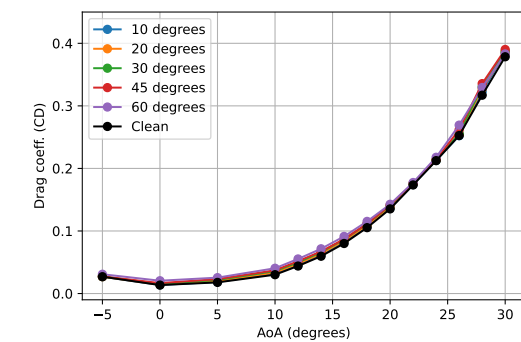
(a) Change in lift coefficient in comparison to clean wing



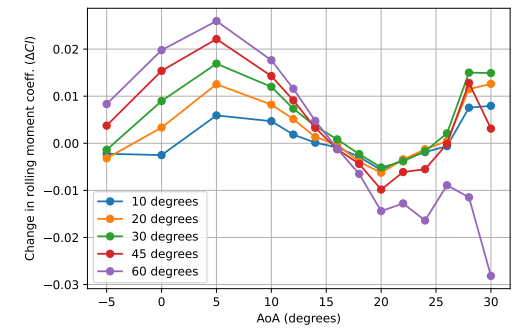
(b) Lift coefficient



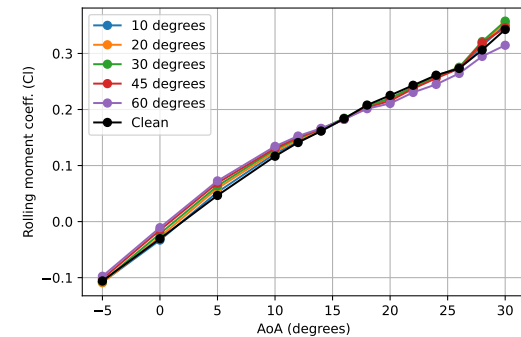
(c) Change in drag coefficient with respect to clean wing



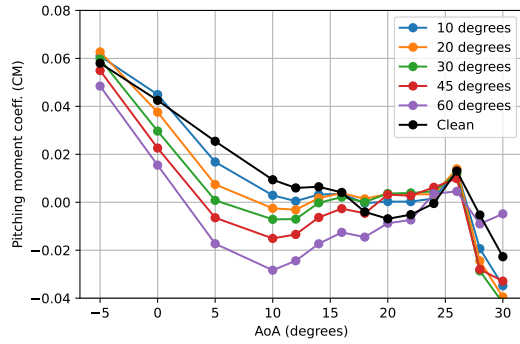
(d) Drag coefficient



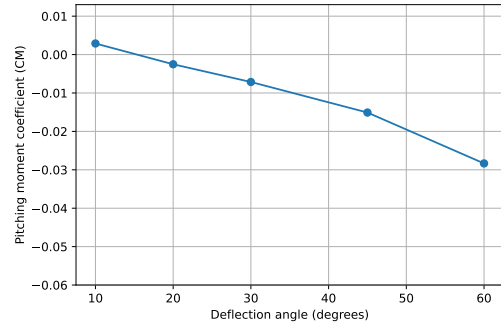
(e) Change in rolling moment coefficient with respect to clean wing



(f) Rolling moment coefficient



(g) Pitching moment coefficient Vs. Angle of attack

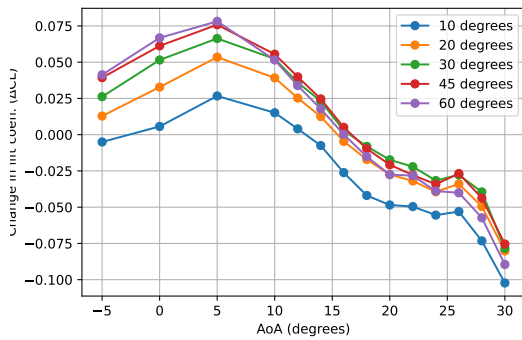


(h) Pitching moment coefficient Vs. Deflection angle

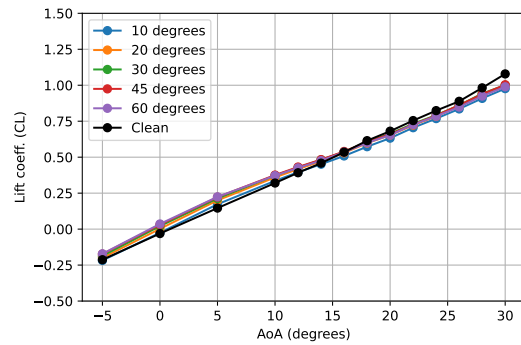
Figure B.8: Results of Flap D Region 2 at 90% of the chord

B.5. Flap E

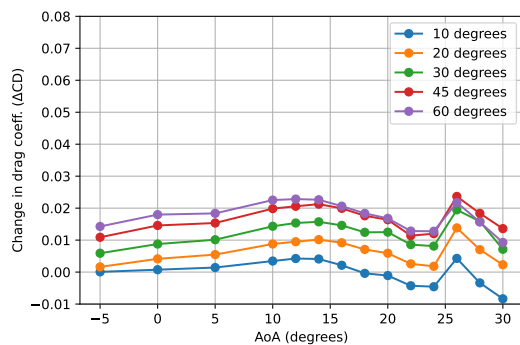
This configuration refers to the flap with an L2 span and chord-wise length of 20% of the local chord in R2. E has been tested in region 2 in the single-flap cases. E shows a maximum of 0.075 increase in lift coefficient, with small differences between 45° and 60° deflection angles. The drag increase is also relatively low given the size of the flap. It produces a significant rolling moment. The pitching moment behavior seems to follow the clean wing however, the onset of a pitch break is around 18°. The change in pitching moment with deflection angle is higher than that of the flaps omn region 1.



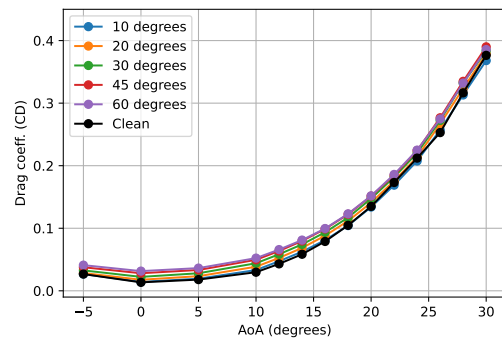
(a) Change in lift coefficient in comparison to clean wing



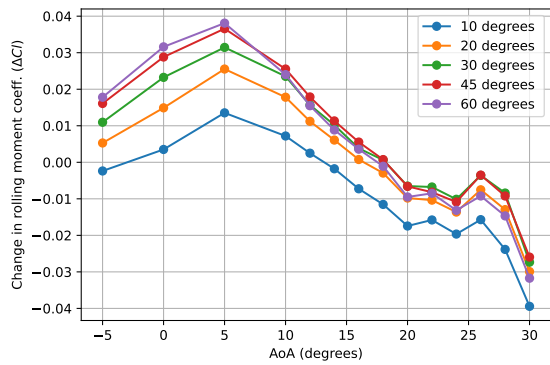
(b) Lift coefficient



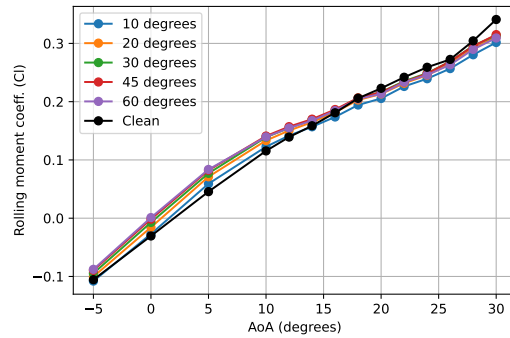
(c) Change in drag coefficient with respect to clean wing



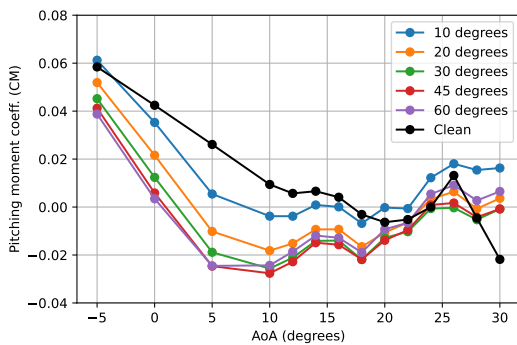
(d) Drag coefficient



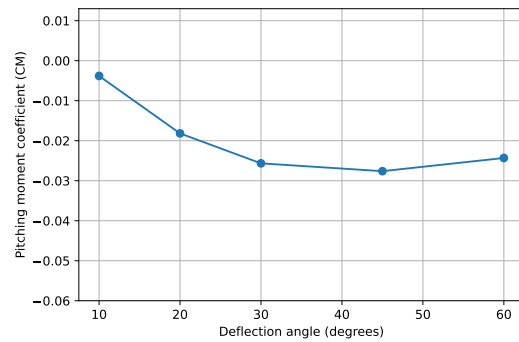
(e) Change in rolling moment coefficient with respect to clean wing



(f) Rolling moment coefficient



(g) Pitching moment coefficient Vs. Angle of attack

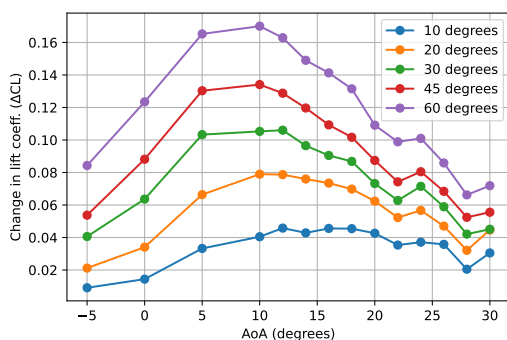


(h) Pitching moment coefficient Vs. Deflection angle

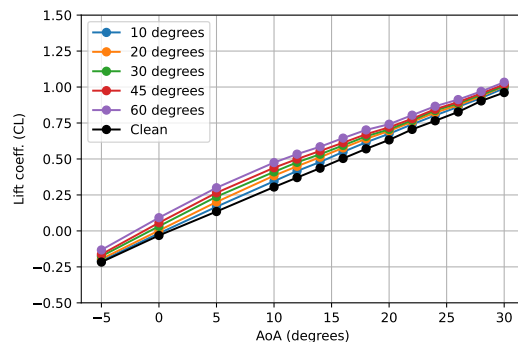
Figure B.9: Results of Flap E in Region 2 at 80% of the chord

B.6. Flaps A and D

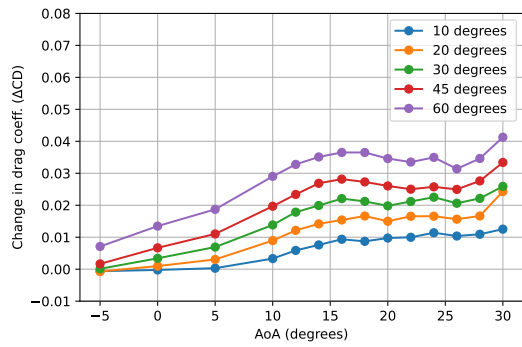
For this configuration A was placed at 0.9C of region 1 and flap D was placed on 0.9C of region 2. Figure B.10 shows great improvement in comparison to the cases where only A was placed at R1 or especially with D placed on region 2. We can see a large increase in the lift coefficient in comparison to the single-flap cases. As expected there is also a large increase in drag. The rolling moment coefficient also has a large increase. Further, the wing seems to be quite stable with a pitch break happening around 22° angle of attack. There is also a small change in the pitching moment with deflection angle.



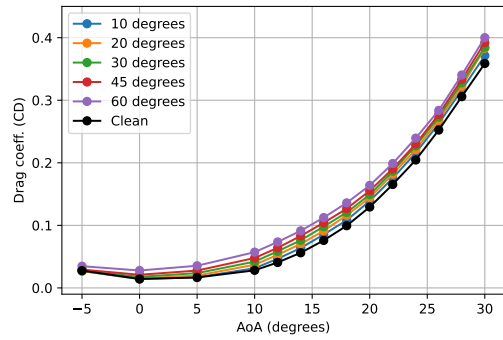
(a) Change in lift coefficient in comparison to clean wing



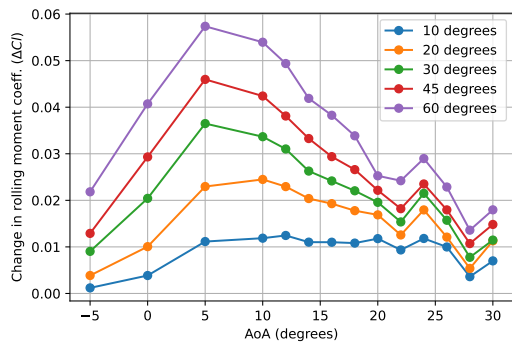
(b) Lift coefficient



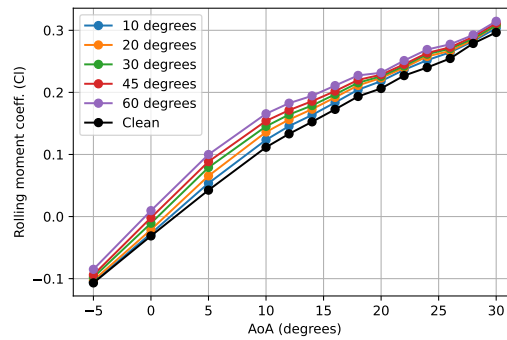
(c) Change in drag coefficient with respect to clean wing



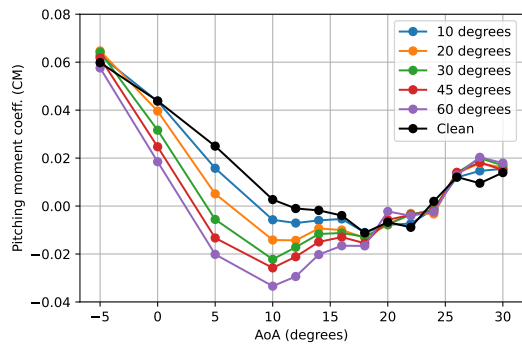
(d) Drag coefficient



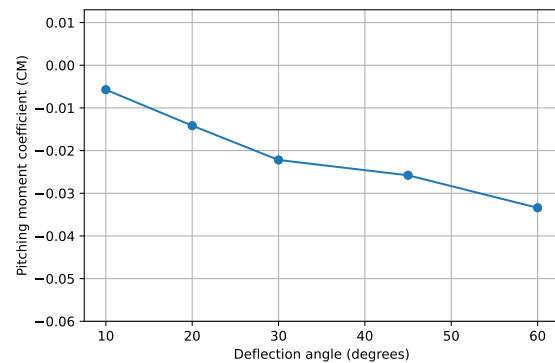
(e) Change in rolling moment coefficient with respect to clean wing



(f) Rolling moment coefficient



(g) Pitching moment coefficient Vs. Angle of attack

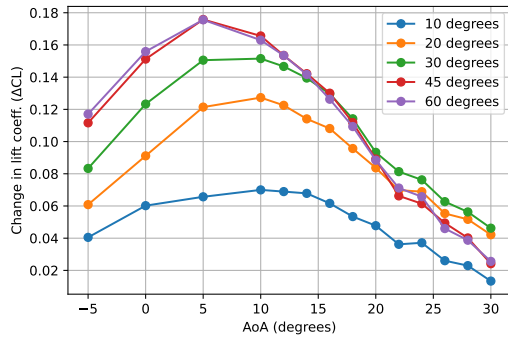


(h) Pitching moment coefficient Vs. Deflection angle

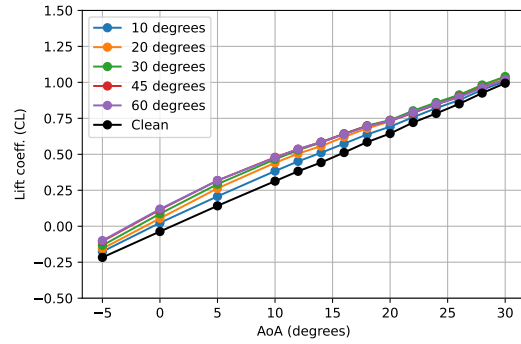
Figure B.10: Results of Flaps A and D at 90% of the chord in both regions

B.7. Flap B on Both Regions

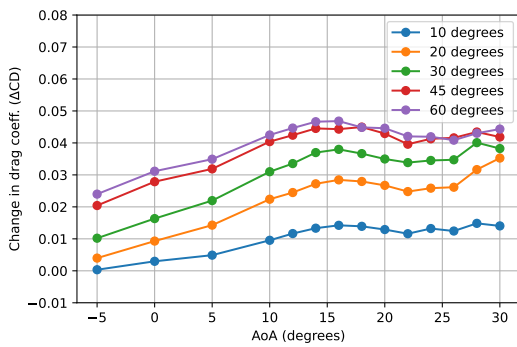
In this configuration, flap B was placed on both region 1 and region 2. The original flap B is sized based on region 1 meaning that the span is the same as region 1 and the chord is 20% of the chord of region 1. Therefore, to achieve the same relative chord length on region 2 a second version of flap B was designed with L1 span but a chord length equal to 20% of the chord of region 2. This configuration is performing quite similar to the B&E case which is expected. The main difference is the rolling moment where there is a smaller increase in this case in comparison to B&E.



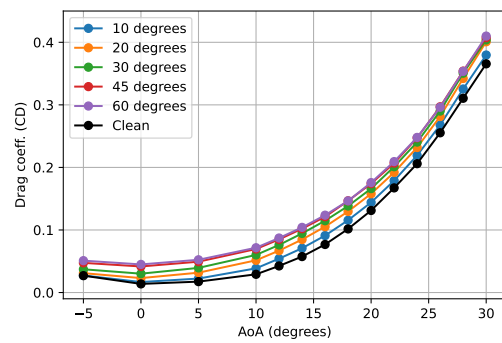
(a) Change in lift coefficient in comparison to clean wing



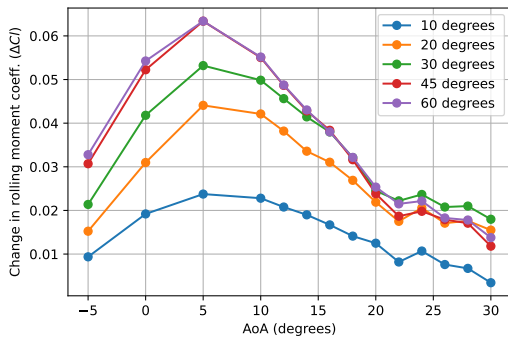
(b) Lift coefficient



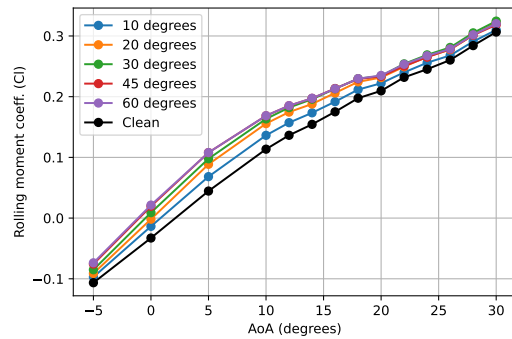
(c) Change in drag coefficient with respect to clean wing



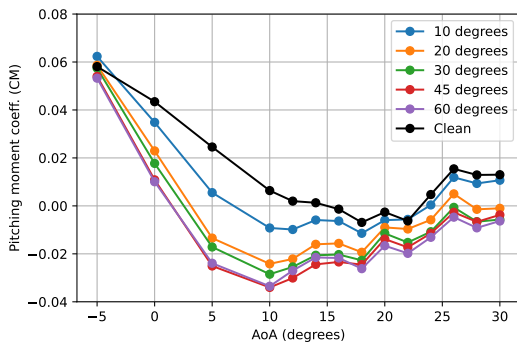
(d) Drag coefficient



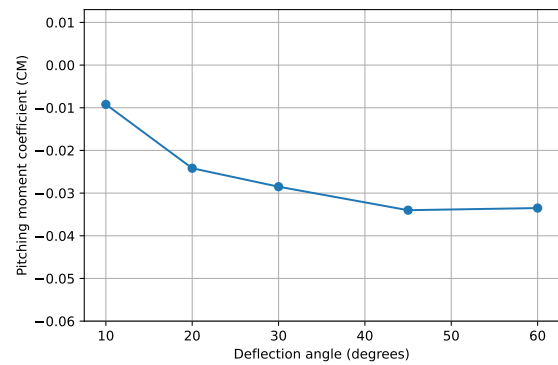
(e) Change in rolling moment coefficient with respect to clean wing



(f) Rolling moment coefficient



(g) Pitching moment coefficient Vs. Angle of attack



(h) Pitching moment coefficient Vs. Deflection angle

Figure B.11: Results of Flap B at 80% of the chord in both regions

C

Wind Tunnel Test Campaign Images

In this appendix the pictures of the half-wing model with various flaps during the wind tunnel test are presented.



(a) A on 09.C R1



(b) B on 0.8C R1



(c) B on 0.8C R2



(d) D on 0.9C R2



(e) E on 0.8c R2



(f) F on 0.7C R2



(g) A and D on 0.9C both regions



(h) B on 0.8C both regions



(i) B and E on 0.8C both regions



(j) C and F on 0.7C both regions



(k) Full-span on 0.8



(l) A on 0.7C R2

Figure C.1: Different flap configurations placed on the half-wing model during the wind tunnel tests